

POLITECNICO DI TORINO

MECHANICAL AND AEROSPACE ENGINEERING DEPARTMENT

Master's Degree Course in Automotive Engineering



Master's Degree Thesis

EXPERIMENTAL-NUMERICAL COMFORT ANALYSIS OF A HEAVY-DUTY VEHICLE

Academic supervisors:

Prof. Mauro VELARDOCCHIA

Prof. Enrico GALVAGNO

Company supervisor:

Dott. Vladi Massimo NOSENZO

Student:

Michele GALFRE'

ACADEMIC YEAR 2018–2019

Index

| | |
|--|-----------|
| INDEX | 2 |
| ABSTRACT | 4 |
| PICTURE INDEX | 5 |
| TABLE INDEX..... | 10 |
| INTRODUCTION | 11 |
| THE COMPANY | 12 |
| IVECO STRALIS | 12 |
| CHAPTER 1. TUNING OF IVECO STRALIS MULTIBODY MODEL IN ADAMS/CAR | 14 |
| 1.1 POSITIONING..... | 15 |
| 1.2 FRONT SUSPENSION | 18 |
| <i>1.2.1 Leaf springs.....</i> | <i>20</i> |
| <i>1.2.2 Steering.....</i> | <i>23</i> |
| 1.3 REAR SUSPENSION | 26 |
| 1.4 SEMI-TRAILER..... | 28 |
| <i>1.4.1 Flexible semi-trailer frame and load distribution.....</i> | <i>28</i> |
| <i>1.4.2 Semi-trailer suspension.....</i> | <i>31</i> |
| 1.5 MASS DISTRIBUTION..... | 32 |
| CHAPTER 2. HANDLING SIMULATIONS | 34 |
| 2.1 PERFORMED MANEUVERS..... | 35 |
| <i>2.1.1 Ramp steer</i> | <i>35</i> |
| <i>2.1.1 Sweep steer</i> | <i>35</i> |
| <i>2.1.3 Step steer.....</i> | <i>36</i> |
| 2.2 RESULTS | 36 |
| CHAPTER 3. MODEL PREPARATION FOR SIMULATIONS | 46 |
| 3.1 FTIRE MODEL | 46 |
| <i>3.1.1 FTire modeling.....</i> | <i>48</i> |
| <i>3.1.2 Iveco Stralis tires</i> | <i>50</i> |
| 3.2 CRG TRACK MODEL | 54 |
| <i>3.2.1 Markbronn pavè.....</i> | <i>57</i> |
| 3.3 TEST PERFORMED AND ACCELEROMETERS POSITIONING..... | 59 |

| | |
|---|-----------|
| 3.4 DRIVER CONTROL FILES AND ADAMS/SOLVER SETTING..... | 61 |
| CHAPTER 4. COMFORT ANALYSIS AND CORRELATION OF THE OBTAINED RESULTS..... | 63 |
| 4.1 COMFORT..... | 63 |
| 4.2 CORRELATION METHODS..... | 66 |
| 4.2.1 <i>PSD estimation</i> | 66 |
| 4.2.2 <i>LCR estimation</i> | 69 |
| 4.3 EXPERIMENTAL-NUMERICAL CORRELATION: UNLOADED CONDITION | 70 |
| 4.3.1 <i>40 km/h constant speed</i> | 71 |
| 4.4 EXPERIMENTAL-NUMERICAL CORRELATION: LOADED CONDITION..... | 76 |
| 4.4.1 <i>40 km/h constant speed</i> | 77 |
| 4.4.2 <i>45 km/h constant speed</i> | 82 |
| 4.3.3 <i>15-30 km/h constant acceleration</i> | 86 |
| CHAPTER 5. CONCLUSIONS AND FUTURE PERSPECTIVES | 90 |
| LIST OF SYMBOLS AND ABBREVIATIONS..... | 92 |
| BIBLIOGRAPHY..... | 93 |
| SITOGRAPHY | 95 |
| ACKNOWLEDGEMENTS..... | 96 |

Abstract

The Master Thesis work has been conducted in the Iveco headquarter in Turin (Italy) with the supervision of the Polytechnic of Turin. It is part of a project that has the aim to develop a reliable multibody model of an Iveco Stralis truck, capable to faithfully reproduce on-road tests.

In automotive market, today more than in the past, it is very important to reduce time to market and, mostly, developing costs before the final production start. So, it is essential to have very predictable models, able to forecast on road behaviors.

The multibody environment used is Adams/Car, produced by MSC Software, while Matlab is chosen for the post-processing environment. Furthermore, a complete 3D model was available in CATIA, a CAD software developed by Dassault Systemes. Altair Hypermesh, MSC Nastran and MSC Adams/View are used to create flexible bodies that are present in the model.

After the introduction, where an overview of the company and of the truck is given, the work is mainly divided in four parts.

The first one is aimed at the tuning of the existing multibody model, in order to obtain a complete and updated model, as close as possible to the real one, from the geometrical and the mechanical point of view. The main topics of this section are: the positioning of all the parts of the model according to the most updated CATIA model, the generation of a new leaf spring, the calibration of the steering system, the revision of the mass distribution and the introduction of a semi-trailer with a flexible frame and a new suspension design.

The second part deals with handling simulations of the truck in two configurations: unloaded (tractor only) and loaded (tractor, semi-trailer and load) conditions. These simulations are necessary to verify the correct behavior of the model performing standard maneuvers.

Subsequently, the preparation of the multibody model for simulations on the pavé track of Markbronn (Germany) proving ground is addressed. In this chapter FTire model, CRG track model, the tests performed by the on-road truck and the numerical simulations settings are discussed.

The final part concerns the first experimental-numerical correlation of comfort analysis measurements in order to evaluate the FTire model and suspension systems behavior of the multibody model. Simulation data and experimental ones are investigated in time and in frequency domain, using two different methods typical of random signals: the level crossing rate (LCR) and the power spectral density (PSD) analysis.

The conclusions regard a discussion of the obtained results and the future perspectives of this project, that surely does not stop here and now. The purpose of having the model that behaves as close as possible to the real one must be pursued also with a view to other studies that can be carried on with this multibody model.

Picture Index

| | |
|--|----|
| Figure 1- Iveco commercial vehicles gamma..... | 12 |
| Figure 2- Iveco Stralis used for on-road test | 13 |
| Figure 3- Iveco Stralis multibody model..... | 14 |
| Figure 4- Iveco Stralis tractor CAD model | 15 |
| Figure 5- Leaner CAD model..... | 15 |
| Figure 6- Complete model of the short wheelbase chassis..... | 16 |
| Figure 7- Sketch model of the short wheelbase chassis | 16 |
| Figure 8- Wireframe tractor model with final positioning. Yellow dots represent the interface nodes of the chassis | 17 |
| Figure 9- Iveco Stralis tractor multibody model | 17 |
| Figure 10- Front suspension CAD model..... | 18 |
| Figure 11- Front suspension multibody model..... | 19 |
| Figure 12- Front antiroll bar CAD model..... | 19 |
| Figure 13- Leaf springs model | 20 |
| Figure 14- Leaf spring profile | 21 |
| Figure 15- Leaf spring force vs displacement characteristic | 22 |
| Figure 16- Steering system top view | 23 |
| Figure 17- Ackerman steering geometry | 23 |
| Figure 18- Steering system..... | 24 |
| Figure 19- Wheel angles vs steering wheel angle. The red line represents the left wheel angle while the blue one the right wheel angle. Negative steering wheel angle denotes a right turn, positive angle a left turn | 25 |
| Figure 20- Steering ratio vs steering wheel angle | 25 |
| Figure 21- Rear suspension CAD model..... | 26 |
| Figure 22- Rear suspension multibody model..... | 26 |
| Figure 23- Rear antiroll bar CAD model..... | 27 |
| Figure 24- Original semi-trailer multibody model | 28 |
| Figure 25- Semi-trailer multibody model..... | 29 |
| Figure 26- Iveco Stralis multibody model..... | 30 |
| Figure 27- Semi-trailer suspension multibody model | 31 |
| Figure 28- Full vehicle performing the step steer maneuver | 34 |
| Figure 29- Ramp steer: steering wheel angle vs lateral acceleration..... | 38 |
| Figure 30- Ramp steer: roll angle vs lateral acceleration | 39 |

| | |
|--|----|
| Figure 31- Ramp steer: sideslip angle vs lateral acceleration..... | 39 |
| Figure 32- Ramp steer: yaw rate vs lateral acceleration..... | 40 |
| Figure 33- Sweep steer: input: steering wheel angle output: lateral acceleration | 41 |
| Figure 34- Sweep steer: input: steering wheel angle output: sideslip angle..... | 41 |
| Figure 35- Sweep steer: input: steering wheel angle output: yaw rate | 42 |
| Figure 36- Sweep steer: input: lateral acceleration output: roll angle | 42 |
| Figure 37- Step steer: lateral acceleration vs time..... | 43 |
| Figure 38- Step steer: roll angle vs time..... | 44 |
| Figure 39- Step steer: sideslip angle vs time | 44 |
| Figure 40- Step steer: yaw rate vs time | 45 |
| Figure 41- Cosin Scientific Software | 47 |
| Figure 42- Flexible ring representing the tire belt..... | 48 |
| Figure 43- Tire regions in FTire thermal model..... | 49 |
| Figure 44- Tire test rig used at ika/fka RWTH Aachen University..... | 50 |
| Figure 45- Tire test bench coordinate system..... | 51 |
| Figure 46- Front tire tread and rim used for measurements | 51 |
| Figure 47- Front tire pressure distribution..... | 52 |
| Figure 48- Rear tire characterization | 52 |
| Figure 49- Rear tire footprint | 53 |
| Figure 50- Curved Reference Line | 54 |
| Figure 51- Regular Elevation Grid | 54 |
| Figure 52- Curved Regular Grid..... | 54 |
| Figure 53- CRG reference line in x-y coordinates | 55 |
| Figure 54- Grid cells height determination..... | 55 |
| Figure 55- CRG representation in u-v-z coordinates..... | 56 |
| Figure 56- CRG representation in x-y-z coordinates..... | 56 |
| Figure 57- To the left CRG transversal road cross section in v-z coordinates at different u positions. To the right CRG longitudinal road cross sections in u- z coordinates at different v positions | 56 |
| Figure 58- CRG file example | 57 |
| Figure 59- Overview of Markbronn test track. Circled in red the Belgian block track..... | 57 |
| Figure 60- Top view of Belgian block track on Adams/Car | 58 |
| Figure 61- Lateral view of Belgian block track on Adams/Car..... | 58 |
| Figure 62- Front axle accelerometer positioning, circled in red..... | 59 |
| Figure 63- Rear axle accelerometer positioning, circled in red..... | 59 |
| Figure 64- Tractor chassis accelerometer positioning, circled in red | 60 |
| Figure 65- PSD of typical road profiles..... | 64 |
| Figure 66- Constant discomfort lines (ISO 2631 standard)..... | 65 |

| | |
|--|----|
| Figure 67- Example of time history signals correlation | 66 |
| Figure 68- Example of PSD signal correlation..... | 69 |
| Figure 69- Example of LCR signal correlation | 69 |
| Figure 70- Accelerometers positioning | 71 |
| Figure 71- PSD of accelerations of front axle left..... | 71 |
| Figure 72- PSD of accelerations of front axle right..... | 71 |
| Figure 73- LCR of accelerations of front axle left | 71 |
| Figure 74- LCR of accelerations of front axle right | 71 |
| Figure 75- Accelerometers positioning | 72 |
| Figure 76- PSD of accelerations of rear axle left | 72 |
| Figure 77- PSD of accelerations of rear axle right | 72 |
| Figure 78- LCR of accelerations of rear axle left..... | 72 |
| Figure 79- LCR of accelerations of rear axle right..... | 72 |
| Figure 80- Accelerometers positioning | 73 |
| Figure 81- PSD of accelerations of frame front left | 73 |
| Figure 82- PSD of accelerations of frame front right..... | 73 |
| Figure 83- LCR of accelerations of frame front left..... | 73 |
| Figure 84- LCR of accelerations of frame front right..... | 73 |
| Figure 85- Accelerometers positioning | 74 |
| Figure 86- PSD of accelerations of frame front left | 74 |
| Figure 87- PSD of accelerations of frame rear right..... | 74 |
| Figure 88- LCR of accelerations of frame front left..... | 74 |
| Figure 89- LCR of accelerations of frame rear right | 74 |
| Figure 90- Accelerometers positioning | 77 |
| Figure 91- PSD of accelerations of front axle left..... | 77 |
| Figure 92- PSD of accelerations of front axle right..... | 77 |
| Figure 93- LCR of accelerations of front axle left | 77 |
| Figure 94- LCR of accelerations of front axle right | 77 |
| Figure 95- Accelerometers positioning | 78 |
| Figure 96- PSD of accelerations of rear axle left | 78 |
| Figure 97- PSD of accelerations of rear axle right | 78 |
| Figure 98- LCR of accelerations of rear axle left..... | 78 |
| Figure 99- LCR of accelerations of rear axle right..... | 78 |
| Figure 100- Accelerometers positioning | 79 |
| Figure 101- PSD of accelerations of frame front left | 79 |
| Figure 102- PSD of accelerations of frame front right..... | 79 |
| Figure 103- LCR of accelerations of frame front left..... | 79 |

| | |
|--|----|
| Figure 104- LCR of accelerations of frame front right..... | 79 |
| Figure 105- Accelerometers positioning | 80 |
| Figure 106- PSD of accelerations of frame rear left..... | 80 |
| Figure 107- PSD of accelerations of frame rear right..... | 80 |
| Figure 108- LCR of accelerations of frame rear left | 80 |
| Figure 109- LCR of accelerations of frame rear right | 80 |
| Figure 110- Accelerometers positioning | 82 |
| Figure 111- PSD of accelerations of front axle left..... | 82 |
| Figure 112- PSD of accelerations of front axle right..... | 82 |
| Figure 113- LCR of accelerations of front axle left | 82 |
| Figure 114- LCR of accelerations of front axle right | 82 |
| Figure 115- Accelerometers positioning | 83 |
| Figure 116- PSD of accelerations of rear axle left | 83 |
| Figure 117- PSD of accelerations of rear axle right | 83 |
| Figure 118- LCR of accelerations of rear axle left..... | 83 |
| Figure 119- LCR of accelerations of rear axle right..... | 83 |
| Figure 120- Accelerometers positioning | 84 |
| Figure 121- PSD of accelerations of frame front left | 84 |
| Figure 122- PSD of accelerations of frame front right..... | 84 |
| Figure 123- LCR of accelerations of frame front left..... | 84 |
| Figure 124- LCR of accelerations of frame front right..... | 84 |
| Figure 125- Accelerometers positioning | 85 |
| Figure 126- PSD of accelerations of frame rear left..... | 85 |
| Figure 127- PSD of accelerations of frame rear right..... | 85 |
| Figure 128- LCR of accelerations of frame rear left | 85 |
| Figure 129- LCR of accelerations of frame rear right | 85 |
| Figure 130- Accelerometers positioning | 86 |
| Figure 131- PSD of accelerations of front axle left..... | 86 |
| Figure 132- PSD of accelerations of front axle right..... | 86 |
| Figure 133- LCR of accelerations of front axle left | 86 |
| Figure 134- LCR of accelerations of front axle right | 86 |
| Figure 135- Accelerometers positioning | 87 |
| Figure 136- PSD of accelerations of rear axle left | 87 |
| Figure 137- PSD of accelerations of rear axle right | 87 |
| Figure 138- LCR of accelerations of rear axle left..... | 87 |
| Figure 139- LCR of accelerations of rear axle right..... | 87 |
| Figure 140- Accelerometers positioning | 88 |

| | |
|---|----|
| Figure 141- PSD of accelerations of frame front left | 88 |
| Figure 142- PSD of accelerations of frame front right | 88 |
| Figure 143- LCR of accelerations of frame front left | 88 |
| Figure 144- LCR of accelerations of frame front right | 88 |
| Figure 145- Accelerometers positioning | 89 |
| Figure 146- PSD of accelerations of frame rear left | 89 |
| Figure 147- PSD of accelerations of frame rear right | 89 |
| Figure 148- LCR of accelerations of frame rear left | 89 |
| Figure 149- LCR of accelerations of frame rear right | 89 |

Table Index

| | |
|---|----|
| Table 1- Ballast weights | 32 |
| Table 2- On-road loading condition | 32 |
| Table 3- Multibody model loading conditions | 33 |
| Table 4- Ramp steer..... | 35 |
| Table 5- Sweep steer | 35 |
| Table 6- Step steer | 36 |
| Table 7- Model characteristics | 37 |
| Table 8- Model characteristics | 37 |
| Table 9- Front tires characteristics | 51 |
| Table 10- Rear tires characteristics | 53 |

Introduction

Vehicle dynamics and comfort are becoming more and more important, mostly with regards to the safety of the driver, of passengers and of pedestrians. The purpose of vehicle dynamics is to guarantee a simple and predictable behavior of the running vehicle and can be considered integral part of the active safety: indeed, it is the central topic for ADAS (Advanced Driver Assistance Systems) and autonomous driving systems. The aim of comfort is to improve the driving experience reducing motion sickness, vibrations and noise that could be annoying for human body.

The commercial vehicles market is becoming very competitive in order to meet customers' demands. Clients, today, ask for products with high performances, high comfort, low fuel consumption and low price. Moreover, trucks are the vehicles that travel the highest number of kilometers every day and transport companies need to reduce the TCO (Total Cost of Ownership) in order to remain competitive in their sector. For this reason, to fulfil buyers' wants, OEM's must improve continuously their industrial vehicles and invest on research.

The driver, the vehicle and the environment provide a single closed-loop and so, evaluate and predict the behavior of this closed system is difficult because there is a mutual interaction between these three elements and there are a lot of variables. Different types of maneuvers are necessary for the description of the dynamic behavior of a vehicle, each of them performed accurately and following standard directives. It is important to perform tests many times and under identical experiments conditions. Only in this way measurements can be compared.

The study of vehicle dynamics involves three different subjects: virtual simulation, test bench analysis and on-road tests. In this thesis, the attention is focused on the first subject, the virtual testing, and on the correlation of simulation data with on-road tests data. In this context, the multibody software used is Adams/Car, which mission is to solve the equations governing the kinematics and the dynamics of a vehicle. Ideally, multibody studies can replace the bench and the on-road tests because virtual approach guarantees identical test conditions and inputs are able to replicate exactly the standard procedures. Approval authorities are starting to look at simulations to release homologation certificates. Nevertheless, on the other hand, experimental confirmation will be always necessary. Virtual simulation allows to obtain great economic savings and time saving, but, at the same time, before "replacing" bench and on-road tests, it is mandatory to have reliable models. For this purpose, a sensitivity analysis and a validation phase must be performed.

The final and validated multibody model could be used not only for handling and comfort simulations, but also for studies like NVH, durability or ADAS systems, in order to continuously improve reliability and safety of future vehicles.

The diagrams present in this thesis, as requested by Iveco company, will lack of the y axis for secrecy reasons.

The Company

Iveco is an industrial vehicle manufacturing company, present all over the world and based in Turin. It was founded, in 1975, from the union of five different companies: Fiat Industrial Vehicles (Italy), OM (Italy), Lancia Special Vehicles (Italy), Magirus-Deutz (Germany) and Unic (France).

These manufacturers joint their skills to become one of the major players in the global transport world. Today Iveco is entirely controlled by CNH Industrial and is an international leader in the development, manufacturing and servicing of a vast range of light, medium and heavy commercial vehicles. It also manufactures city and intercity buses and special vehicles for military uses, for civil protection and for specific missions like, for example, fire-fighting.

Iveco is present in all five continents. It consists in 27 production plants, in 6 research centers, in 5'000 points of sales and service and it counts more than 25'000 employees all around the world.

Considering commercial vehicles, the light segment is represented by the Iveco Daily, with a range of weight from 2.8 tons up to 7 tons. The medium vehicles category is characterized by the Eurocargo, with a range between 7 and 19 tons. Concluding, the Stralis and the Trakker represents the range of weights that goes from 19 to 72 tons. Each category is characterized by hundreds of different types of configurations (wheelbase, number of axles, 4x2 or 4x4 drive, type of cabin, etc.).



Figure 1- Iveco commercial vehicles gamma

Iveco Stralis

Iveco Stralis, the subject of this thesis, belongs to heavy-duty vehicle category. Concerning weights, its working range is between 18 and 44 tons, the maximum allowed weight as indicated in European directives. Its production started in 2002 in substitution of two previous models: the Eurostar and

the Eurotech. It is manufactured in the Spanish Iveco plant and it has been subjected to different restyling during the years. There are a lot of configurations and so an alphanumeric code is used for classification. For instance, the model used for on-road tests discussed in this work, has the code AS 440 S 48 T/P, that means:

- AS indicates the cabin type;
- 440 is the maximum weight on the ground (tons*10);
- S indicates the model, so, in this case stands for Stralis;
- 48 is the engine power (CV*10);
- T distinguishes the tractor from the lorry model;
- /P deals with the type of the front and the rear suspensions.

Since a truck has to carry heavy loads, the tractor could have more than 2 axles and the rear axles have twinned wheels. For this reason, there is another classification defined according to ISO norms, for instance 6x2(x2). In this case:

- 6 represent the total number of the wheels;
- 2 stands for the number of the driving wheels;
- 2 is the number of the steering wheels.

According to this standard, a couple of rear twinned wheels is considered only as a wheel. The propulsors used in Iveco Stralis, named Cursor, are straight-six engines. The available displacements go from 7'790 cm³ to 12'880 cm³ and the power ranges between 310 and 570 CV. In the picture below is showed the model used for on-road test performed in Markbronn proving ground, situated in Germany.



Figure 2- Iveco Stralis used for on-road test

Chapter 1. Tuning of Iveco Stralis multibody model in Adams/Car

The first part of this work is focused on the tuning of the available Iveco Stralis multibody model in Adams/Car environment. The debug phase is started with the positioning of each part of the model according to the last release of the CATIA CAD model and is continued with the fixing of some inaccuracies concerning the front suspension, the rear suspension, the cabin, the engine properties and the gear ratios. It is followed the introduction of a flexible semi-trailer frame and a new semi-trailer suspension. At the end the mass distribution has been revised in order to meet the real test conditions.

Adams/Car represents the widely used software among OEMs to evaluate lateral and longitudinal dynamics of a vehicle. The particularity of modeling with a multibody approach is that parts are modelled like infinitely rigid elements, i.e. 6 dof bodies. In reality, in Adams/Car, it is possible to introduce flexible bodies containing the modal analysis of the system, making the model more and more complex and accurate.

Adams/Car modeling is devised in three steps: template, subsystem, assembly. The template, which defines the topology of the system, is the starting point of the modeling. The subsystem, that recalls the layout described in the template previously created, permits to change some parameters and obtain different configurations of the same model. The final step is characterized by the assembly, in which different subsystems can be matched together in order to create increasingly complete systems. Only after the creation of the assembly, that can be a suspension assembly or a full vehicle assembly, it is possible to perform simulations. This methodology permits to have an extreme flexibility because it allows to change configuration modifying, adding, or replacing parts in order to have an overview of results and chose the best arrangements.

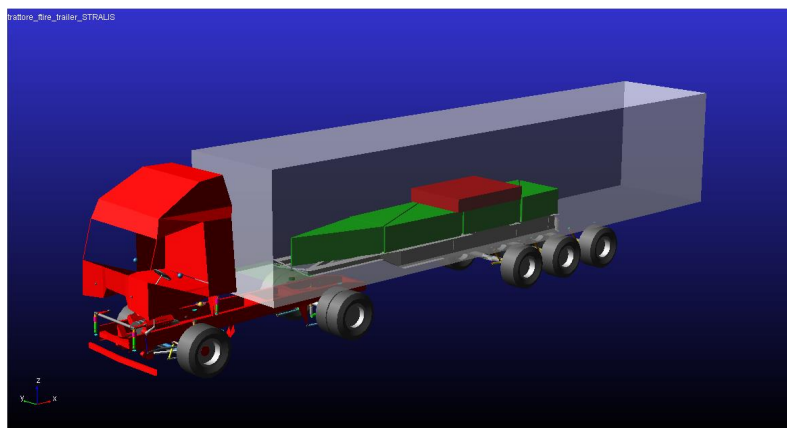


Figure 3- Iveco Stralis multibody model

1.1 Positioning

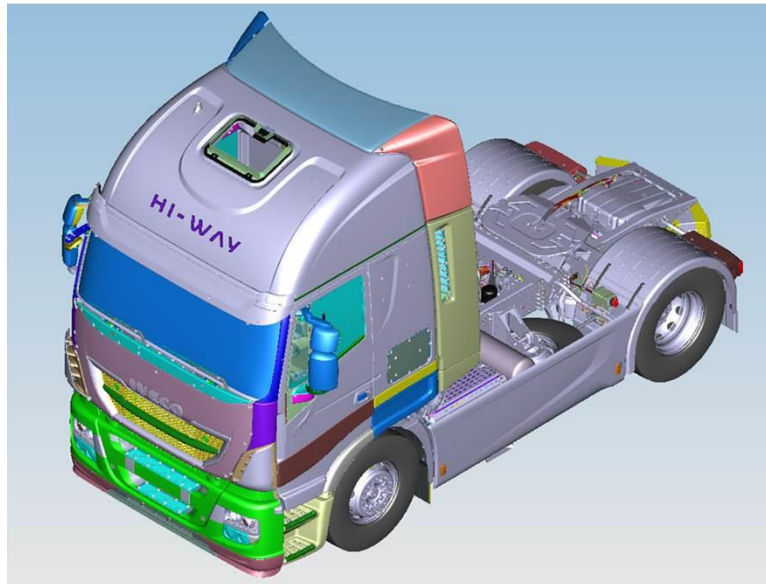


Figure 4- Iveco Stralis tractor CAD model

Starting from a complete and updated CATIA CAD model, a leaner model is created. The necessary subsystems for evaluating the correct positions and dimensions of all the parts in the Adams/Car model are the tractor body, the front suspension, the rear suspension and the cabin suspension system.

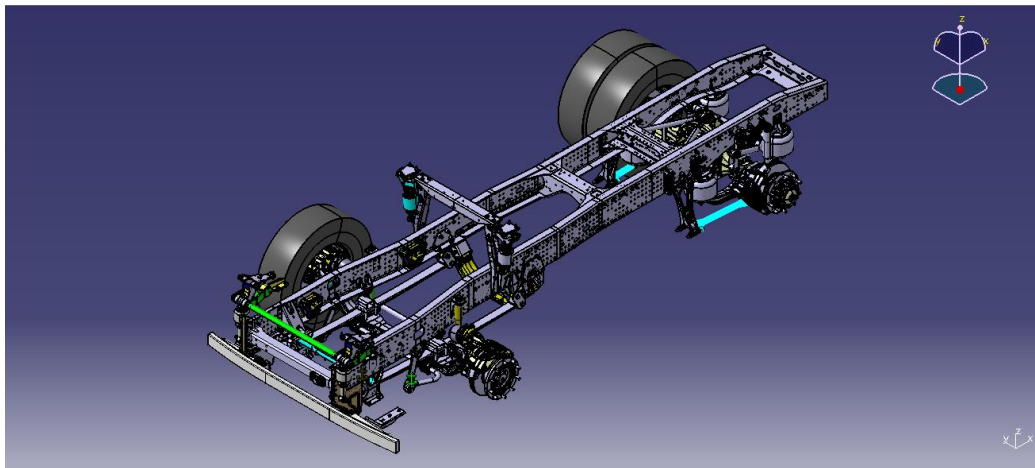


Figure 5- Leaner CAD model

From the lean CAD model, all the positions of the multibody model have been updated. In this way there is a perfect correspondence between the CATIA model and the Adams/Car model concerning the location of each part. Notice that, both in CATIA and in Adams/Car, the reference frame is oriented in this way, according to right hand convention: the x-axis coincides with the vehicle one

and is rearward, the z-axis is perpendicular to the road surface and is upward while the y-axis points to the right. The origin of the global reference frame, positioned near the front axle, does not match any point of the vehicle, but it has been chosen the same in Adams/Car and CATIA for having correspondence between 3D and multibody models.

Respect the previous model, a new chassis with short wheelbase has been introduced. In fact, originally there was an incongruence between the interface parts, created for a short wheelbase body but associated to a long wheelbase frame.

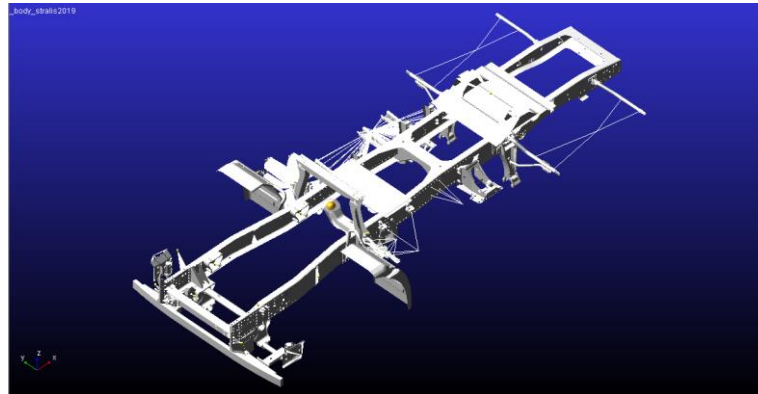


Figure 6- Complete model of the short wheelbase chassis

The cabin and its suspensions have been completely repositioned according to the interface nodes present on the new body.

The cabin and the body are flexible parts because being very large elements, their influence on the dynamic behavior of the system is not negligible. The introduction of flexible bodies is possible thanks to specific functions of Adams/Car and the procedure is described in this chapter at the section 1.4.1. In the multibody model are used sketch of the cabin and of the chassis in order to reduce the computation power, but they behave perfectly like the complete models concerning deformations and vibration modes.

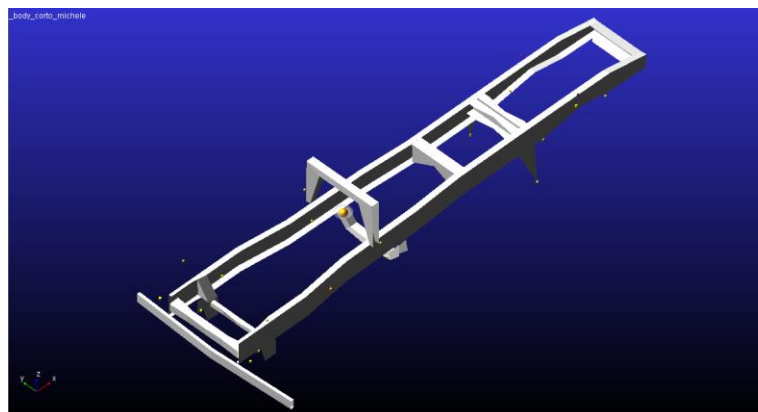


Figure 7- Sketch model of the short wheelbase chassis

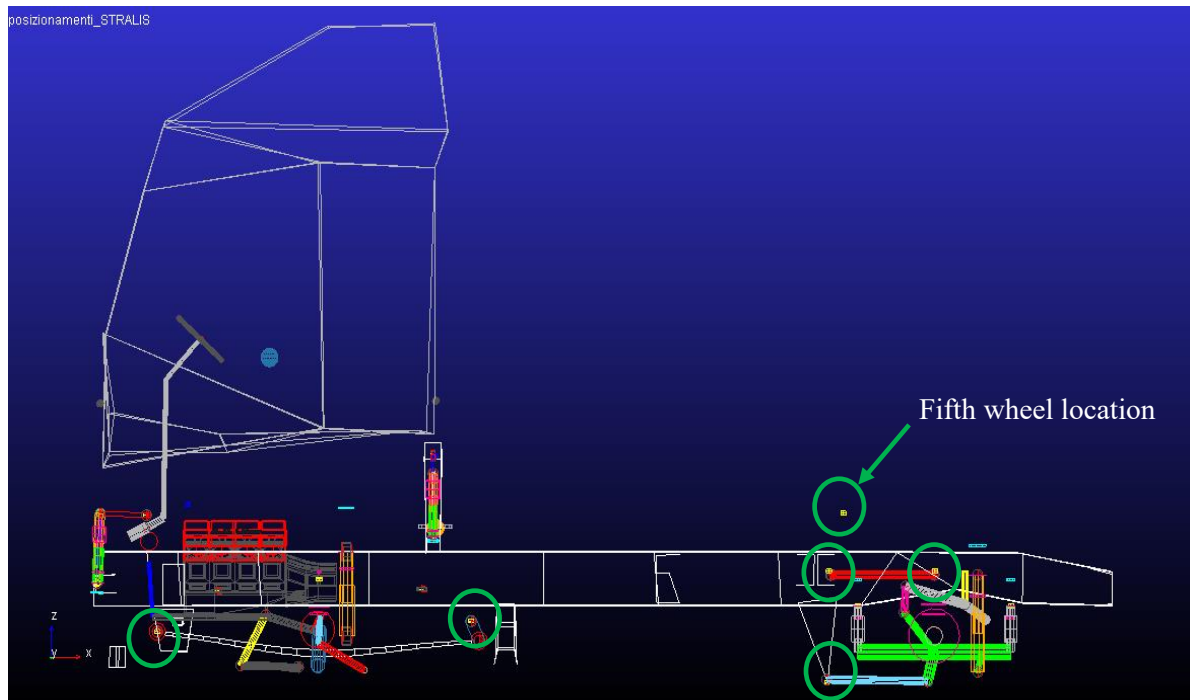


Figure 8- Wireframe tractor model with final positioning. Yellow dots represent the interface nodes of the chassis

In [Figure 8](#) it is possible to see the positioning of parts respect yellow interface nodes. Some of these nodes are circled in green. The [Figure 9](#) represent the complete tractor multibody model.

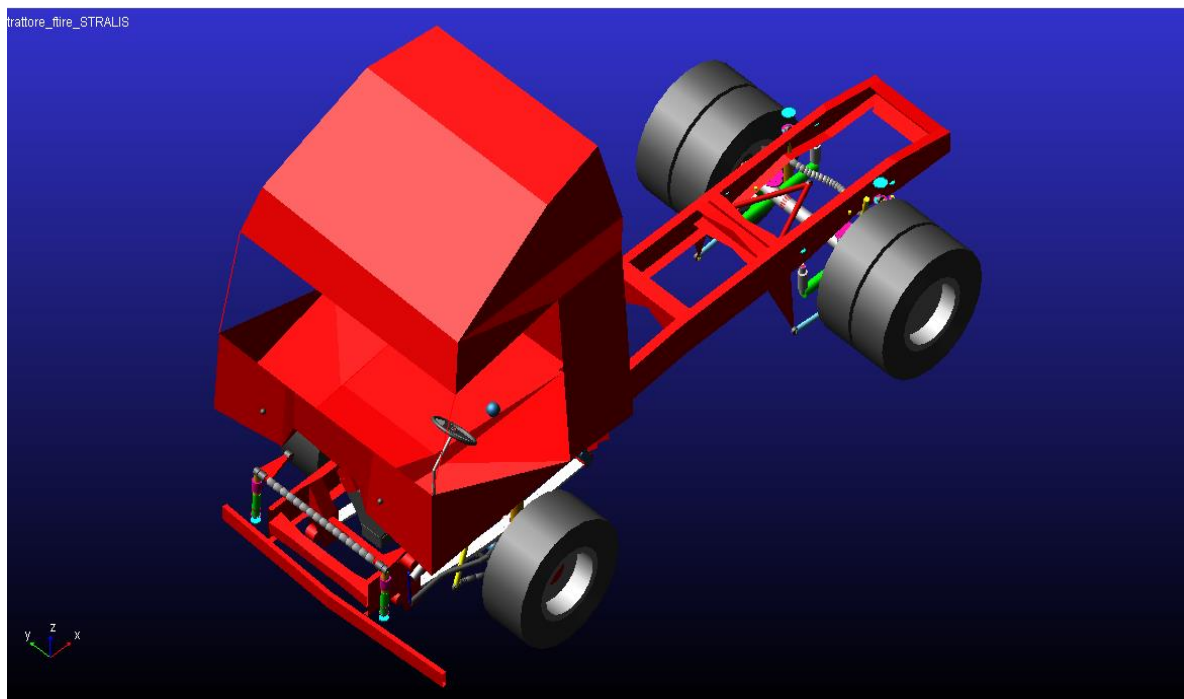


Figure 9- Iveco Stralis tractor multibody model

1.2 Front suspension

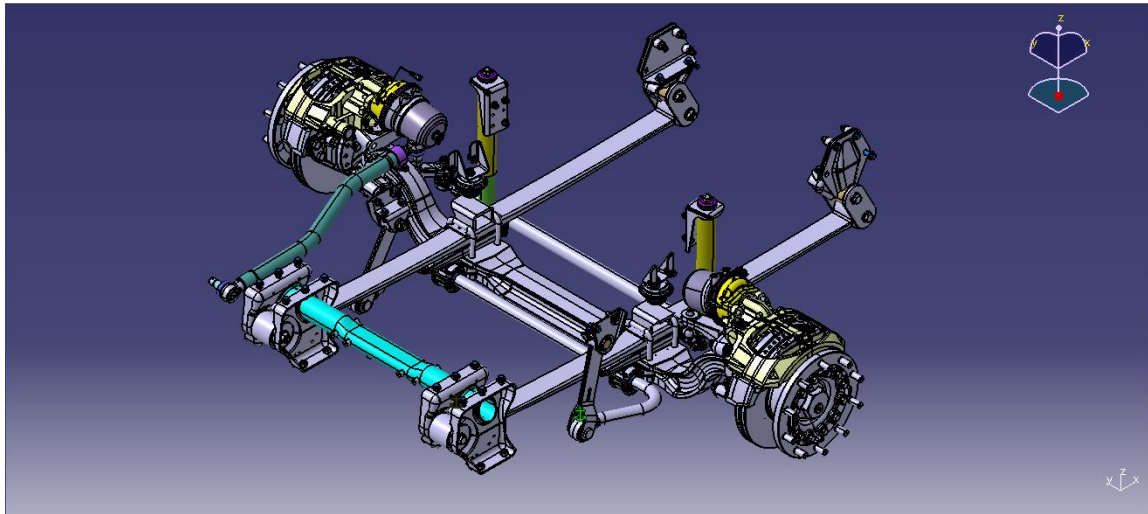


Figure 10- Front suspension CAD model

The principal task of a suspension system is to exchange static and dynamic forces between the vehicle and the road surface. Its major objective is to avoid the detachment of the wheels and reduce the vibrations coming from road imperfections and roughness, improving comfort.

Concerning Adams/Car front suspension model represented in [Figure 11](#), it is subdivided in four different subsystems that are matched together to complete the suspension assembly. These subsystems are:

- front suspension, that contains the rigid axle, the wheel hubs, the uprights, the shock absorbers, the tie-rods and part of steering leverage;
- leaf spring, with the two mono-leaf with variable thickness;
- front antiroll bar;
- steering, that comprises the steering wheel, the steering shafts and the pinion.

The wheels are part of a further subsystem.

The leaf spring and the steering system will not be addressed in this section but in the following subchapters.

The front suspension system, depicted in [Figure 11](#), is of dependent type and is characterized by a rigid axle (12), linking the two front wheels. It is connected to the chassis by means of two leaf springs (10), rigidly clamped to the top surface of the axle, two shock absorbers (11) and the front antiroll bar (9).

Basically, no change to the topology was performed compared to the previous model.

The property files belonging to the shock absorbers, to the bushings and to the axle bump-stops have been updated in order to meet directives coming from engineering office.

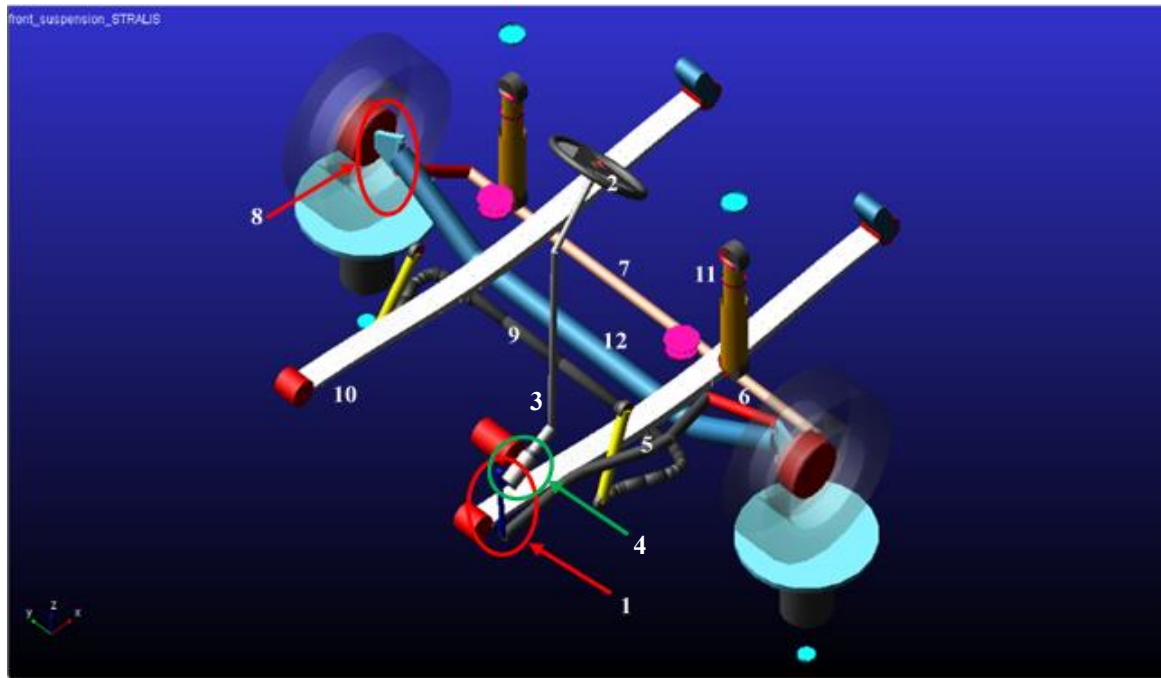


Figure 11- Front suspension multibody model

- | | |
|-------------------------|------------------------|
| 1- Pitman arm | 7- Transversal tie rod |
| 2- Steering wheel | 8- Right upright |
| 3- Steering shafts | 9- Front antiroll bar |
| 4- Pinion | 10- Leaf springs |
| 5- Longitudinal tie rod | 11- Shock absorbers |
| 6- Left upright | 12- Front axle |

The front antiroll bar (9), like the rear one, is modeled as linear beam thanks to the Adams/Car specific function. In this way, it is not completely rigid because it follows the Eulero-Bernoulli formulation. It is shaped like a cylindrical hollow bar, made of steel, curved and linked to the axle by means of two bushings and to the chassis by means of two rigid elements. It is useful to reduce rolling along a curve ensuring a better stability.

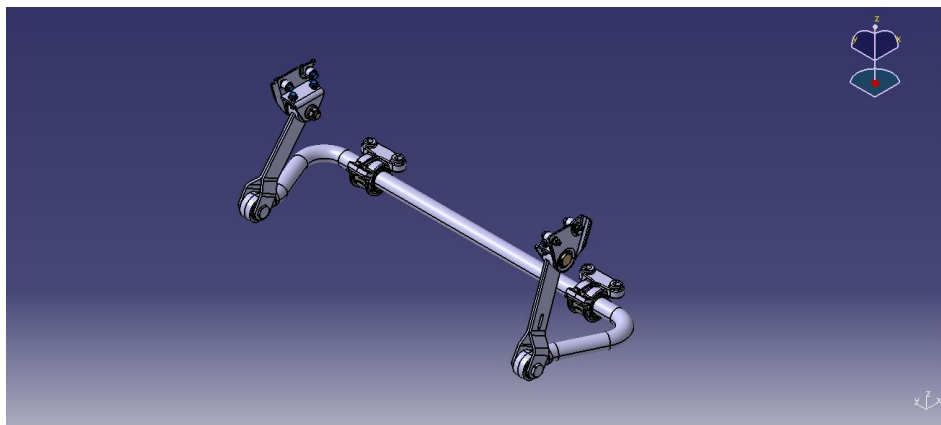


Figure 12- Front antiroll bar CAD model

1.2.1 Leaf springs

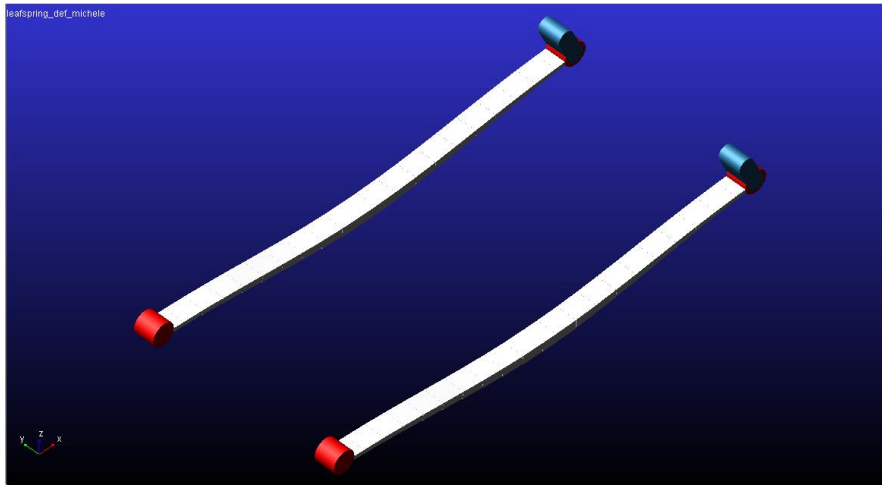


Figure 13- Leaf springs model

The primary component of the front suspension modelling is represented by the leaf springs which constitute an independent subsystem. The original leaf spring has been modified in order to adapt geometrical and mechanical properties to the drawing values, coming from engineering department. Moreover, in the existing leaf model, there is a leaf element that compenetrates the eyes and this could give problem on the behavior of the spring.

To generate the leaf springs, the Adams/Car tool named Leaf Toolkit is used. This tool is specific for the creation of leaf springs. It works dividing the leaves, in this case the only leaf, in a series of elements connected together through Adams beam elements. It uses the discrete beam approach so the resulting model will be flexible, as normal for a spring. The number of elements that create the leaf are defined by the user, but they don't influence the mechanical properties of the system. Their aim is to approximate in an improved way the leaf profile: in fact, the number of these elements has been reduced respect the previous model, in order to decrease the computing power. Leaf Toolkit works both in Adams/View and in Adams/Car and starts with the definition of the geometry of the leaves, the characteristics of the eyes, the shackle features and the material properties. After that, it is possible to perform a static analysis, with which mechanical properties such as stiffness are checked. Then the preload can be set, and the leaf spring assembly created, with the right and the left one. At the end of these passages, it is possible to transfer the created model in Adams/Car and subsequently assembled in a suspension or full-vehicle assembly.

Technical drawings and the CAD model are provided by the engineering office. According to the toolkit sequence, the design of the new leaf spring starts with the creation of the OG profile file (original geometry profile). In this section are necessary the following geometry characteristics of the spring:

- number of leaves;

- eye type (berlin, up, down);
- beam elements length;
- fore/aft spring length;
- fore/aft camber eight;
- clamp length;
- thickness.

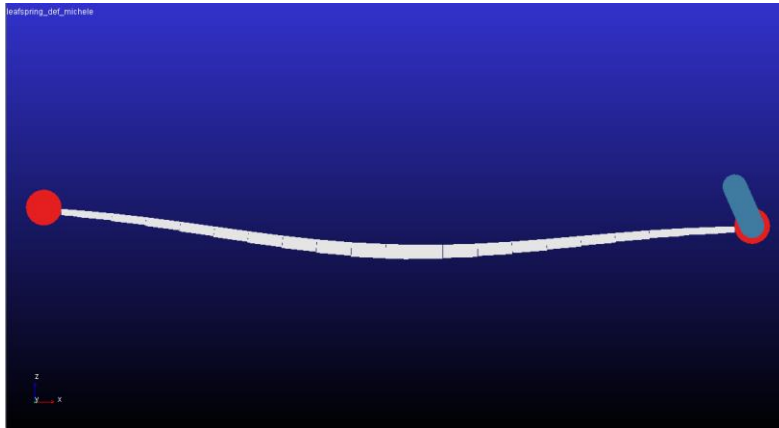


Figure 14- Leaf spring profile

From these information a file with extension .lef is created. The file contains the coordinates and the thickness of each element that composes the leaf spring. The Stralis leaf spring is a mono-leaf with variable thickness. Consequently, this file has to be modified because it assumes the thickness constant. Therefore, it is used an Excel sheet with proper functions to generate the correct leaf profile. After this passage, the OG file is re-imported in the toolkit and the leaf spring creation section can begin. In this section are necessary information about the width of the leaf and of interleaf forces (these last are not needed having only one leaf). In the following section regarding the attachments, information about the shackle and of the axle seat must be inserted. The leaf is connected to the chassis thanks to the front and the rear eye of berlin type. The rear eye is linked to a shackle that is clamped to the truck frame. The last part of the design phase regards the material properties in which the Young modulus, the shear modulus and the damping are adjusted in order to meet the real mechanical characteristics.

After this design phase, analysis can be performed to verify the stiffness of the system; so, a quasi-static vertical test has been performed and the force vs displacement diagram has been plotted. Different changes have been performed before reaching the target. Thanks to this iterative process it has been possible to verify that the stiffness is not influenced by the number of elements per leaf, by the eye's diameter and by shackle dimensions. The width of the leaf has been slightly reduced respect to the drawing value, in order to simulate the tapered edges, that cannot be reproduced with

this tool. The most modified characteristic has been the clamp length that being the thickest portion, directly influence leaf performances. In fact, this dimension has been reduced to about 60% respect the technical specifications, to reach a reasonable stiffness value. Furthermore, to obtain the desired stiffness, the Young module and the shear module have been lowered a little, otherwise it remains too high. Thanks to these modifications the correct mechanical properties have been reached.

[Figure 15](#) illustrates the force vs displacement characteristic of the leaf spring. As the figure shows, the trend is almost linear, according to drawing directives.

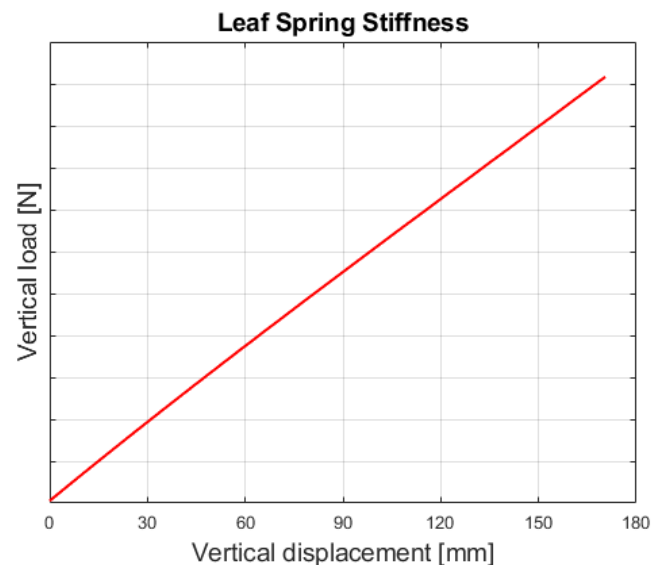


Figure 15- Leaf spring force vs displacement characteristic

The final phase regards the creation of the preloaded model, the creation of the assembly with the two leaf springs and the export of the model to Adams/Car. In this part, also the axle position can be chosen. In Adams/Car template builder environment, the leaf spring model is complete of mount parts, bushing and communicators that must be updated in order to correctly work with the other subsystems. So, the position of the leaves is adjusted, the bushing property file corrected with the ones provided by Iveco and the mount parts and communicators opportunely modified.

1.2.2 Steering

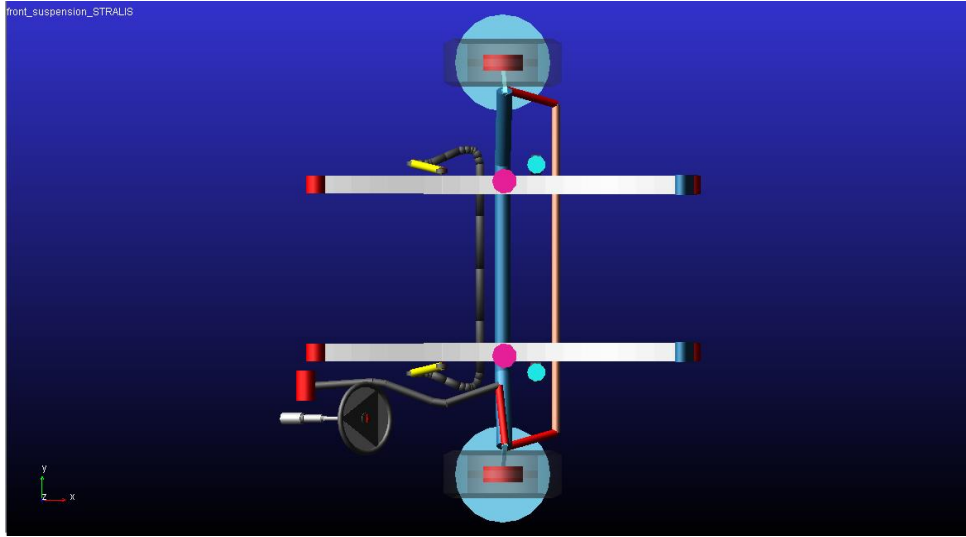


Figure 16- Steering system top view

The steering system belonging to the previous model has been modified in order to meet the target of steering ratio, defined as follows:

$$\text{Steering ratio} = \frac{\text{steering wheel angle}}{(\text{left wheel angle} + \text{right wheel angle})/2}$$

Actually, the steering ratio is variable, but for the type of analysis conducted in this thesis, it can be considered constant. Moreover, the previous model does not follow the Ackermann steering condition: in fact, the outer wheel of the turn rotated more than the inner one, so all the forces were exerted only on the outer wheel. The hardpoints of the steering system model have been modified following the directives coming from the engineering department.

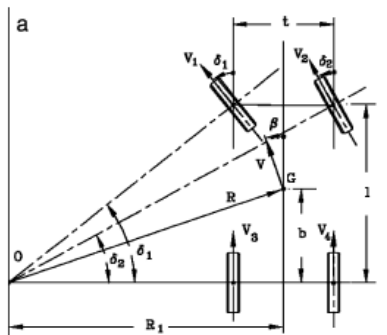


Figure 17- Ackerman steering geometry

Ackerman steering:

$$\cotg(\delta_1) - \cotg(\delta_2) = \frac{t}{l}$$

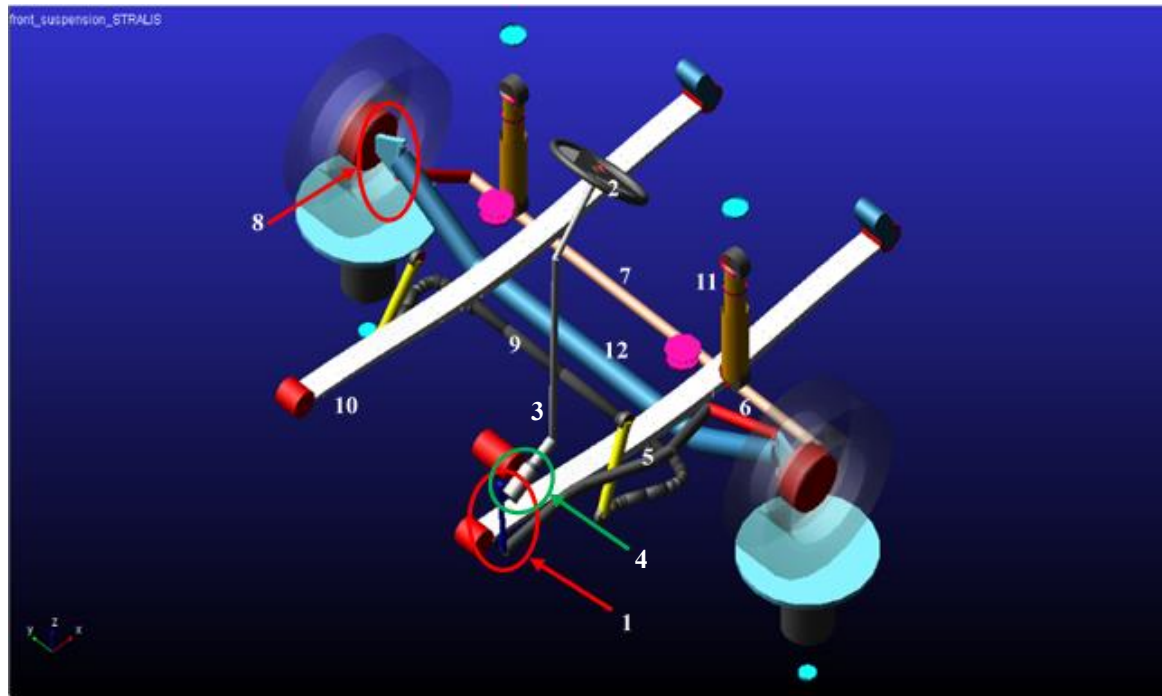


Figure 18- Steering system

- | | |
|-------------------------|------------------------|
| 1- Pitman arm | 7- Transversal tie rod |
| 2- Steering wheel | 8- Right upright |
| 3- Steering shafts | 9- Front antiroll bar |
| 4- Pinion | 10- Leaf springs |
| 5- Longitudinal tie rod | 11- Shock absorbers |
| 6- Left upright | 12- Front axle |

Observing [Figure 18](#), the steering of the wheels can be described: the Pitman arm (1) is guided by the steering wheel (2) through steering shafts (3) and a pinion (4). Steering shafts are linked together by means of convel joints: the upper one is connected to the steering wheel thanks to a bushing which simulates the torque stiffness while the lower one to a reduction gear. The Pitman lever rotates about y -direction making the longitudinal tie rod (5) translating in x -direction, which, in the other extremity, is connected to the left upright (6). This translational motion makes the left upright to rotate about z -direction, producing the rotation of the left wheel. At the same time, the left upright is connected to the transversal tie rod (7), that translates along y . This movement produces the rotation of the right upright (8) making the right wheel steering.

The steering system is modeled in such a way that it works even if the cabin subsystem is not present. In fact, it is connected to the truck cabin and to the frame both. Moreover, the predisposition in case of right-hand drive is present.

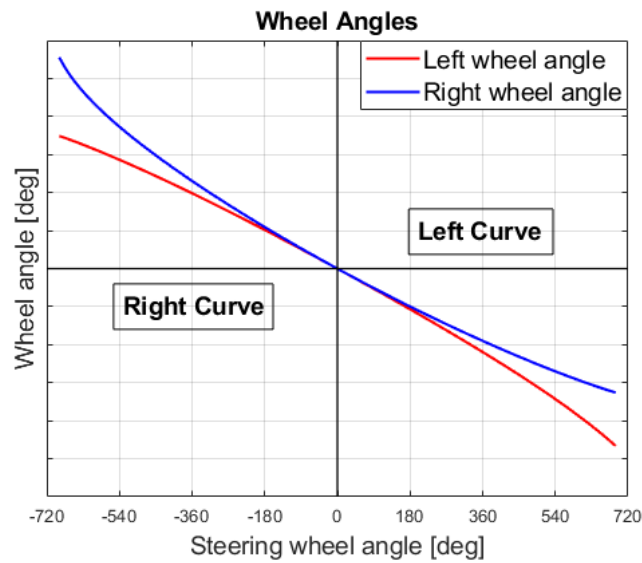


Figure 19- Wheel angles vs steering wheel angle. The red line represents the left wheel angle while the blue one the right wheel angle. Negative steering wheel angle denotes a right turn, positive angle a left turn

[Figure 19](#) shows the left and the right wheel angles in case of a curve. It is possible to verify that in case of a right turn, the right wheel (represented by the blue line) steers more than the left one (represented by the red line). The opposite happens in case of a left curve.

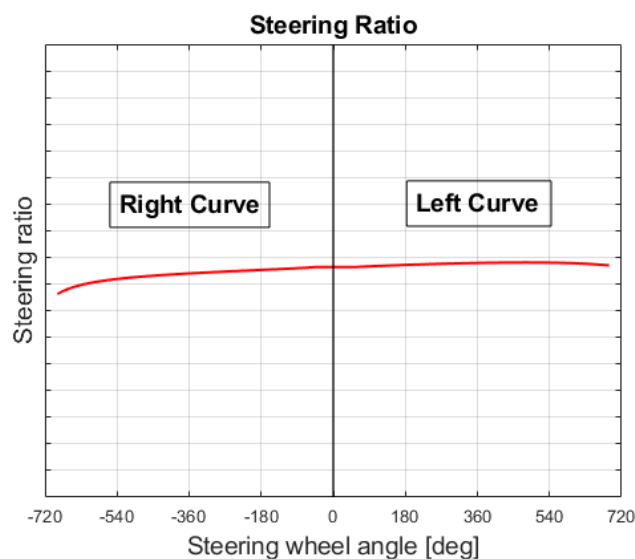


Figure 20- Steering ratio vs steering wheel angle

[Figure 20](#) represents the trend of the steering ratio. It slightly varies between left and right curve due to the steering system geometry, which has been designed according to engineering office directives. Major differences can be noticed at the end of the stroke, but this does not influence the symmetric truck behavior (left and right curve) in handling and comfort simulations, in which the steering wheel angle ranges between $+100^\circ$ and -100° .

1.3 Rear suspension

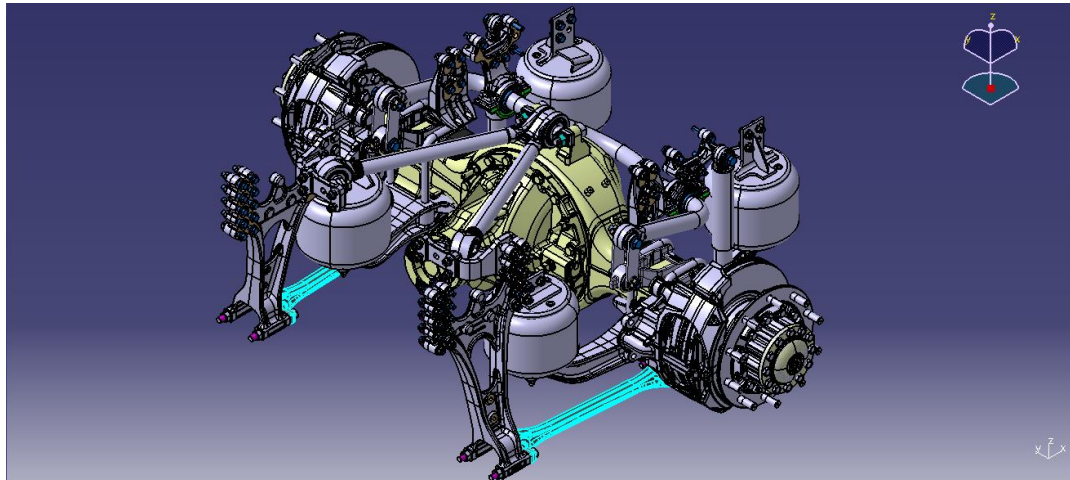


Figure 21- Rear suspension CAD model

The rear suspension system is also of dependent wheels type but obviously it is quite different respect the front one. Looking at [Figure 22](#), it is characterized by a rigid axle (1) that connects the rear twinned wheels. In the CAD model it is possible to notice that it is part of the differential box and contains the drive shafts. At the borders of this axle, two longitudinal elements (2) are present. On these elements a couple of air springs (3) and a shock absorber (4) link the axle to the truck frame.

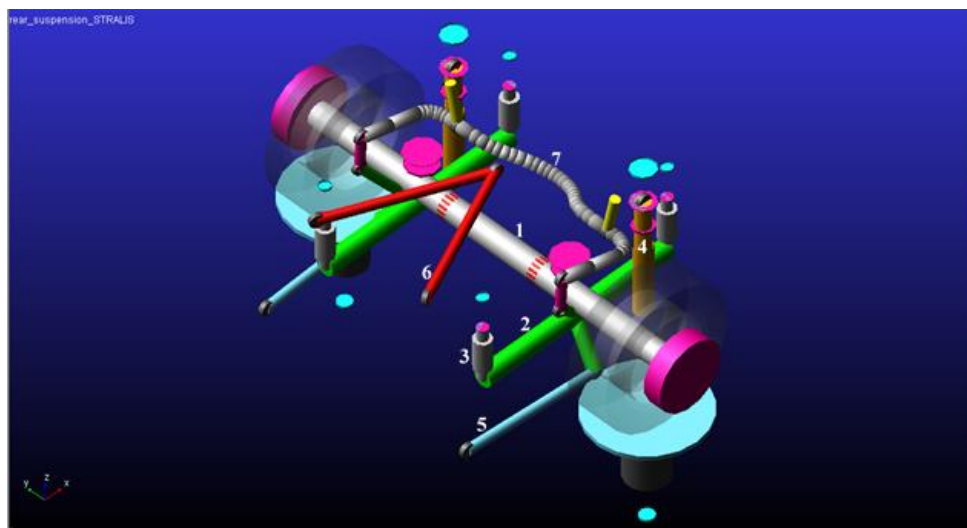


Figure 22- Rear suspension multibody model

- | | |
|--------------------------|----------------------|
| 1- Rear axle | 5- Tie rods |
| 2- Longitudinal elements | 6- V rod |
| 3- Air springs | 7- Rear antiroll bar |
| 4- Shock absorbers | |

Another important component is the V rod (6) that connects the rear axle to the chassis, constraining the motion of the suspension. Instead, two longitudinal tie rods (5) constrain the longitudinal motion.

Finally, the rear antiroll bar (7) completes the rear suspension assembly. Also in this case the bar is part of a different subsystem and it is modeled like a linear beam, with a certain degree of flexibility. The previous model did not work properly because it resulted completely constrained to the frame, so communicators have been modified.

As far as the twinned wheels is concerned, they are fixed together and their position is defined by means of parameter variables included in the rear suspension templates. These variables define the position of each wheel respect the hub, the toe and the camber angle.

The property files that determine the behavior of the air springs and of the shock absorbers have been provided by Iveco engineering office.

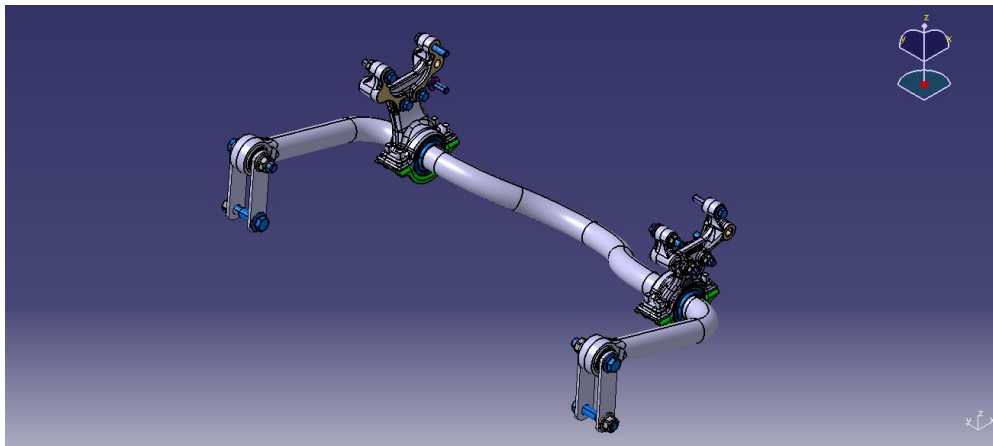


Figure 23- Rear antiroll bar CAD model

1.4 Semi-trailer

The Iveco Stralis configuration under study is the one with tractor and semi-trailer. The semi-trailer is not an Iveco product, but it is manufactured by specialized manufacturer. It is connected to the tractor by means of a link called “fifth wheel”. The existing semi-trailer model is completely rigid and it has been modeled thanks to information coming from the web, because of the lack of technical drawings and measurements directly taken on the product. Its template comprises big box that represents the cargo space, three axles with their suspension system and a red mass that can be moved in order to change the position of the center of mass and simulate the loading condition. In this thesis work the semi-trailer model has been updated with the introduction of the flexible frame and the modeling of a new suspension.

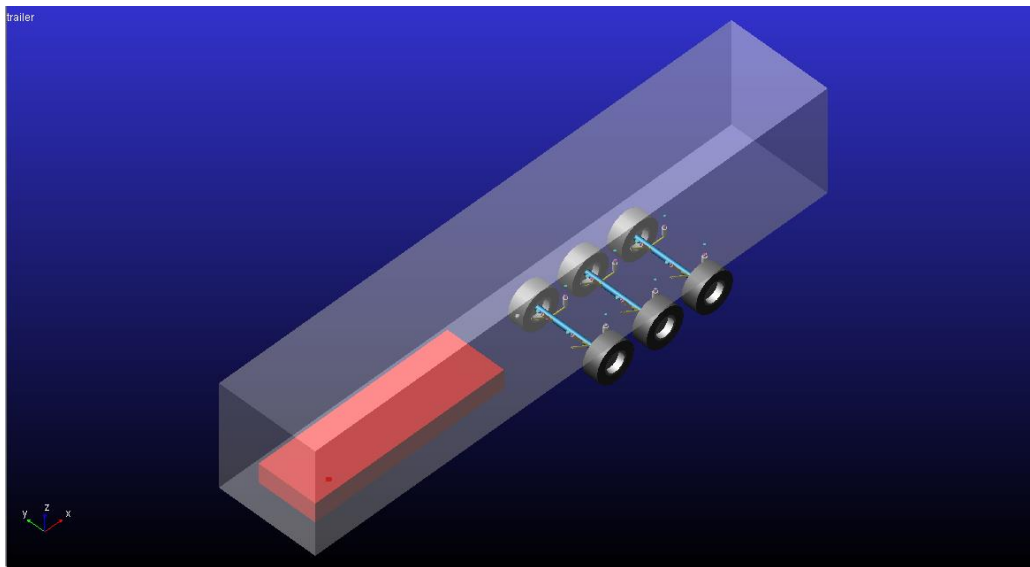


Figure 24- Original semi-trailer multibody model

1.4.1 Flexible semi-trailer frame and load distribution

The new semi-trailer model is characterized by more components. The most significant innovation is the flexible frame which gives its contribution in the dynamic behavior of the entire model. In fact, for larger components is important to describe the correct comportment as far as is concerned stiffness and damping because they influence the whole mechanical assembly.

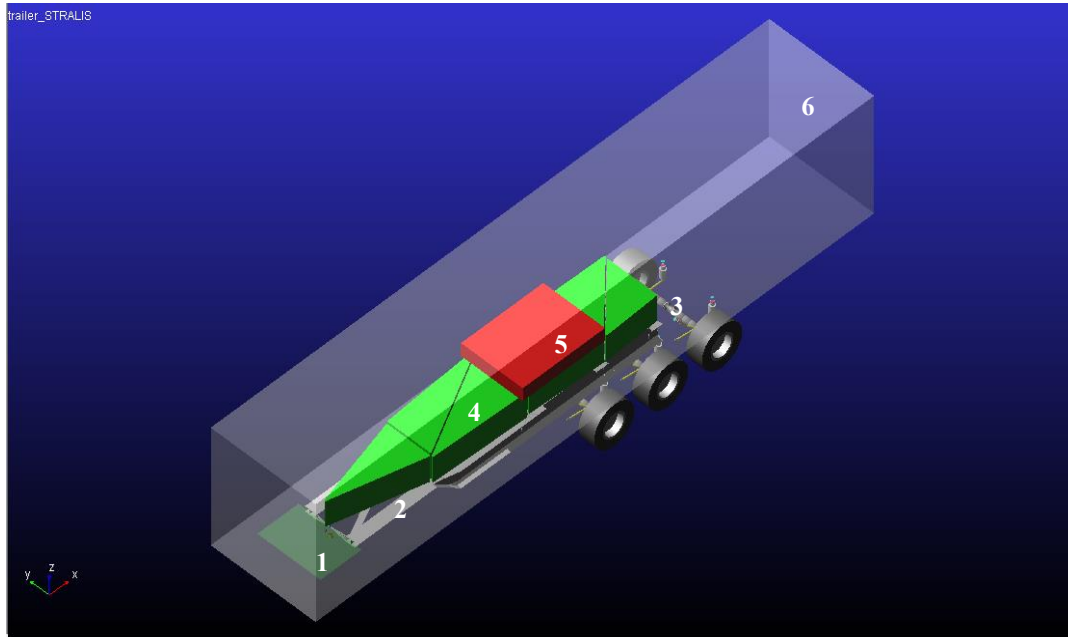


Figure 25- Semi-trailer multibody model

- | | |
|-----------------------|--|
| 1- Front rigid part | 4- Masses connected to the flexible body |
| 2- Flexible frame | 5- Floating mass |
| 3- Semi-trailer axles | 6- Cargo space |

Looking at [Figure 25](#), the semi-trailer template is divided in three main parts: a front one (1), rigid, positioned in front of the fifth wheel; a central one (2), flexible, characterized by the chassis of the semi-trailer; a rear one, rigid, at which the three semi-trailer axles (3) and the floating mass (5) are connected.

As far as central part is concerned, it is characterized by a flexible body. This means that under dynamic loads it does not behave like a rigid element, but it deforms and vibrates. This can happen thanks to the possibility to insert in Adams/Car the file containing the modal analysis of the bodies. This file is produced using other software specific for vibration studies. It has been obtained starting from shell elements exported from the 3D CAD model. This model containing surfaces has been imported in Altair Hypermesh in order to generate a fine mesh and prepare the FEM model for the following passage. In Hypermesh environment interface nodes are created. These nodes do not belong to the mesh ones but are different entities whose displacement is related to several mesh nodes and vice versa. This passage is necessary because forces are never exchanged by one point only but by a surface. Interface points are important because they define the location where other subsystems are connected and they exchange static and dynamic forces with the chassis. After this step the FEM model of the truck body with the interface nodes is imported in MSC Nastran, where the modal analysis is performed. From this analysis an output file with extension .mnf is produced

and imported in Adams/Car environment thanks to the “switch to flexible” command. This file contains the vectors of the mode shapes and the natural frequencies of the system.

All these passages have been performed by the engineering office and the .mnf file has been made available for the aim of this thesis work.

Performing full-vehicle analysis different options are available concerning flexible bodies. In fact, they can be set as:

- Rigid Body: Adams/Car ignores all the modes during the simulation, so the body is totally considered rigid;
- Constant: it means that inertia properties are unaffected by deformation;
- Partial Coupling: some invariants are disabled reducing CPU power and simulation time but with low impact on results;
- Full Coupling: this formulation is used to achieve full accuracy;
- Custom: the user has the possibility to select the invariants to disable.

In order to get reliable results and do not waste time, the simulations are performed with “Partial Coupling” configuration instead of “Full Coupling” and a simplified body model is used.

In the Iveco Stralis model, showed in [Figure 26](#), the flexible bodies present are the tractor cabin (1), the tractor chassis (2) and the semi-trailer frame (3). They are switched to “Rigid body” option if they are not the subject of the simulation.

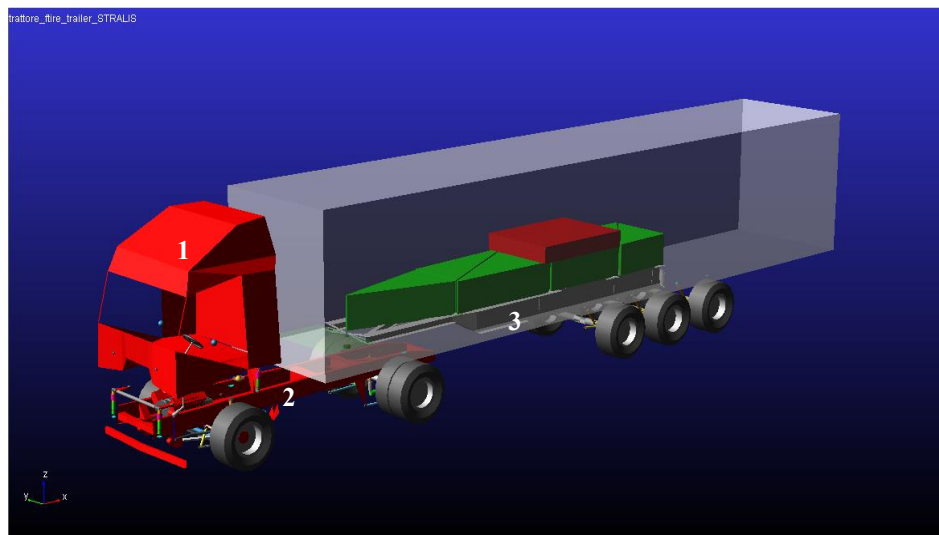


Figure 26- Iveco Stralis multibody model

*1- Tractor cabin
2- Tractor chassis*

3- Semi-trailer frame

A new load distribution has been introduced. Several masses directly connected to the semi-trailer chassis have been created in order to distribute the load on all the frame. Each mass has a triangular

shape and it is constrained to the frame in three points by means of three bushings, opportunely modified. A total of seven masses have been created and they exchange forces directly with the nodes of the semi-trailer chassis. In this way they give their contribution on the frame behavior. Another mass is created in order to adjust the total load of the trailer and change the position of the center of mass. It is connected to the rear part of the trailer and its load is discharged on the three axles of the semi-trailer.

1.4.2 Semi-trailer suspension

A new semi-trailer suspension has been generated. Previous suspension characteristics were collected on the web because not available in the Company, being the semi-trailer not an Iveco product. The new suspension has been designed in base of experimental measures coming from the semi-trailer used during on-road tests.

It consists of an axle hinged into two longitudinal arms connected to the semi-trailer frame by a couple of shock absorbers and air springs.

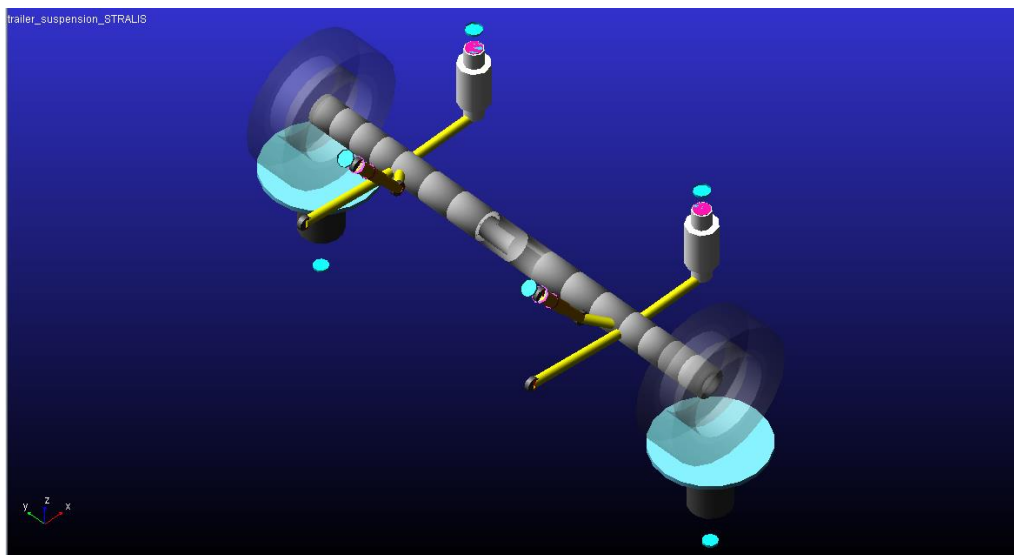


Figure 27- Semi-trailer suspension multibody model

All the positions of hardpoints and of the elements have been updated following the directives coming from the engineering office. The mass and the inertia properties are not available, so they have been computed by Adams/Car thanks to the geometry and selecting the proper material. The axle that connects the right and the left wheel is created using the function “Non-Linear Beam” in order to give a certain degree of flexibility to the system.

1.5 Mass distribution

Mass distribution has been the last task of the first part of thesis work. In this part masses have been modified in order to meet real on-road test conditions. To this purpose four ballast have been created on the tractor flexible chassis, in correspondence of the interface nodes between the shock absorbers and the frame. In this way it is possible to obtain a correct weight distribution between left and right wheels and front and rear axles.

In the tractor model without ballasts there is a significant weight unbalance between left and right side of the truck, especially concerning the rear axle. For this reason, the ballast weights have been set as indicated in [Table 1](#):

| Ballast weights [kg] | |
|----------------------|-----|
| Front axle right: | 0.1 |
| Front axle left: | 94 |
| Rear axle right: | 0.1 |
| Rear axle left: | 845 |

Table 1- Ballast weights

On-road test loading conditions have been two: unloaded and loaded condition. The unloaded condition is characterized by the tractor only while the loaded one by the tractor and the semi-trailer. The loadings characterizing the truck during on-road tests are presented in [Table 2](#).

| Unloaded condition [kg] | |
|-------------------------|-------|
| Front axle: | 4'750 |
| Rear axle: | 2'800 |
| Total weight: | 7'550 |

| Loaded condition [kg] | |
|-----------------------|--------|
| Front axle: | 6'800 |
| Rear axle: | 11'200 |
| Semi-trailer weight: | 22'000 |
| Total weight | 29'550 |

Table 2- On-road loading condition

The loadings that has been possible to reach in the multibody model are shown in [Table 3](#).

| Unloaded weights [kg] | |
|-----------------------|-------|
| Front axle: | 4'745 |
| Rear axle: | 2'805 |
| Total weight: | 7'550 |

| Loaded weights [kg] | |
|----------------------|--------|
| Front axle: | 6'471 |
| Rear axle: | 11'163 |
| Semi-trailer weight: | 22'000 |
| Total weight | 29'550 |

Table 3- Multibody model loading conditions

The ballasts remain unchanged between the loaded and the unloaded case.

In the multibody model, it has not been possible to reach the perfect load distribution concerning the loaded case, especially regarding the front axle, because increasing the load on the front part of the semi-trailer (that discharges only on the fifth wheel and not on the semi-trailer axles), the simulation goes in error. After a consultation with the engineering office, it has been concluded that the problem could be in the flexible models that reach big deformations. In fact, setting them “Rigid”, the error disappears.

Chapter 2. Handling simulations

In this section handling simulations are presented. Before proceeding with tests that are object of this study, it is important to know if the vehicle behaves correctly performing standard lateral dynamics maneuvers. Three kind of test are performed:

- ramp steer;
- sweep steer;
- step steer.

These maneuvers are normed by ISO standards for passenger vehicles. In simulations of the Stralis multibody model are used the standards adopted by Iveco for commercial vehicles. They follow the same procedures of ISO tests, but they are adapted to heavy-duty vehicles limits.

Handling maneuvers have been performed with the two vehicle configurations used for the comfort analysis in Markbronn proving ground: the unloaded (tractor only) and the loaded (tractor semi-trailer and load) conditions. The test settings are maintained the same for the two load cases.

The two configurations are characterized by the following flexible bodies: tractor cabin, tractor chassis and the semi-trailer body.

As far as is concerned Adams/Solver setting, the integrator GSTIFF is used, with formulation I3 and H_{\max} equal to $5.0 \cdot 10^{-3}$ seconds. GSTIFF I3 integrator is the Adams/Car default one and is considered to be very robust and efficient in terms of results and simulation time. The H_{\max} sets the maximum time step that the integrator is allowed to take in order to not lose very short events.

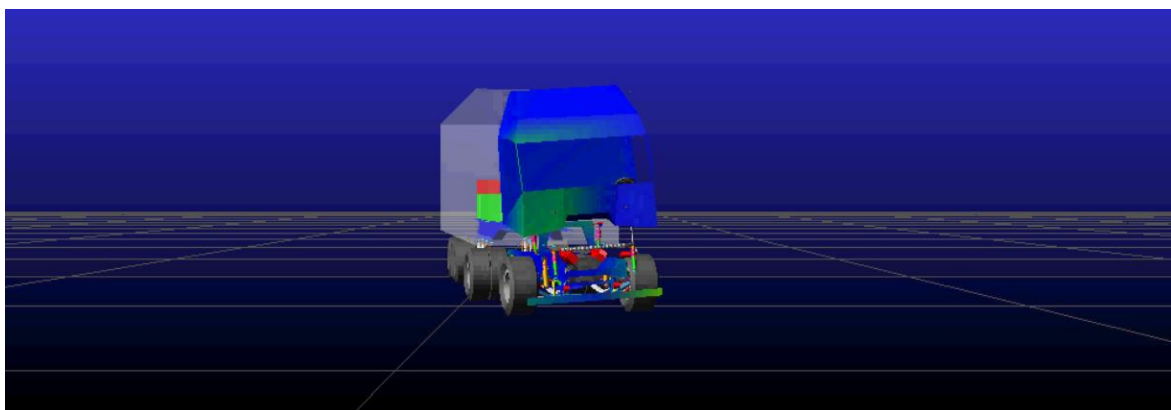


Figure 28- Full vehicle performing the step steer maneuver

2.1 Performed maneuvers

2.1.1 Ramp steer

This type of test, that refers to the ISO 4138:2004 norm, is performed at 60 km/h and applying a steering input that constantly increase in time, with a rate of 10 deg/s. In this test, as the ISO norm suggests, it has been chosen to maintain the throttle constant although the speed decrease during the steering event. The maneuver ends when the test limit condition is achieved. In this case it has been decided to stop the test when the vehicle loses adherence.

In [Table 4](#) the principal settings of the driver control file are showed.

| Ramp steer | |
|--------------------|--------------|
| Static set-up | Straight |
| Speed | 60 [km/h] |
| Ramp starting time | 5 [s] |
| Steering ramp | 10 [deg/s] |
| End condition | $t > 25$ [s] |

Table 4- Ramp steer

2.1.1 Sweep steer

This test refers to the ISO 7401:2003 norm. It is performed at 60 km/h and it consists in a continuous inusoidal steering input. Even in this case the throttle is maintained constant despite the speed decrease during the maneuver. The steering amplitude is fixed and corresponds to the steering angle that, in a steady-state lateral test, provides a certain lateral acceleration. In this case it has been chosen the steering angle that at 60 km/h provides a lateral acceleration of 0,4 g: 50 degree. The steering frequency is continuously increased, starting from 0.2 Hz up to 2 Hz.

In [Table 5](#) the principal settings of the driver control file are showed.

| Sweep steer | | | |
|---------------------|-----------|-------------------|--------------|
| Static set-up | Straight | Initial frequency | 0.2 [Hz] |
| Speed | 60 [km/h] | Final frequency | 2 [Hz] |
| Sweep starting time | 5 [s] | Frequency rate | 0.05 [Hz/s] |
| Steering angle | 50 [deg] | End condition | $t > 42$ [s] |

Table 5- Sweep steer

2.1.3 Step steer

As the sweep steer, also this test refers to the ISO 7401:2003 norm. It is performed at 70 km/h maintaining the throttle constant during the maneuver. It is characterized by a steering input suddenly applied and then maintained in order to evaluate the transient behavior of the vehicle. The steering input must be very fast: 0.15 s and its amplitude fixed and corresponding to the steering angle that, in a steady-state lateral test, provides a certain lateral acceleration. In this case, it has been chosen 50 degree.

It is important to verify that the vehicle does not rollover performing this test.

In [Table 6](#) the principal settings of the driver control file are showed.

| Step steer | |
|--------------------|--------------|
| Static set-up | Straight |
| Speed | 70 [km/h] |
| Step starting time | 5 [s] |
| Steering angle | 50 [deg] |
| Step duration | 0.15 [s] |
| End condition | $t > 12$ [s] |

Table 6- Step steer

2.2 Results

In the following pages the principal results concerning lateral dynamics are presented.

The unloaded condition concerns the tractor only with the driver and a passenger, each one weighing 75 kg. Pacejka tire models are used for these manouvers.

The loaded condition concerns the tractor with the driver and a passenger, each one weighing 75 kg, the semi-trailer and the load, for a total load of 29'550 kg. Pacejka tire models are used for the tractor and the semi-trailer.

The Adams/Car default road friction coefficient is maintained.

In [Table 7](#) and [Table 8](#) are reported the principal characteristics of models used for handling simulations, the load distribution and the kind of simulations performed.

| | | |
|--------------------------|---------------------------|----------|
| Model | Tractor | |
| | Tractor chassis: | Flex |
| | Semi-trailer body: | - |
| | Tires: | Pacejka |
| Loading condition | Unloaded | |
| | Front axle: | 4'745 kg |
| | Rear axle | 2'805 kg |
| | Semi-trailer: | - |
| | Total: | 7'550 kg |
| Simulations | Ramp steer | |
| | Sweep steer | |
| | Step steer | |

Table 7- Model characteristics

| | | |
|--------------------------|---------------------------------|-----------|
| Model | Tractor and semi trailer | |
| | Tractor chassis: | Flex |
| | Semi-trailer body: | Flex |
| | Tires: | Pacejka |
| Loading condition | Loaded | |
| | Front axle: | 6'471 kg |
| | Rear axle | 11'163 kg |
| | Semi-trailer: | 22'000 kg |
| | Total: | 29'550 kg |
| Simulations | Ramp steer | |
| | Sweep steer | |
| | Step steer | |

Table 8- Model characteristics

Ramp steer

The principal results are plotted in function of the lateral acceleration. Ramp steer simulation is performed at 60 km/h with a rate of increase of the steering angle of 10 deg/s, for both the load conditions. The lateral acceleration has been changed in sign in order to have clearer graphs.

In [Figure 29](#) is possible to notice that the lateral acceleration increases equally and linearly for both the configurations until 0.4 g. Above 0.4 g, the loaded condition reaches higher steering wheel angle for equal lateral acceleration, but it shows non-linearity starting from 0.45 g. In the loaded configuration, the limit condition is reached before than the one with the tractor only. The understeering gradient K_{us} can be considered equal for the two configurations and being bigger than zero it means that the vehicle has an understeering behavior in the linear part of the graph.

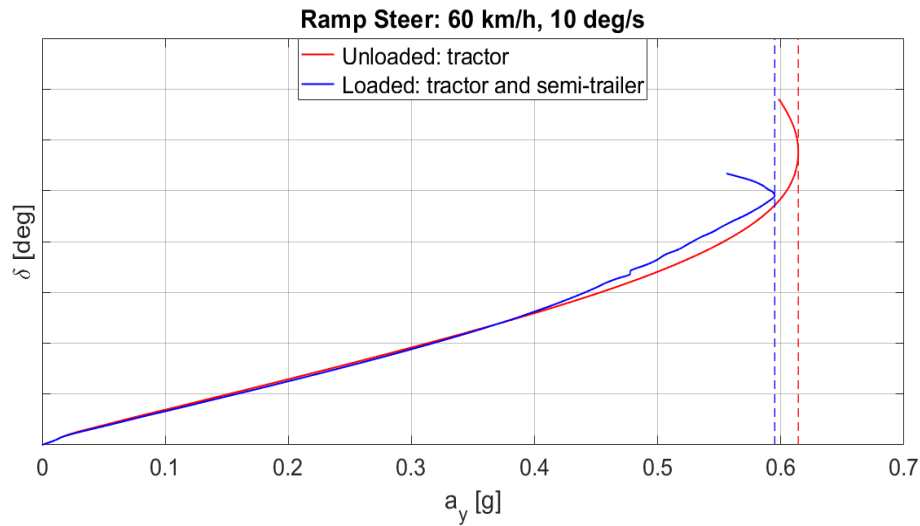


Figure 29- Ramp steer: steering wheel angle vs lateral acceleration

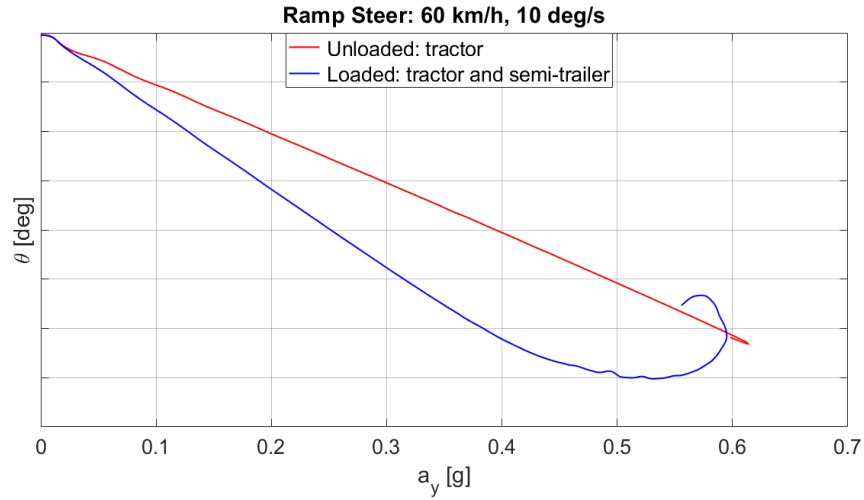


Figure 30- Ramp steer: roll angle vs lateral acceleration

In [Figure 30](#) are showed the roll angles of the tractor flexible chassis, of the two configurations, in function of the lateral acceleration. It is possible to see that in the loaded condition, the roll angle increases rapidly respect the unloaded one, because of the semi-trailer influence. Over 0.4 g the loaded condition shows non-linearity probably due to the non-linear behavior of some components. It is evident that the vehicle does not rollover also in the loaded configuration, because of the relatively low center of mass of the whole system.

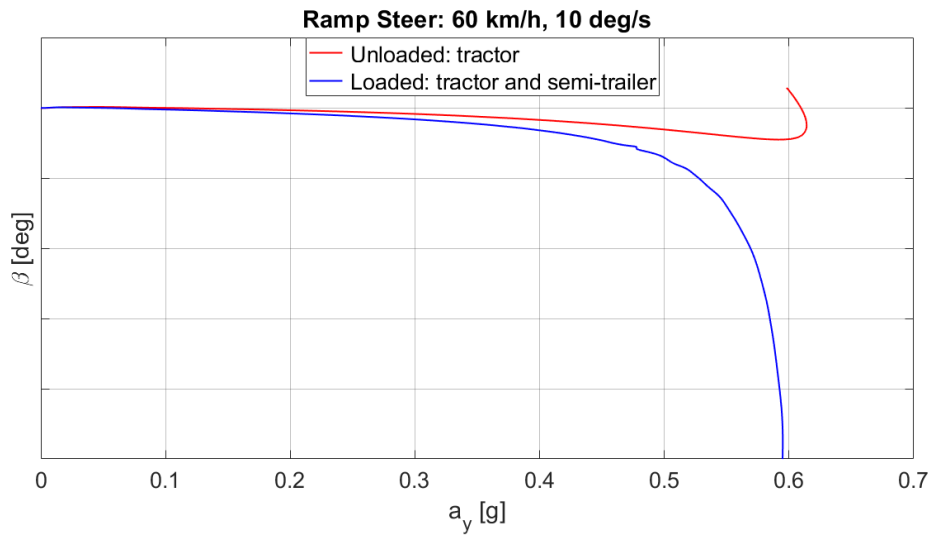


Figure 31- Ramp steer: sideslip angle vs lateral acceleration

[Figure 31](#) shows the behavior of the sideslip angle increasing the lateral acceleration. Looking in the graph, it is clear that the sideslip of the loaded condition is higher and starts to increase rapidly over 0.45 g respect the unloaded one. The unloaded condition sideslip angle shows an abnormal

behavior changing direction. Generally, the common behavior of the sideslip angle of passenger vehicles is more similar to the blue one. The sideslip gradient K_β cannot be computed because of the non-linearity of the obtained results. Generally, in passenger cars the first part of this curve is linear and the sideslip gradient can be calculated as follows:

Sideslip gradient:

$$K_\beta = \frac{\beta}{a_y}$$

The yaw rate increase linearly increasing the steering wheel angle and consequently the lateral acceleration, as could be seen in [Figure 32](#). Its behavior can be considered equal for both the configurations until 0.5 g, then in the loaded condition it increases rapidly.

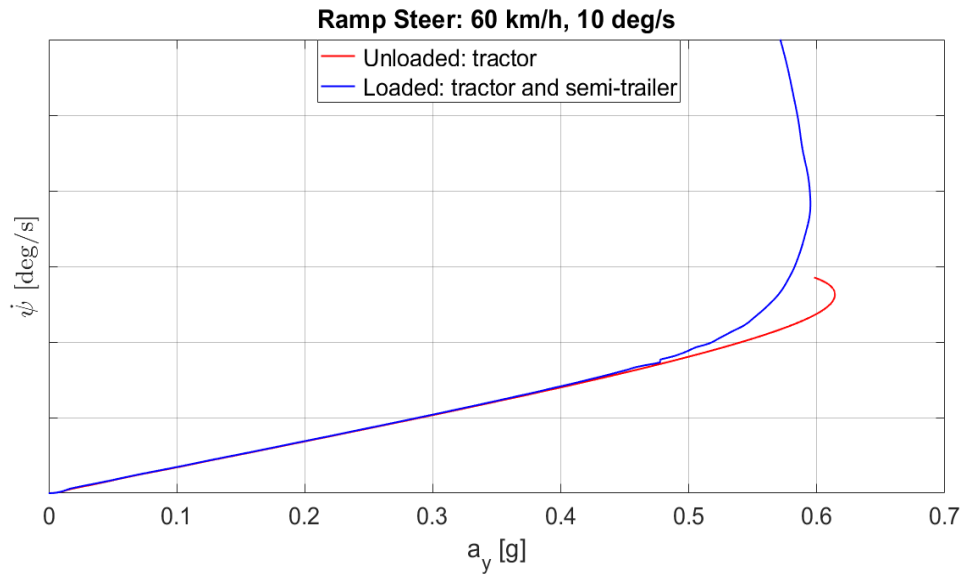
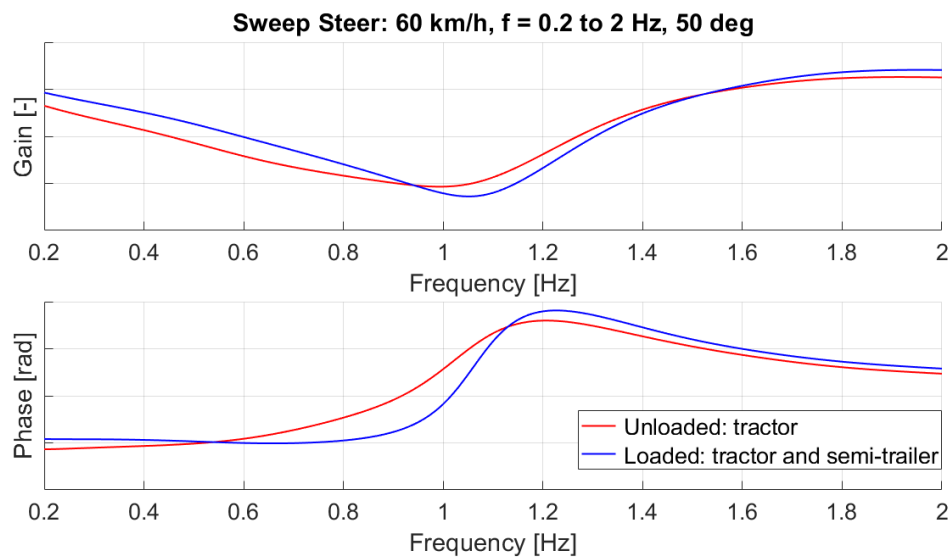


Figure 32- Ramp steer: yaw rate vs lateral acceleration

Sweep steer

The principal results are plotted using Bode diagrams in order to be more significant. Sweep steer simulation is conducted at 60 km/h, with a sinusoidal steering input of amplitude 50 deg and a frequency that goes from 0.2 Hz to 2 Hz, for both the configurations. In the following diagrams are plotted the gain, which influences the amplitude of the response, and the phase, which impacts the delay time of the response. It is important during the developing of the vehicle dynamics to maximize the gain and minimize the delay times. In this way the vehicle will be reactive in the response to the driver inputs.

[Figure 33](#) shows the lateral acceleration response to the input steering wheel angle, in frequency domain.



*Figure 33- Sweep steer:
input: steering wheel angle
output: lateral acceleration*

[Figure 34](#) shows the sideslip angle response to the input steering wheel angle, in frequency domain.

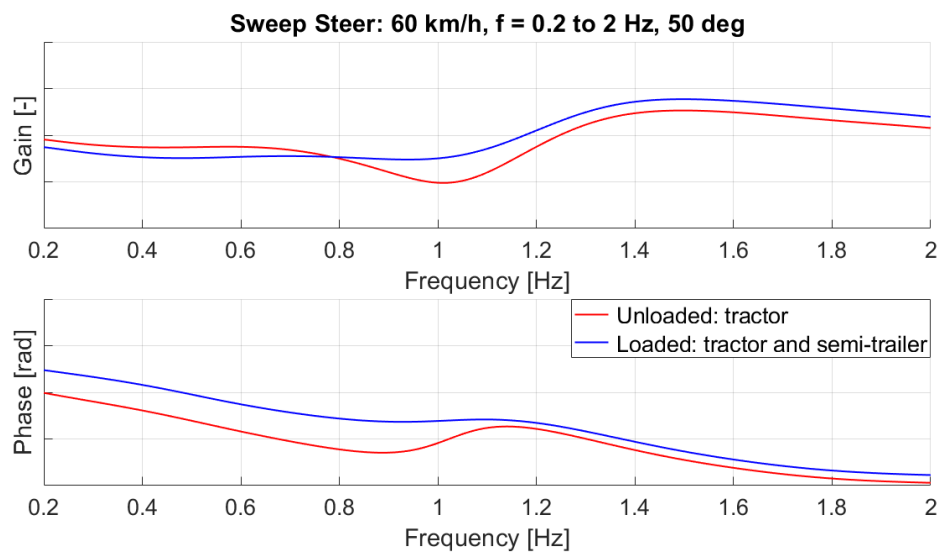


*Figure 34- Sweep steer:
input: steering wheel angle
output: sideslip angle*

[Figure 35](#) shows the yaw rate response to the input steering wheel angle, in frequency domain.

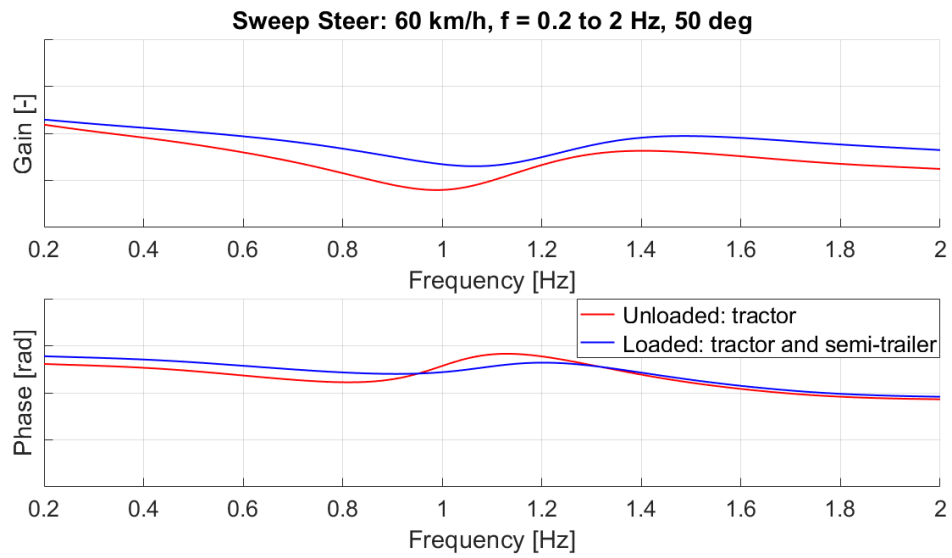


*Figure 35- Sweep steer:
input: steering wheel angle
output: yaw rate*

[Figure 36](#) shows the roll angle response to the input lateral acceleration, in frequency domain.

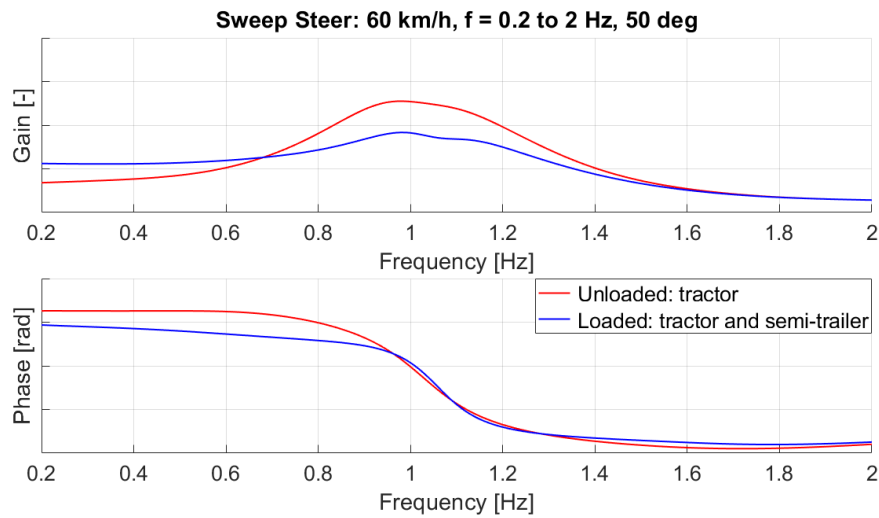


*Figure 36- Sweep steer:
input: lateral acceleration
output: roll angle*

Step steer

The principal results are plotted in function of time. Step steer simulation is performed at 70 km/h with a step steering angle of 50 deg reached in 0.15 s, for both the loading conditions. The lateral acceleration, the roll angle and the sideslip angle have been changed in sign in order to be clearer.

In [Figure 37](#) is possible to notice the lateral acceleration behavior of the two configurations. The oscillation at high frequency between 5 and 5.5 seconds is due to the engine movement immediately after the steering input application. In fact, it is connected to the chassis by means of bushings. The trend of the curve at low frequency between 5.5 and 8 seconds is due to the cabin shaking, because it is provided of an own suspension system. It can be seen that the lateral acceleration, after reaching the maximum value, it starts to decrease because of the speed reduction during the maneuver.

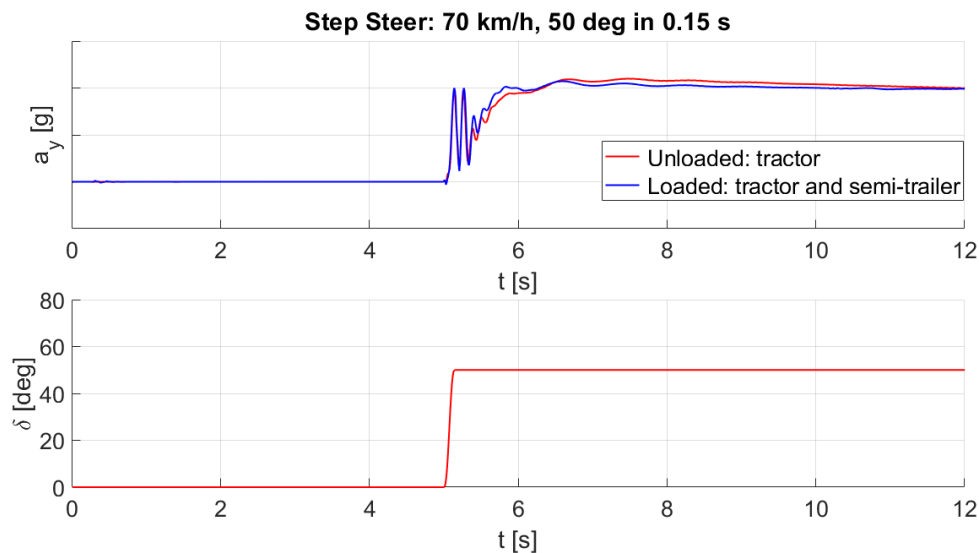


Figure 37- Step steer: lateral acceleration vs time

In [Figure 38](#) is possible to notice the roll angle behavior of the two configurations. The loaded configuration achieves higher roll angle values. The trend of the curve at low frequency between 5.5 and 8 seconds is due to the cabin shaking, as said before. In this case also, after reaching the maximum value, the trend of the curves is decreasing due to the reduction in speed during the maneuver. It is clear that in this test, that can be considered similar to an emergency maneuver, the rollover it is not reached for both the configurations.

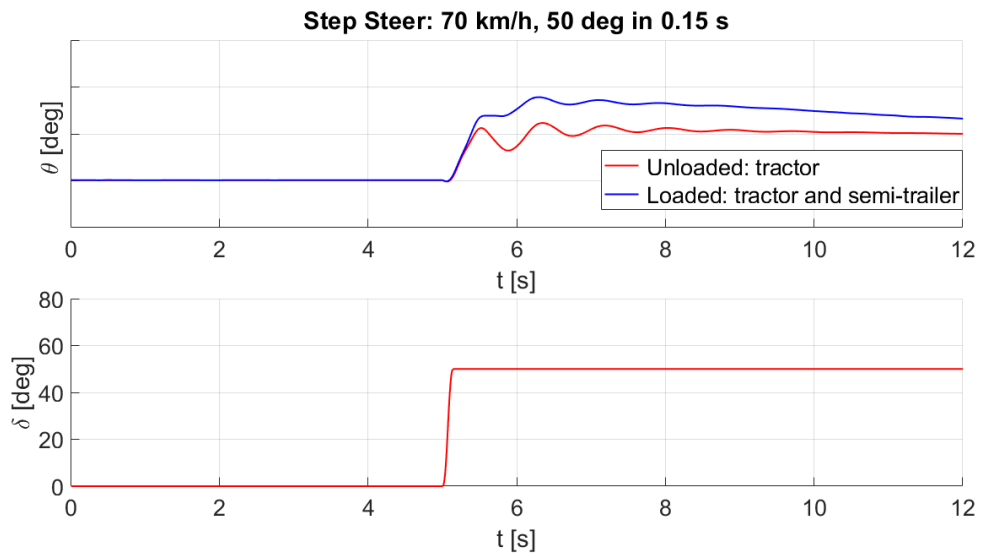


Figure 38- Step steer: roll angle vs time

[Figure 39](#) shows the sideslip angle behavior of the two configurations.

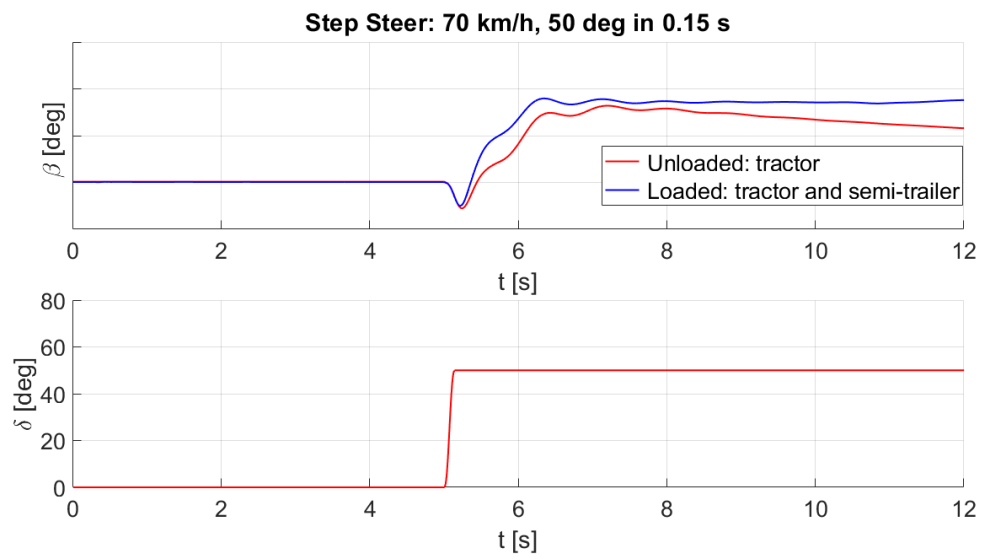


Figure 39- Step steer: sideslip angle vs time

[Figure 40](#) shows the yaw rate behavior of the two configurations.

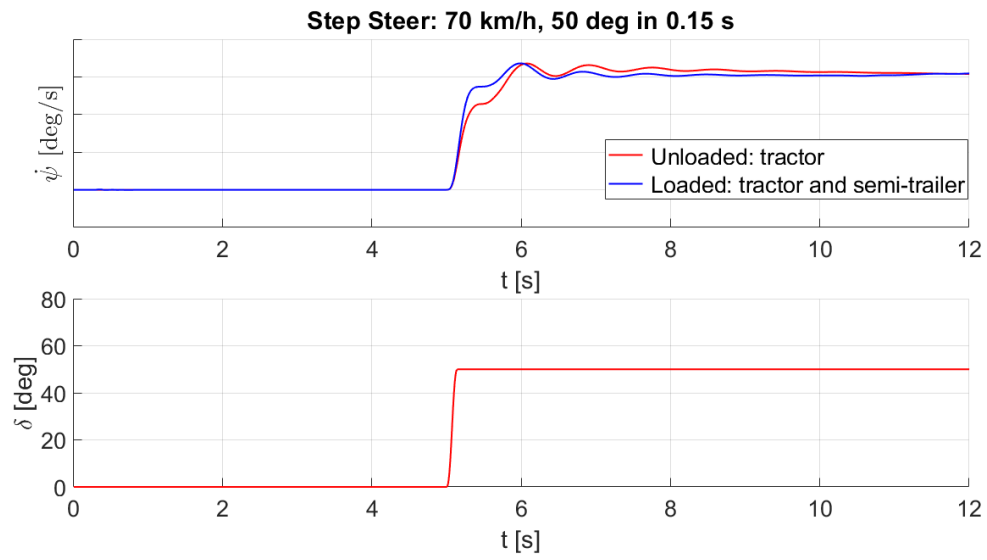


Figure 40- Step steer: yaw rate vs time

Chapter 3. Model preparation for simulations

After the development the subsystems of the Iveco Stralis truck model and the handling simulations, the focus will be on the preparation of the model for comfort analysis in order to obtain consistent results for the subsequent correlation with experimental data.

This chapter addresses the implementation of FTire model in substitution of the previous Pacejka tire model, with the consequent increase in the accuracy of the Adams/Car multibody model. A little overview on FTire model and Iveco Stralis tires characterization is given.

Following, an overview of .crg (Curved Regular Grid) track file is given with the deepening on the Belgian block path used in this comfort study. An accurate 3D reproduction of the track situated in Markbronn proving ground is available for simulations.

Finally, the on-track tests performed, the accelerometers positioning, the creation of the driver control files for numerical simulations and the setting of the Adams/Solver and are discussed.

Thanks to these precautions it is possible to faithfully reproduce the real test conditions and start the simulations, which will be discussed in the following chapter.

3.1 FTire Model

The Pacejka model PAC2002 is the industrial standard used by manufactures to simulate a tire and to conduct the primary dynamics studies. This model has been introduced by Hans B. Pacejka and it is based on the so called “Magic Formula”, because it has no physical meanings. Each tire is characterized by about twenty coefficients obtained performing experimental tests. Although it is an excellent mean, it shows some critical issues. For example, it does not work properly for very low speeds or for frequencies higher than 15 Hz. PAC2002 is implemented in the standard version of Adams/Car software.

An important improve has been done with the introduction of FTire model. The acronym FTire means “Flexible Structure Tire Model” and it denotes the most complete tool for tire dynamics simulation present nowadays in the vehicle industry. It is a 3D nonlinear model that refers entirely to analytical means in order to reproduce tire behavior using classical mechanical and thermodynamic laws. FTire can be used for vehicle comfort simulations, prediction of road loads due to irregularities and for handling studies. It can be compared to a FEM model of the wheel and the contact between the tire and the road is not characterized by one point only but by a local contact patch pressure distribution. For these reasons the results coming from FTire model are very consistent and show very good correlation with experimental measures. Due to the complexity of

this model approach, simulations take significantly longer time respect the same simulation performed by PAC2002 tire model. FTire model has been developed by Cosin Scientific Software and it can be used in Adams/Car thanks to a specific Cosin's tool.

During simulations, FTire model is able to take into account most of the aspects that characterize the tire on-road behavior, such as:

- The structural dynamics and belt dynamics,
- Frequency range up to 200 Hz due to road surface irregularities,
- The thread wear, mass and stiffness imbalances and radius variation,
- The distribution of the belt temperature,
- The air volume vibration,
- The tire slipping on the rim in case of large torques,
- The flexible rim behavior,
- The sidewall contacts.

FTire model lets the engineer to have a very reliable model that can be used to simulate every condition of a tire during its entire lifecycle. In fact, different variables can be inserted in the model such as user-defined wear, temperature distribution, rim flexibility models, large camber angles and misuse scenarios. It works also with rigid time-invariant and time variant road surfaces and flexible and deformable road surfaces such as mud and sand.

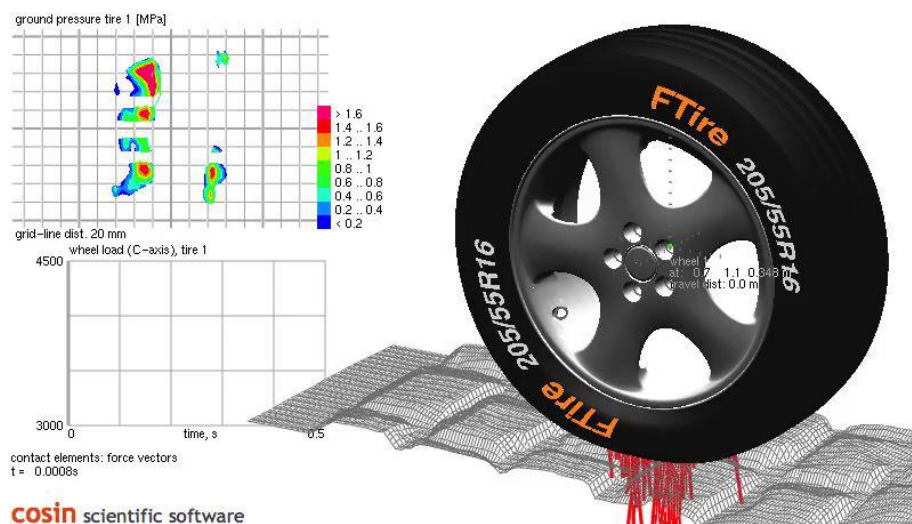


Figure 41- Cosin Scientific Software

3.1.1 FTire modeling

The model behind an FTire is characterized by different physical models:

- Mechanical model
- Thermal model
- Thread wear model
- Air volume vibration model
- Flexible and viscoplastic rim model

Mechanical model

The mechanical model that is part of FTire is characterized by a flexible ring, showed in [Figure 42](#), that represents the tire belt. This ring is subdivided in a finite number of elements which are connected together by means of springs and bending stiffnesses. On each element is present a series of blocks representing the tire tread, containing mechanical properties such as stiffness and damping in every direction (radial, tangential and lateral). Concerning the blocks radial deformation, it depends on the road surface, while the lateral and tangential deflections depend on the tire slipping velocity respect to the ground. Tread blocks are positioned following parallel lines, in this way they can deform and shape the road profile in longitudinal and transversal directions both.

The forces coming from the road surface are transferred to the rim that, being flexible, influences the wheel behavior. These forces are computed integrating all the ones acting on the flexible ring.

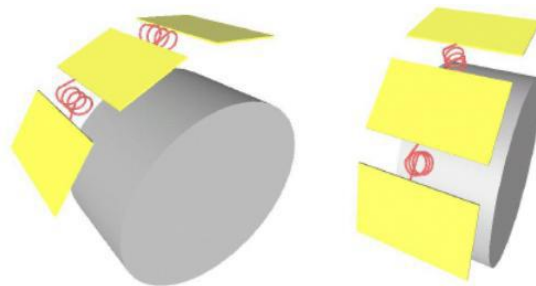


Figure 42- Flexible ring representing the tire belt

Thermal model

This model is particularly important in case of tires in which the friction properties strongly depends on temperature. It is mainly characterized by three submodels. The first one computes the actual inflation pressure taking into account the air mass, the tire temperature, the actual tire interior volume and the inflation pressure of the tire in normal conditions. The second one regards the heat generation, due to the power loss in damping and friction, and the heat transfer model. It takes into account three temperatures: the one of the tire structures (sidewalls, belt, air volume), the one of the

tread without contact patch and the one of the tread involved in the contact patch. The third component considers the rubber temperature as an additional variable to the slipping velocity and the ground pressure.

[Figure 43](#) shows the tire regions considered in the thermal model.

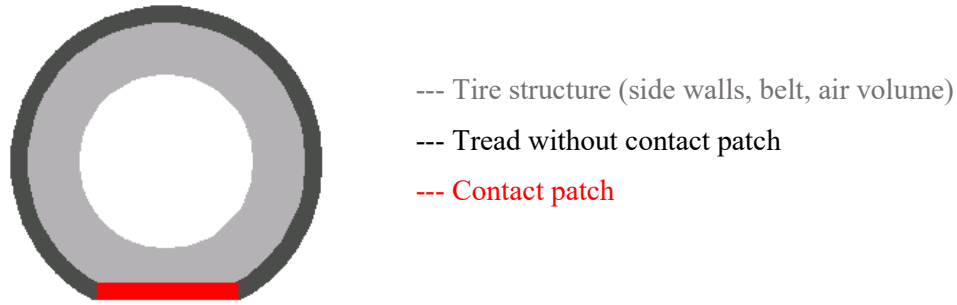


Figure 43- Tire regions in FTire thermal model

Thread wear model

This model is able to compute the wear rate because of the power loss due to the road friction. Power loss can be computed as follow:

$$P_{loss} = F_{friction} * v_{slip}$$

Tread element's temperature T and normal force F_N are available thanks to the thermal and mechanical model. The wear rate $\frac{dh}{dt}$ can be considered as follows:

$$\frac{dh}{dt} = -f(P_{loss}, T, F_N)$$

Tread wear computation is important because it affects: the tire cross section, the tread radial and shear stiffness, the contact patch pressure distribution, the heat capacity and the tire mass. As consequence it affects the overall tire stiffness and so the handling behavior of the vehicle.

Air volume vibration model

This model describes the filling gas behavior due to the deformations of rolling tires. The variation of air pressure, air density and air speed inside the tire could impair the reaction forces on the tire structure and the rim, especially at high frequencies.

Flexible and viscoplastic rim model

The forces coming from the contact patch are transferred to the right and the left rim flanges. In FTire model the rim is no more considered rigid, but it is flexible and can pursue plastic deformation if elastic region is overcome. When a tire is characterized, an internal flexible rim model is present, but there is the possibility to call an external model written by the user if different rims are mounted on the same tire.

3.1.2 Iveco Stralis tires

The tires mounted on the Iveco Stralis used for on-road tests and the ones used for the multibody model are the same and they correspond to:

- Front tires: Continental ContiHybrid HS3 (M+S) 385/55 R22.5 160K 11.8J
- Rear tires: Continental ContiEcoPlus HD3 (M+S) 315/70 R22.5 154L 11.8J



Figure 44- Tire test rig used at ika/fka RWTH Aachen University

These tires have been characterized for Iveco by fka mbH Aachen, Germany, with the support of ika/fka RWTH Aachen University, Germany. Different tire measurements have been performed, such as: tests in static condition, tests in steady state rolling conditions, footprints detection and cleat tests. The tire test bench coordinate system is showed in [Figure 45](#).

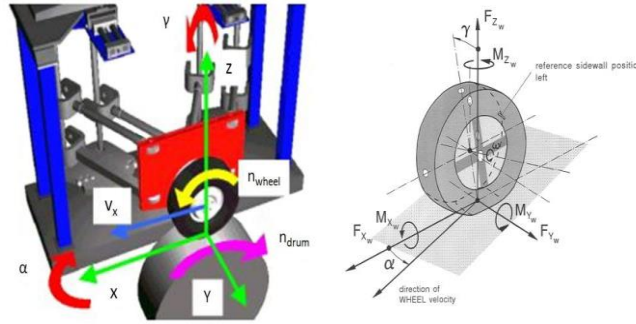


Figure 45- Tire test bench coordinate system

Different tests conditions with variation of vertical loads, inflation pressure and camber angles are necessary to completely characterize the tire.

Tires characterization costs are very high (in the order of tens of thousands of euros) and for a company with many vehicles that can mount hundreds of different types of tires is a very important expense. For these reasons not all the data and measurements will be showed.

Front tires



Figure 46- Front tire tread and rim used for measurements

In the table below are reported the principal measurements concerning front tires.

| Front tires characteristics | | | |
|-----------------------------|-----------------------|-------------------------|-----------|
| Manufacturer | Continental | Nominal diameter | 994.55 mm |
| Name | ContiHybrid HS3 (M+S) | Actual diameter | 959.2 mm |
| Type | Truck | Thread depth | 14 mm |
| Design | F | Tread width | 320 mm |
| Actual width | 385 mm | Tire mass | 71.4 kg |
| Actual aspect ratio | 55% | Rim diameter | 22.5" |
| Load index | 160 | Rim width | 298.45 mm |
| Inflation pressure | 8.50 bar | Rim mass | 43.55 kg |

Table 9- Front tires characteristics

[Figure 47](#) shows a typical footprint obtained after measurements, in the following test condition:

- Load F_z : 17660 N
- Tire inflation pressure: 8.5 bar
- Camber Angle: 0.00°

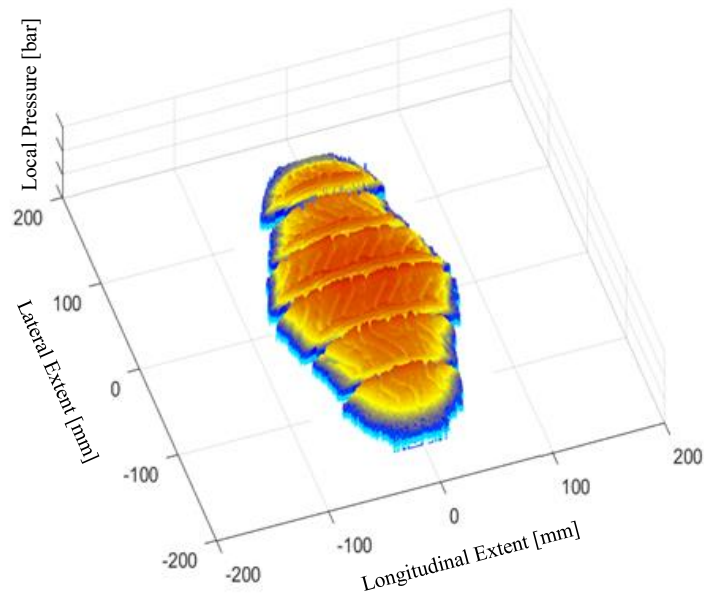


Figure 47- Front tire pressure distribution

Rear tires



Figure 48- Rear tire characterization

In [Table 10](#) are reported the principal measurements concerning rear tires.

| Rear tires characteristics | | | |
|----------------------------|------------------------|-------------------------|------------|
| Manufacturer | Continental | Nominal diameter | 1012.5 mm |
| Name | ContiEcoPlus HD3 (M+S) | Actual diameter | 1007.35 mm |
| Type | Truck | Thread depth | 16.2 mm |
| Design | R | Tread width | 262.9 mm |
| Actual width | 315 mm | Tire mass | 62.05 kg |
| Actual aspect ratio | 70% | Rim diameter | 22.5" |
| Load index | 154 | Rim width | 9" |
| Inflation pressure | 7.50 bar | Rim mass | 37 kg |

Table 10- Rear tires characteristics

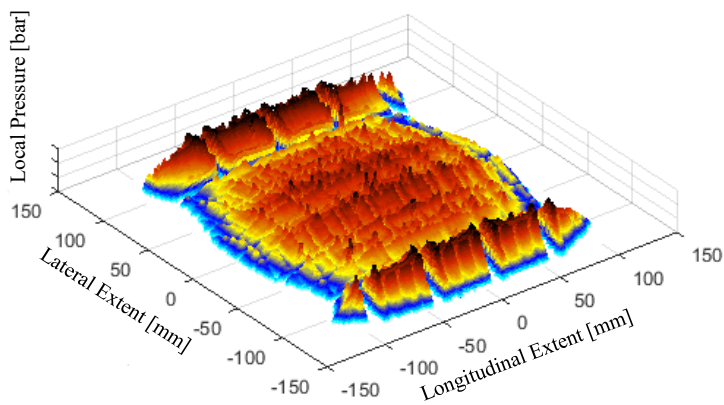


Figure 49- Rear tire footprint

[Figure 49](#) shows the rear tire footprint obtained after measurements.

3.2 CRG Track Model

With a complex and accurate tire model like FTire it is also important to have good road surface representations in order to perform very complete vehicle dynamics simulations, such as vehicle handling, NVH, ride comfort and durability. To have increasingly precise and reliable models that can represent every on-road condition is become crucial nowadays for vehicle OEMs, especially for the development of autonomous vehicles and their upcoming introduction in the market.

The project that led to the creation of the CRG (Curved Regular Grid) format is called OpenDRIVE and has begun in 2005 by VIRES GmbH, a German simulation technology company. At the beginning, with the help of Daimler AG, they built a database of road surfaces for driving simulators, but the problem was that each customer required different formats. Thus, they decided to standardize them, and other German companies like BMW, Audi, Porsche and Volkswagen start to support this mission defining the objectives of this research. This cooperation led to the creation of a common open source tool for detailed road surfaces description, available to everybody and with a common format, the OpenCRG.

OpenCRG is a 3D representation of road surfaces. The acronym CRG, as said before, means “Curved Regular Grid” and it refers to the road description technique. This method is characterized by a “Curved Reference Line” that is the representation of the road map in the global coordinate system (x - y axis). The global reference system is transformed in a grid, the “Regular Elevation Grid” that is described by the u axis, which coincides with the reference line, and the v axis that is perpendicular to u axis. Each grid cell contains height information completing the road surface description with the longitudinal and the transversal road slope.

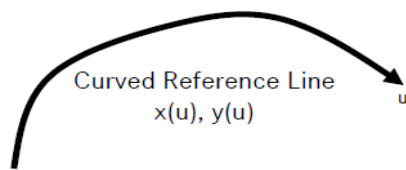


Figure 50- Curved Reference Line

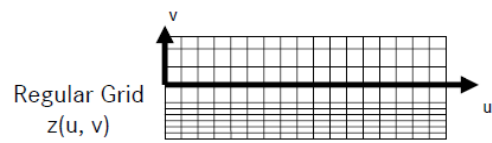


Figure 51- Regular Elevation Grid

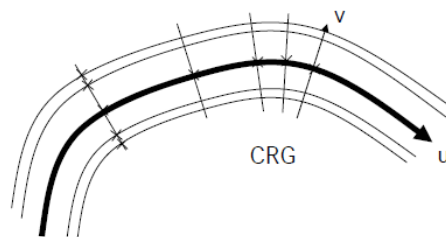


Figure 52- Curved Regular Grid

The data necessary for this model to precisely describe the road surface can be obtained thanks to laser scanning, for example: TLS, “Terrestrial Laser Scanning”, or MLS, “Mobile Laser Scanning”. To this purpose, vehicles with high-resolution equipment for road surface measurement are used. A preprocessing of the recorded data is necessary to have consistent information, to delete noises and to have an efficient data storage.

After this phase the CRG grid cells have to be filled with elevation data. To do this the u and v coordinates of the cell location are converted in x - y coordinates of the global reference system and these are taken as the center of a circle with a defined radius. This circle limits the laser scanned points cloud and the average height is computed. The mean height is then stored in the CRG cell. In this way measured data of 3D road profiles are directly obtained and stored in .crg format in the computer of the vehicle that is performing the measurements. All this process has been developed in a Matlab script by the above-mentioned German companies and made available open source for everyone. In the following images it is possible to see what explained above and the Matlab output of a .crg file reading.

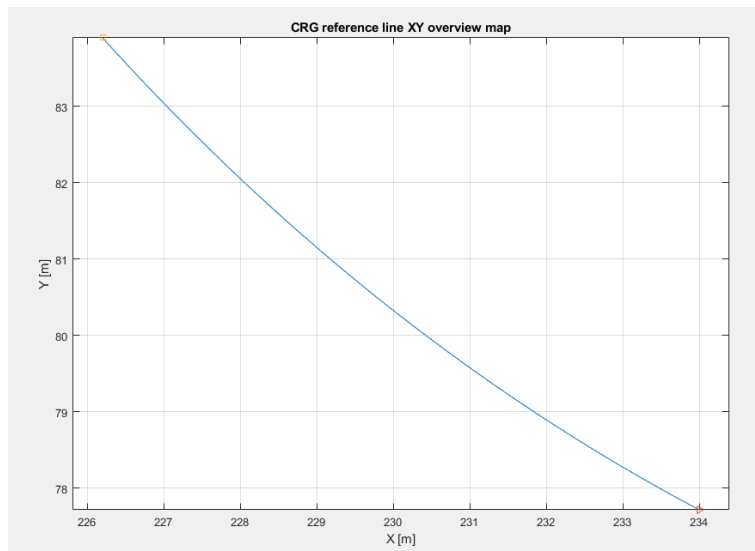


Figure 53- CRG reference line in x - y coordinates

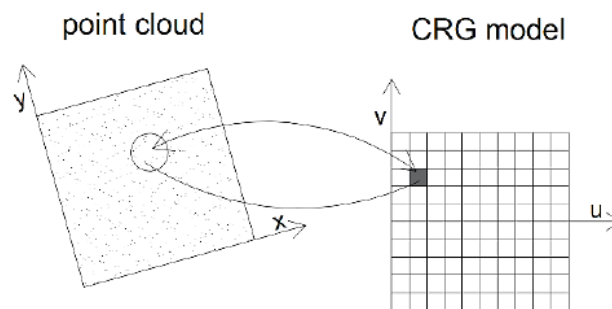


Figure 54- Grid cells height determination

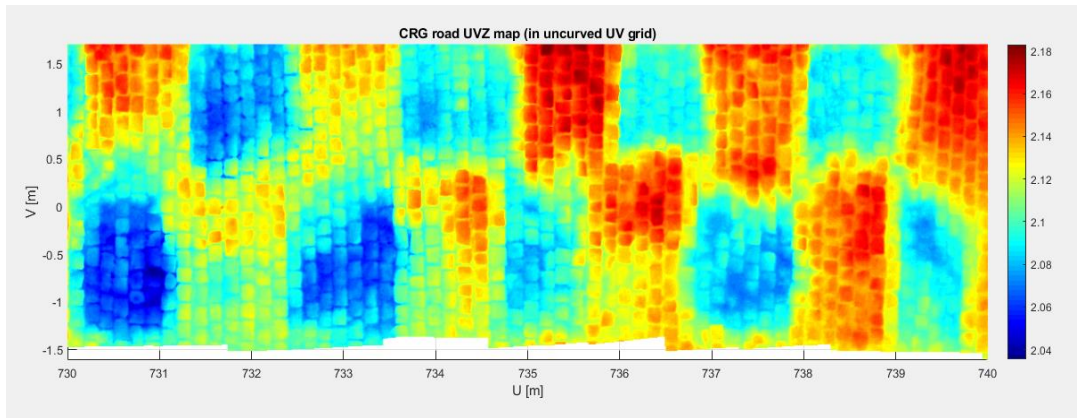


Figure 55- CRG representation in u-v-z coordinates

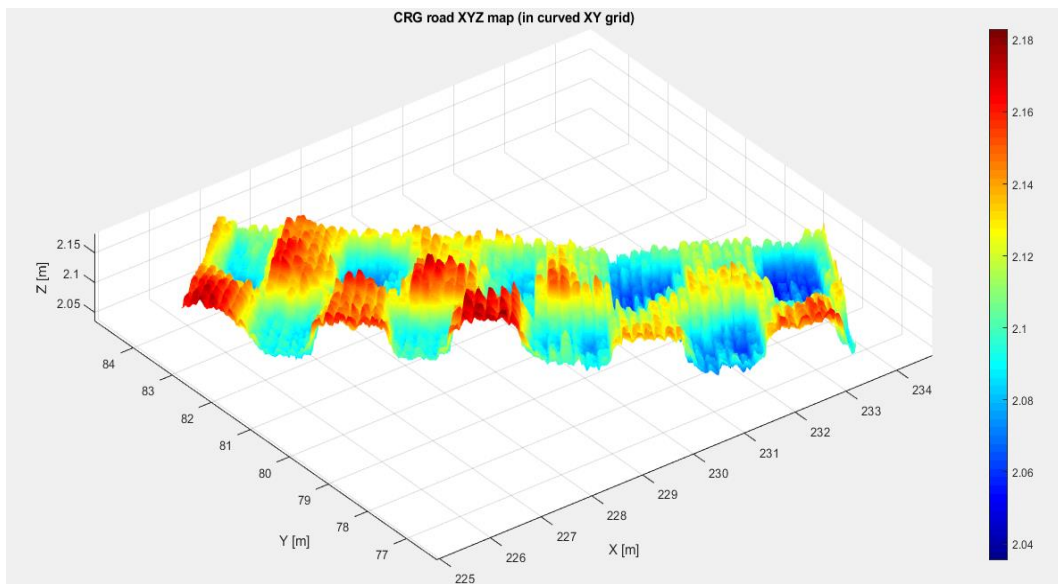


Figure 56- CRG representation in x-y-z coordinates

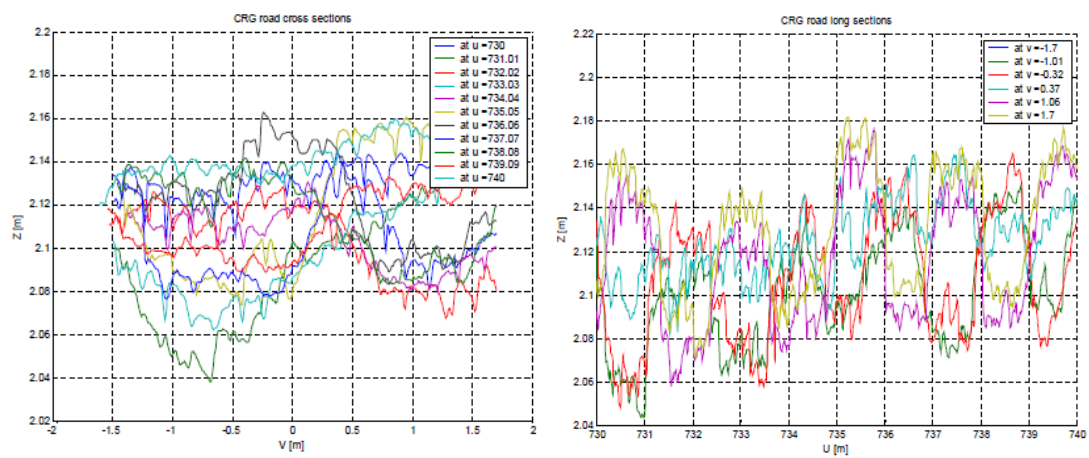


Figure 57- To the left CRG transversal road cross section in v-z coordinates at different u positions.
To the right CRG longitudinal road cross sections in u- z coordinates at different v positions

The [Figure 59](#) shows a Google Maps overview of Markbronn proving ground. Circled in red it is possible to see the location of the Belgian block track, that has been laser scanned and the 3D surface obtained using OpenCRG technique and format.

In [Figure 60](#) and [Figure 61](#) it is showed the Adams/Car 3D visualization of the Markbronn Belgian block track, that has a very detailed resolution of 1x1x0.1 cm in x-y-z directions.

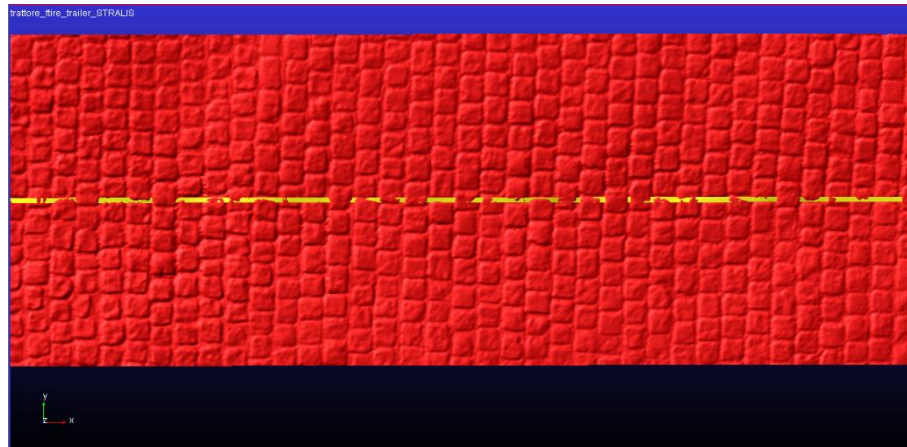


Figure 60- Top view of Belgian block track on Adams/Car

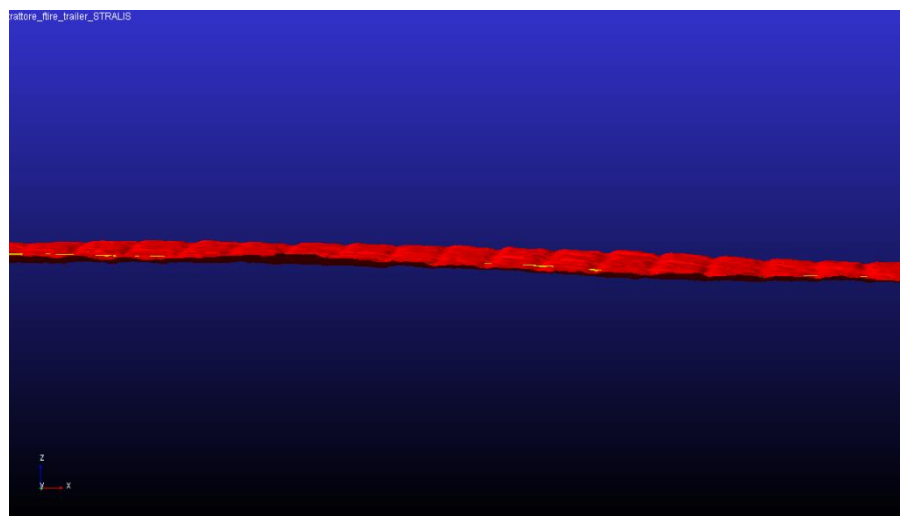


Figure 61- Lateral view of Belgian block track on Adams/Car

3.3 Test Performed and Accelerometers Positioning

Belgian block is one of the hardest paths that can be driven by a vehicle. In fact, it is part of the hundreds of tests that are performed during vehicle development. In this type of track, due to high accelerations, it is possible to evaluate ride comfort, NVH, bolt tightening resistance, interior and exterior parts resistance, components durability and other vehicle critical issues. Consequently, this kind of test is of fundamental importance in order to correlate the multibody model with the real vehicle. The final goal is to have a very complete model and tune it so that behaves like the real one, with the purpose of reduce developing time and costs.

Four different Belgian block tests done in Markbronn will be discussed in this thesis work, one performed in “unladen” condition (only the tractor) and three in “laden” condition (tractor, semi-trailer and load):

- Unloaded test has been performed at 40km/h, at constant speed;
- Loaded tests have been performed at:
 - 40 km/h, at constant speed;
 - 45 km/h, at constant speed;
 - 15-30 km/h, at constant acceleration.

Accelerometers, aimed at the data recording, have been positioned on the edges of front and rear axles, approximately as shown in [Figure 62-63](#), and on the chassis, near the interconnection between the shock absorbers and the tractor frame ([Figure 64](#)).

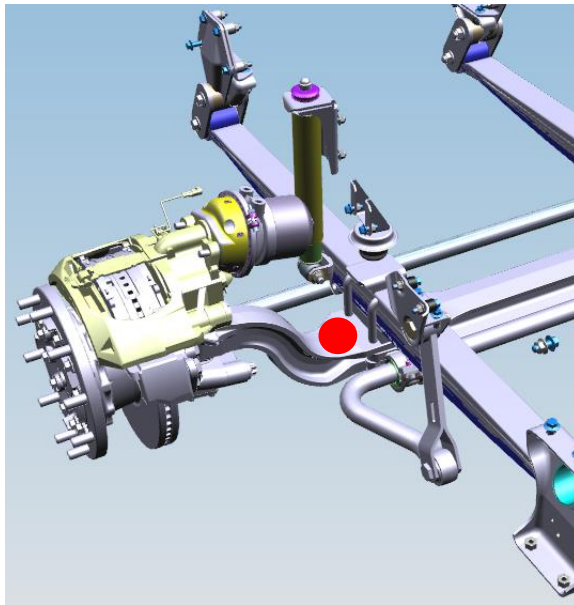


Figure 62- Front axle accelerometer positioning, circled in red

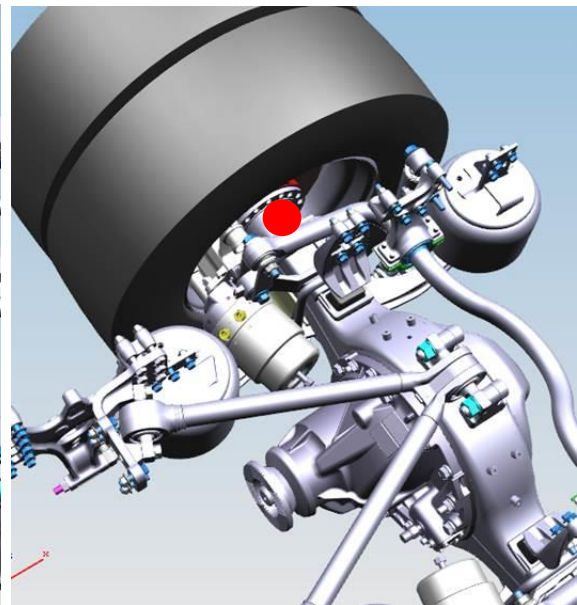


Figure 63- Rear axle accelerometer positioning, circled in red

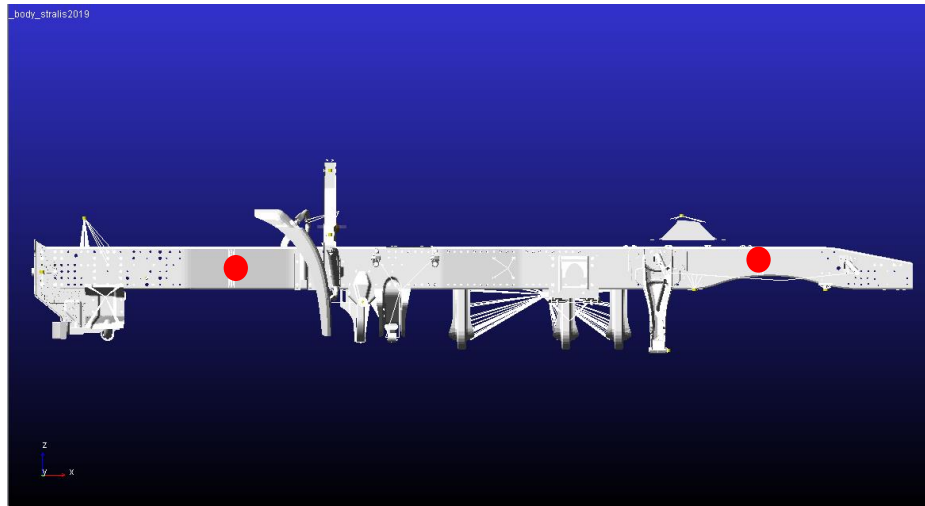


Figure 64- Tractor chassis accelerometer positioning, circled in red

Output data coming from accelerometers have been stored, disturbances removed and re-sampled at 100 Hz (Adams/Car default sampling frequency) by the engineering office. Files coming from engineering department contains signals in time domain so, being random signals, they must be transformed in frequency domain in order to be compared with signals coming from Adams/Car simulations.

Unfortunately, no information about accelerometer type and characteristics are available, so measurements are assumed to be corrects.

Concerning the multibody model, special “Requests” have been created and set in Adams/Car in order to record accelerations. They have been located in the same positions as the accelerometers of the on-road test truck.

3.4 Driver Control Files and Adams/Solver Setting

With the multibody model complete and functioning and the on-road tests data available, the following steps concerns creation of the driver control files which simulates the maneuvers performed by the driver on track, and the setting of the Adams/Solver, in order to choose the best integrator for this type of simulations.

Four different driver control files have been created, one for each type of test. The major problematics of this part of work have been the maintaining of the trajectory of the track by the vehicle and the speed maintenance because the track is not flat and there are some holes.

The first problem has been solved finding the right compromise between the oscillation respect the trajectory center, and the misalignment at the beginning of the track. In fact, if a parameter concerning the trajectory planning of the driver control file is set too low, the vehicle starts perfectly aligned with the center of the path, but after 3-4 seconds of simulation it starts to oscillate with increasing frequency with respect the center line, until the vehicle gets out of the road. On the contrary, if this parameter is set too high, the vehicle runs along the road misaligned with respect to the center, but it does not oscillate. The right parameter value has been reached after an iterative process. Probably to have a perfect maintenance of the road center, some default parameters concerning the steering PID controller should be modified, but for this study is good enough the compromise reached, also because during on-road tests it is impossible to maintain the perfect center line by the driver.

The problem concerning the speed and acceleration maintenance has been solved modifying the engine and transmission ratio parameters. In fact, making this kind of simulation, it has been discovered that the engine torque vs rpm characteristic and the transmission ratios were not corresponding to the engine and the transmission mounted on the on-road test vehicle. Moreover, the behavior is different if the truck is loaded and unloaded. In fact, the driver control file corresponding to 40 km/h constant speed, works differently in the two loading conditions. So, different initial conditions must be set in the driver control files.

With reference to the Adams/Solver settings, after a meeting with the engineering department and the MSC Software support, it has been decided to use GSTIFF as integrator with formulation SI2 and H_{\max} equal to $1.0 \cdot 10^{-4}$ seconds. GSTIFF is a method of dimensional integration very precise and fast for the evaluation of displacements and a wide range of quantities linked to the motion analysis. The formulation SI2 provides an improvement to the integration method in order to have a better control of speeds and accelerations errors. It gives very good results also with wide

frequency oscillations. Instead, H_{\max} sets the maximum time step that the integrator is allowed to take.

Using this kind of instructions, the output data needed for this thesis work are computed more accurately than using other types of integrators.

Chapter 4. Comfort analysis and correlation of the obtained results

4.1 Comfort¹

It is difficult to define comfort because it is a complex and very subjective parameter. But, at the same time, it is becoming more and more important for the customer choice. It is related to vibrations perceived in the cockpit by the passengers. Driving comfort, together with vibrational and acoustic comfort, has a strong impact on vehicle safety. SAE (Society of Automotive Engineers) divides comfort as follows:

- ride: low frequencies up to 5 Hz;
- shake: intermediate frequencies between 5 and 25 Hz;
- harshness: high frequencies between 25 and 100 Hz;
- noise: acoustic phenomena from 100 to 22 kHz.

Internal vibrations

Internal vibrations are due to the vehicle itself. The main sources are rotating parts: the wheels, the driveline and the engine. The main reason of these excitation is imbalance.

Concerning the tires, they may show structural and geometrical irregularities like, for example, eccentricity. The tire-wheel assembly is a mechanical element characterized by elasticity and damping and so it can filter higher vibrations due to tire-road contact. Subsequently, these are further filtered by suspensions and finally they are perceived on-board as noise.

The excitations produced by the driveline are generally transmitted to the chassis by its soft mountings.

The engine is a great source of noise and vibrations due to inertial forces of reciprocating elements and variations of the driving torque. For this reason, the design of engine suspensions results very complex. They should be soft to insulate the chassis from engine vibrations but at the same time they must be stiff to avoid large relative motion between engine and vehicle.

Another contribution to the noise is due to aerodynamics. Aerodynamic noise is caused by vortices and flow detachment on the front part of the vehicle.

¹ Genta Giancarlo, Morello Lorenzo. (2009). “The Automotive Chassis. Volume 2: System Design”, Springer.

Generally, it is important to reduce vibrations that could cause discomfort, but at the same time, a complete suppression of excitation and noise could be undesirable and dangerous because they convey useful information to the driver and can give warnings in case of anomalies.

External vibrations

External vibrations are due to the roughness of the road surface. It is important to study these excitations because they are responsible of the vertical load F_z at the tire-road contact. A large variation of F_z reduces the tire ability to exert forces in x and y direction.

Road vibrations cannot be studied using a deterministic approach because they are random signals and so must be treated using stochastic methods such as power spectral density.

ISO (International Organization of Standardization) divides road surfaces in 8 classes of power spectral density, from A to H. Classes between A and D are typical of hard-surface roads, with increasing roughness. Classes E and F are typical of natural surface roads, pavé or bad maintained roads G and H classes correspond to road with very important disconnections. In the figure below are showed the typical power spectral densities of the before mentioned road classes.

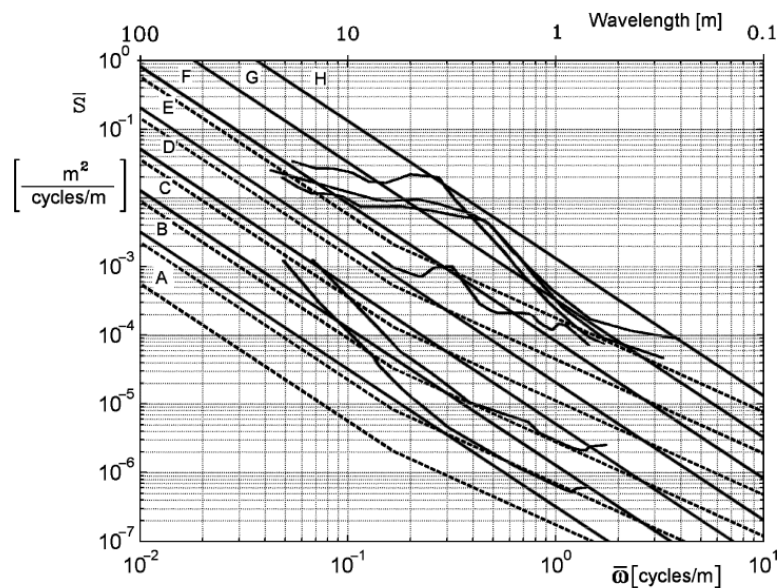


Figure 65- PSD of typical road profiles

The frequency on x axis is in cycles/m because the function that describes the road profile $h(x)$ is in function of space and not in function of time.

Human body perception

Different studies have been conducted on the vibration perception of human body. ISO 2631 standard divides between vibrations that occur with a frequency that ranges between 0.5 Hz to 80 Hz that can cause discomfort and fatigue, and between vibrations that occur with a frequency that ranges between 0.1 Hz and 0.5 Hz that may cause motion sickness.

In the subsequent plot is possible to see the root mean square of accelerations causing a reduction of physical efficiency, in function of frequency. It is possible to notice that the critical range of frequencies for human body is between 4 Hz and 8 Hz.

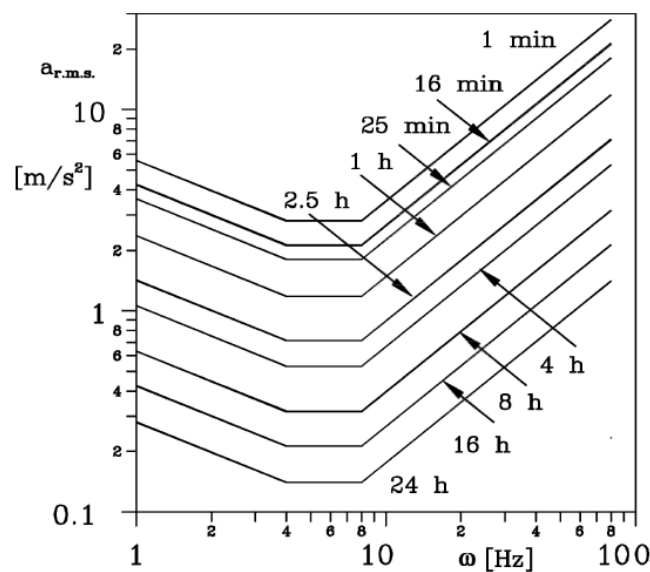


Figure 66- Constant discomfort lines (ISO 2631 standard)

Natural frequencies of sprung and unsprung masses should be placed far from frequencies that produce discomfort. Lower natural frequencies, the ones linked to the sprung masses should be placed above 1 Hz to avoid motion sickness but below 4 Hz. Higher natural frequencies are due to unsprung masses motion and should be higher than 10 Hz.

The study linked to this thesis concerns vibrations between 0 and 20 Hz and, as said in the introduction, regards a first correlation among experimental and numerical accelerations. Properly, it is not a comfort study aimed at improving the driver and passenger driving experience, but a preliminary evaluation of the FTire model and suspension systems response of the multibody model respect the on-road truck, performing the same track in the same test conditions. The multibody model developed is multipurpose because can be used not only for handling but also for studies concerning comfort, durability and fatigue.

4.2 Correlation methods

In this section the correlation of the numerical and experimental data, concerning the comfort analysis, is presented. The vertical accelerations, recorded by the accelerometers on track and by the requests opportunely positioned in the multibody model, will be compared in terms of power spectral density (PSD). This choice has been done because we are dealing with random signals that do not carry adequate information in time domain. Instead, they are meaningful in frequency domain, because they show the power content at each frequency of the sinusoids in which the signal can be subdivided. What is obtained is only an estimation of the power spectral density because of the numerous approximations that this analysis method requires.

An alternative representation of the correlation, using level crossing rate (LCR), will be given. This technique is widely used in telecommunication field. LCR measures how many times per second a stochastic process crosses a given level.

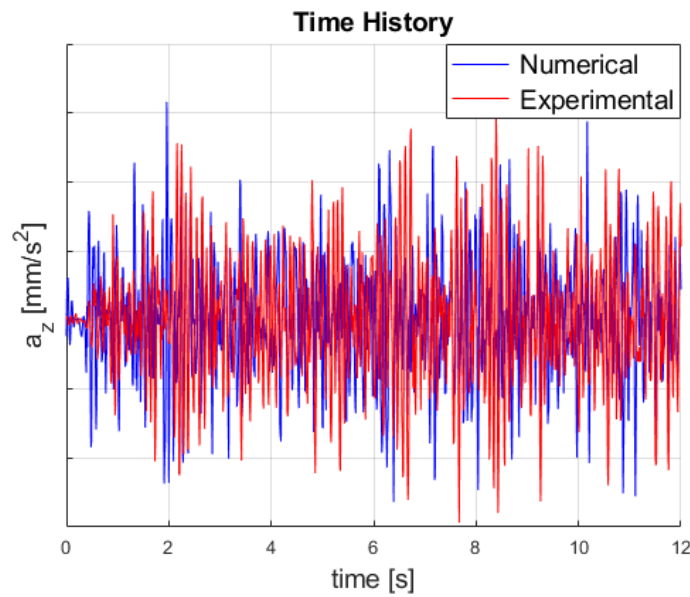


Figure 67- Example of time history signals correlation

4.2.1 PSD estimation

The output signals of accelerometers positioned on the truck and of the requests defined in the model are accelerations in time domain, obtained sampling with a frequency equal to 100 Hz. So, the correlation object of this study is between two discrete, non-deterministic (random) signals. For this reason, is necessary a comparison in frequency domain, between the power spectral content of the signals.

The Fourier's theorem helps in these situations because it says that a complex signal can be always represented by the superposition of an infinite number of sinusoids. If the signal is periodic, it can be treated with the Fourier series. Our signals are non-periodic, or better their period can be considered infinite, so they can be decomposed by the Fourier transform which is a generalization of Fourier series.

The Fourier transform of a function $x(t)$ is given by:

$$X(f) = \int_{-\infty}^{+\infty} x(t) * e^{-j2\pi ft} dt$$

The Fourier's transform has important properties:

- Linearity: if the transform of two signals is known, it is possible to compute the transform of the combination of the two signals.
- Independence by time: if the time history of a signal is translated, the absolute value of the transform $|X(f)|$ does not change and the phase displacement varies linearly with f . This property is very important because it is impossible to have an exact correspondence of the time history of the path traveled by the truck and the one traveled by the model.
- Independence by frequency domain: this property is the dual of the previous one.
- Convolution: the complex convolution operation can be substituted by a simple multiplication of the Fourier transform of the two functions.

The problem is that it is not possible to compute the transform between $-\infty$ and $+\infty$ in case of a finite time interval and a discrete number of samples. The discrete Fourier transform (DFT) overcomes this fact considering the signal as a periodic function with period equal to the time interval. Here is introduced the concept of windowing, that means that we suppose our signal of infinite length multiplied by a rectangular window which value is equal to 1 during a certain time period and 0 elsewhere. The effect of windowing introduces the impossibility to compute the effective spectrum of the signal but only an estimation, because of the finite number of samples.

The power spectral density is defined as the square modulus of the Fourier transform of the signal:

$$S(\omega) = \lim_{T \rightarrow \infty} \frac{1}{T} \left| \int_{-\frac{T}{2}}^{+\frac{T}{2}} x(t) * e^{-i\omega t} dt \right|^2$$

The DFT formulation is:

$$S(\omega) = \sum_{n=-\infty}^{+\infty} x(n) * e^{-j\omega n}$$

This estimation of the PSD is also known as periodogram.

The computation of the DFT can be very expensive in terms of computational power in case of a lot of samples. So, it has been introduced by Cooley and Tukey in 1965 an algorithm able to reduce the number of computations: the fast Fourier transform (FFT).

The passages necessary to study the PSD of a signal are the followings:

- Signal acquisition: it is characterized by sampling frequency.
- Trend removing: it consists into the removing of trends that can affect the signal and are not necessary for the signal analysis.
- Mean value removing: it is mandatory in signal analysis. If the signal is characterized by a mean value different from zero, it can be considered as $x = x_0 + k$. Doing the square modulus, the double product $2x_0k$ generates power leakage.
- Windowing: there are different type of windows. The windows type depends on the type of signal that as to be analyzed. For random, narrow-band signals, the most used windows are Hamming and Hanning. For this study it has been chosen the Hanning window.
- Fast Fourier transform and parameters selection: there are not exact FFT parameters to be chosen, it depends by the signal and by what we want to check. It is an iterative process.

All what concerns the PSD estimation is resumed by the PWELCH function in Matlab.

The parameters used have been the followings:

- Sampling frequency (fs): 100 Hz;
- Number of points to apply FFT (nfft): 2 next power of two of number of samples;
- Windows type: Hanning (symmetric type);
- Windows segment length: 512;
- Overlap percentage: 50%

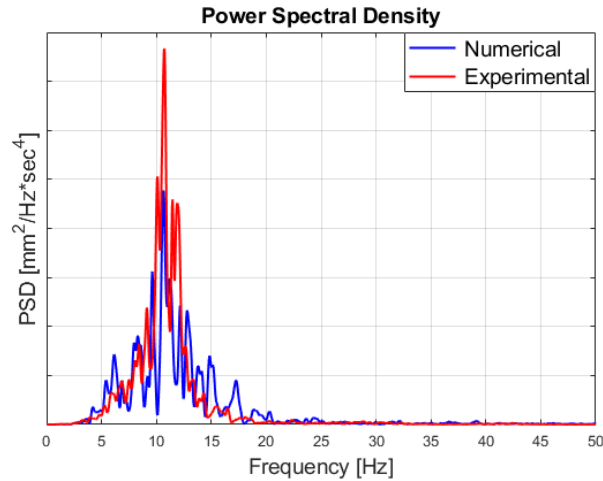


Figure 68- Example of PSD signal correlation

4.2.2 LCR estimation

Level Crossing Rate is a correlation method used to quantify how often a stochastic signal crosses, in positive or negative direction, a defined level.

It is a technique adopted firstly in the aeronautical industry to count, in a simple way, accelerations that exceeded certain discrete levels. Iveco testing and simulations departments use LCR method to qualify signals (accelerations, strains, forces) in order to detect the reached levels and also to allow the comparison among several signals. Moreover, it is widely used in durability and fatigue analysis in order to evaluate the consistency of the loads versus the number of occurrences.

On x-axis it is represented the number of times the defined level is crossed, in logarithmic scale.

On y-axis there are the vertical accelerations crossed by the signal, divided in levels.

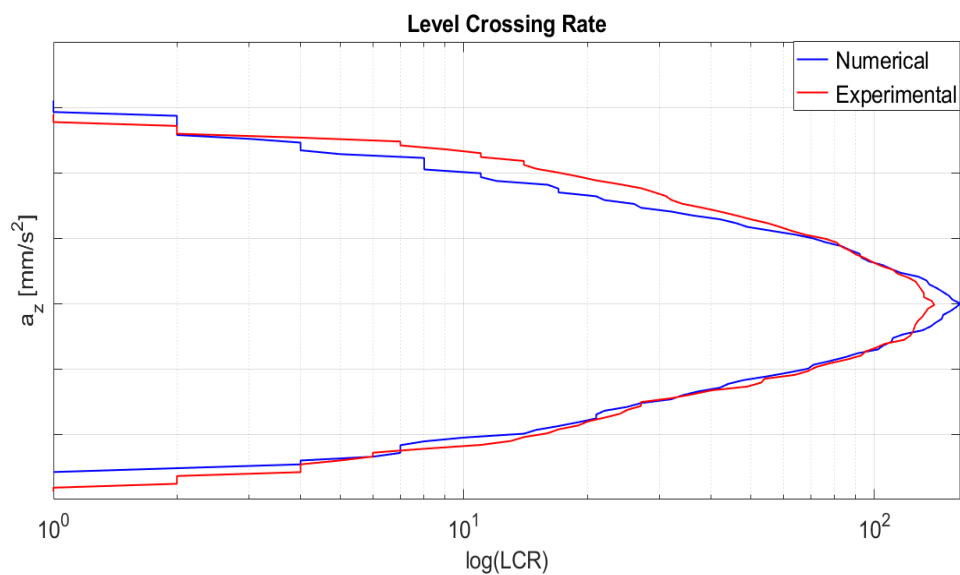


Figure 69- Example of LCR signal correlation

4.3 Experimental-numerical correlation: unloaded condition

In the following sections, the principal results obtained with unloaded condition on Belgian block track, are showed in terms of correlation between numerical and experimental results. The vertical accelerations recorded by the accelerometers positioned on axles and on the tractor chassis are compared in frequency domain using power spectral density (PSD) and using the level crossing rate (LCR) technique.

Concerning the PSD representation, the range of frequency meaningful for this study is between 0 and 20 Hz, even if the complete graph goes from 0 to 50 Hz, the Nyquist frequency.

The LCR representation is done in logarithmic scale in order to have a clearer situation.

4.3.1 40 km/h constant speed

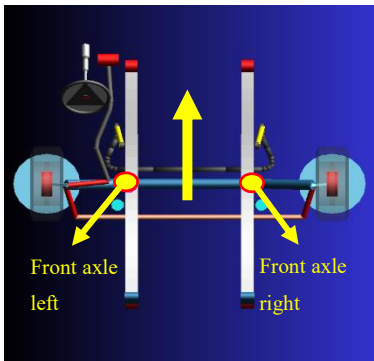


Figure 70- Accelerometers positioning

| Front axle left: | Front axle right: |
|---|---|
| <div> <div> <div>PSD: a_z Front Axle Left</div> </div> <div> <p>Figure 71- PSD of accelerations of front axle left</p> </div> </div> | <div> <div> <div>PSD: a_z Front Axle Right</div> </div> <div> <p>Figure 72- PSD of accelerations of front axle right</p> </div> </div> |
| <div> <div> <div>LCR: a_z Front Axle Left</div> </div> <div> <p>Figure 73- LCR of accelerations of front axle left</p> </div> </div> | <div> <div> <div>LCR: a_z Front Axle Right</div> </div> <div> <p>Figure 74- LCR of accelerations of front axle right</p> </div> </div> |

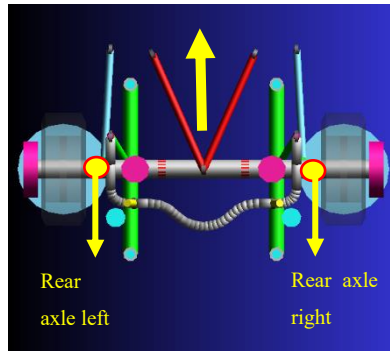
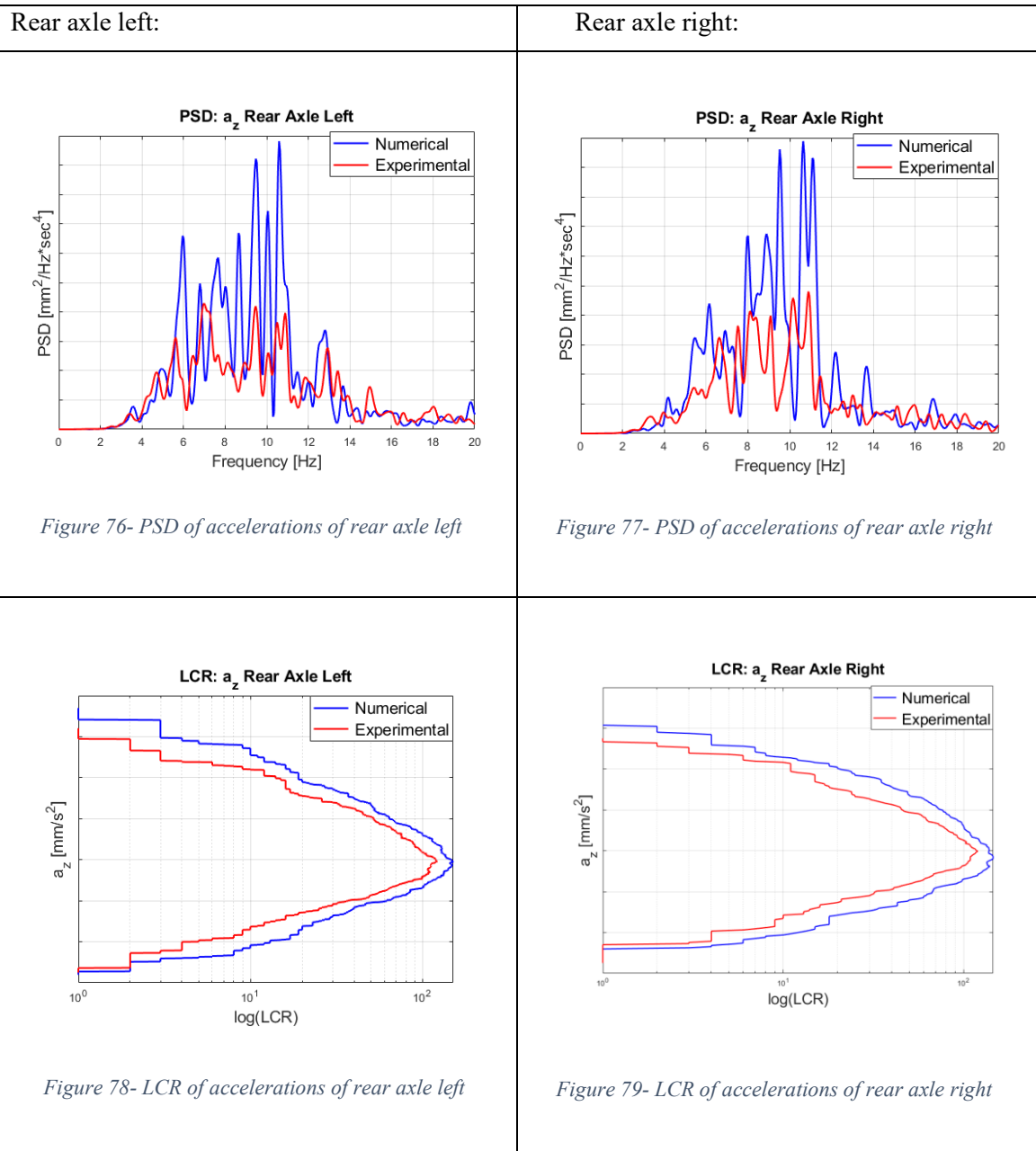


Figure 75- Accelerometers positioning



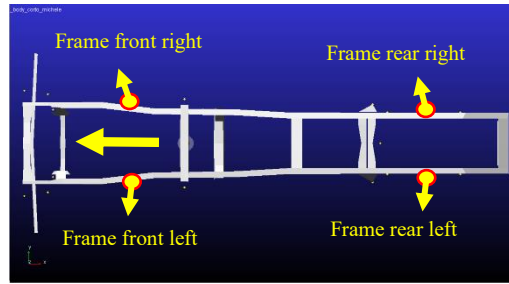


Figure 80- Accelerometers positioning

Frame front left:

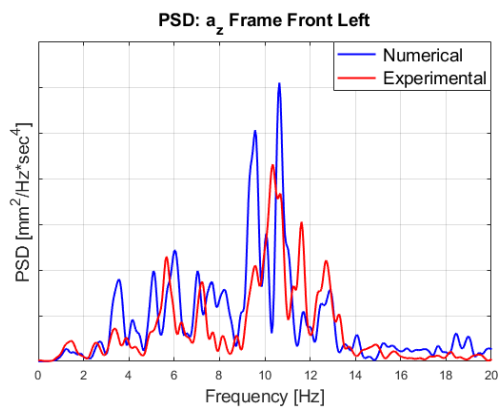


Figure 81- PSD of accelerations of frame front left

Frame front right:

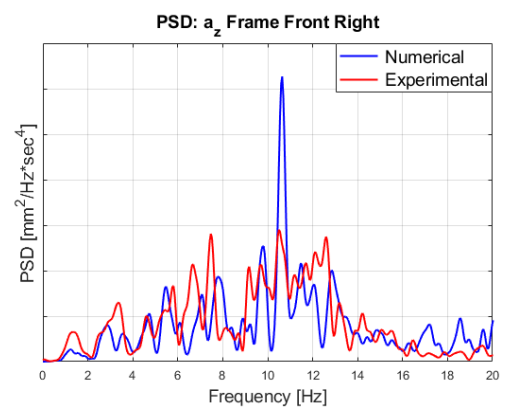


Figure 82- PSD of accelerations of frame front right

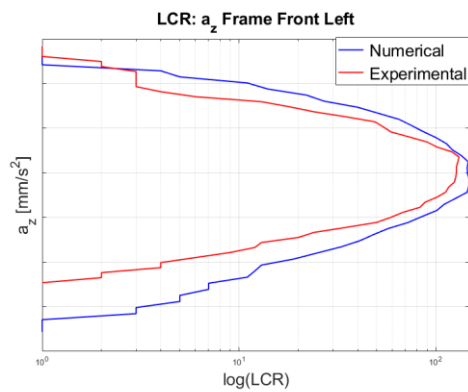


Figure 83- LCR of accelerations of frame front left

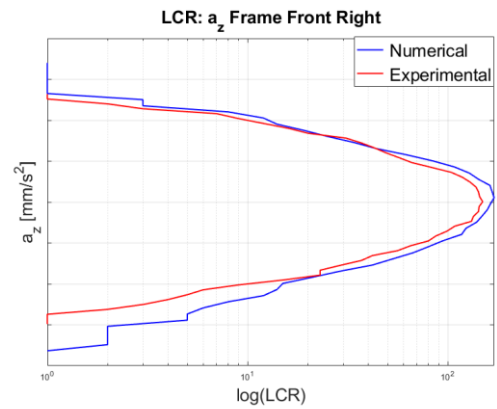


Figure 84- LCR of accelerations of frame front right

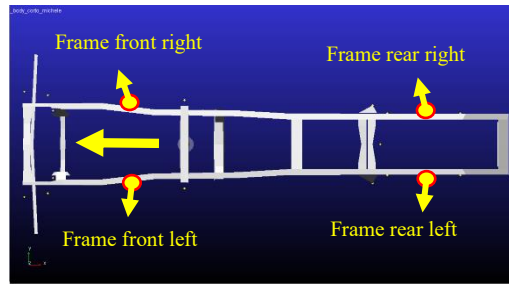


Figure 85- Accelerometers positioning

Frame rear left:

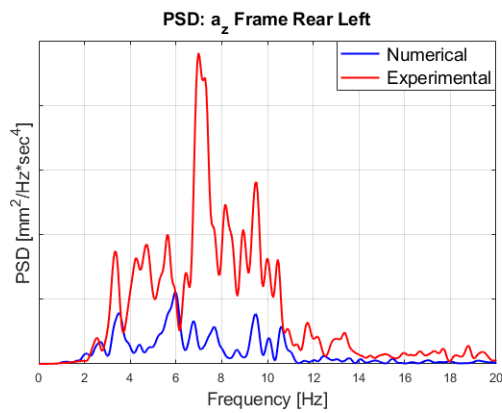


Figure 86- PSD of accelerations of frame front left

Frame rear right:

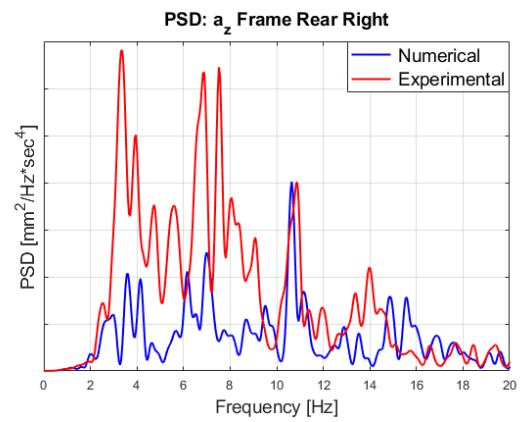


Figure 87- PSD of accelerations of frame rear right

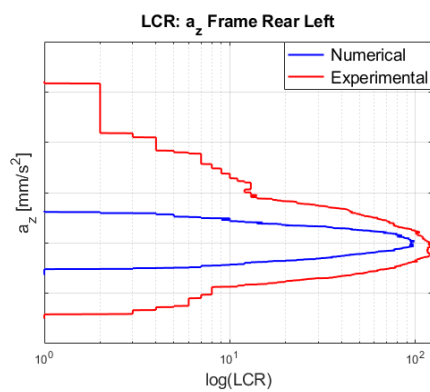


Figure 88- LCR of accelerations of frame front left

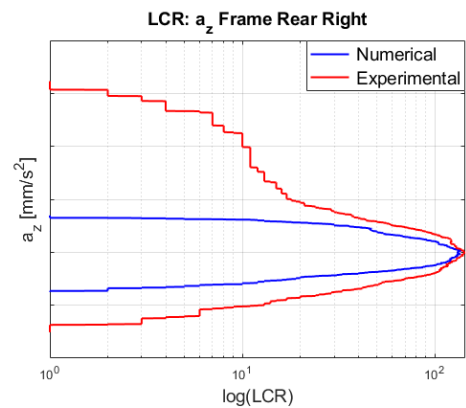


Figure 89- LCR of accelerations of frame rear right

The results obtained in the unloaded condition are very satisfactory, especially with regards to the accelerations recorded on the front and the rear axles. In fact, the bands of frequencies showed by

PSD diagrams correspond and the number of passages and the amplitudes represented by LCR graphs are similar.

Differences are noticed between the accelerometers positioned on the frame, especially the rear ones. The bands of frequencies showed by PSD are respected but the amplitudes are different in PSD and LCR diagrams both. The reason can be linked to the behavior of the rear air-springs and bushings not matching with the real ones.

4.4 Experimental-numerical correlation: loaded condition

In the following sections, the principal results obtained with loaded condition on Belgian block track, are showed in terms of correlation between numerical and experimental results. The considerations done in [section 4.3](#) are always true.

4.4.1 40 km/h constant speed

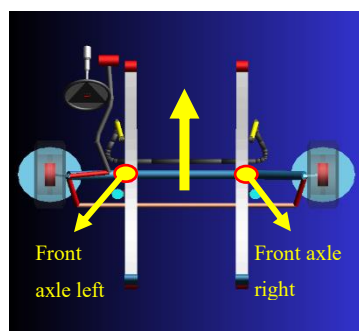


Figure 90- Accelerometers positioning

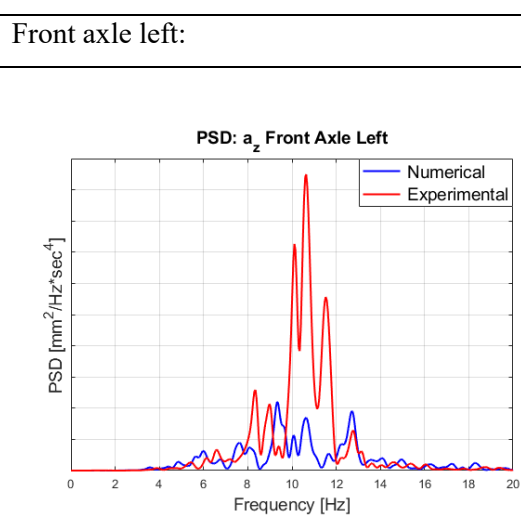


Figure 91- PSD of accelerations of front axle left

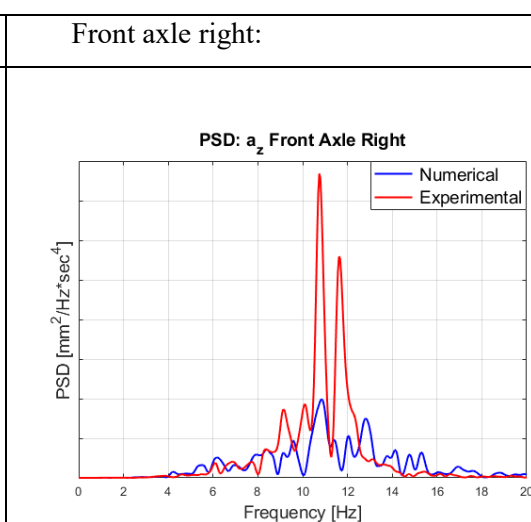


Figure 92- PSD of accelerations of front axle right

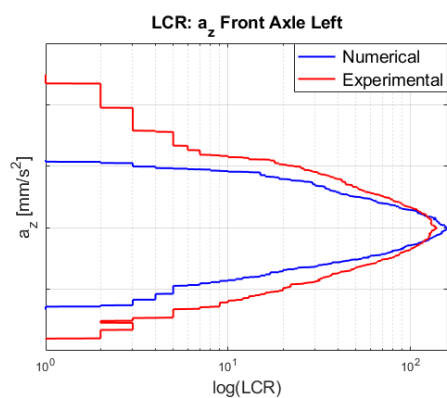


Figure 93- LCR of accelerations of front axle left

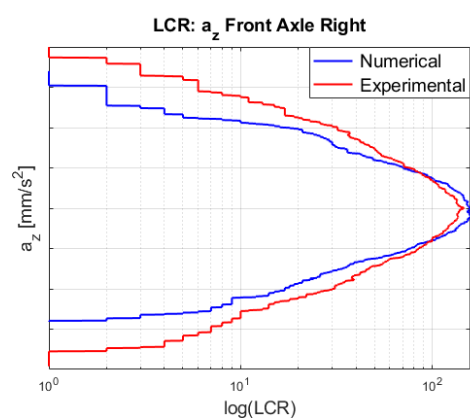


Figure 94- LCR of accelerations of front axle right

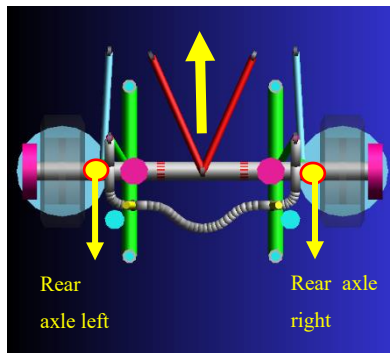


Figure 95- Accelerometers positioning

Rear axle left:

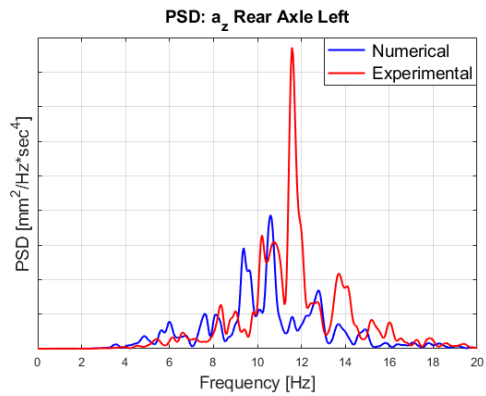


Figure 96- PSD of accelerations of rear axle left

Rear axle right:

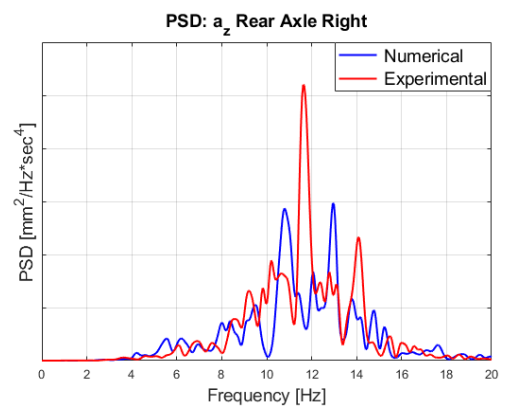


Figure 97- PSD of accelerations of rear axle right

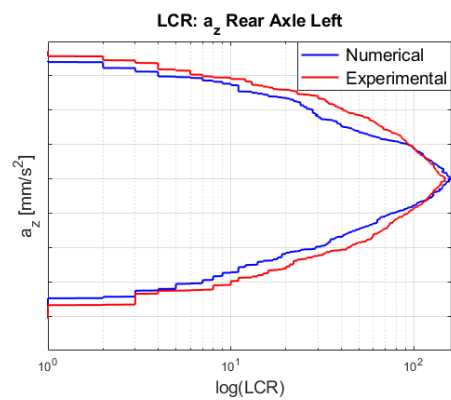


Figure 98- LCR of accelerations of rear axle left

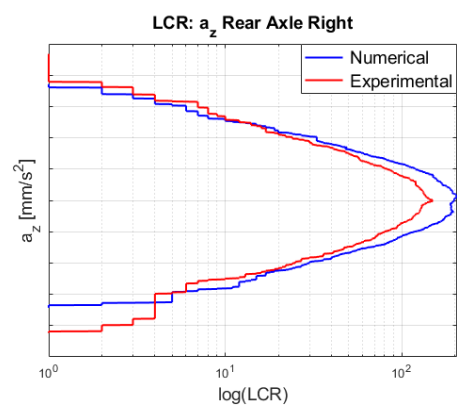


Figure 99- LCR of accelerations of rear axle right

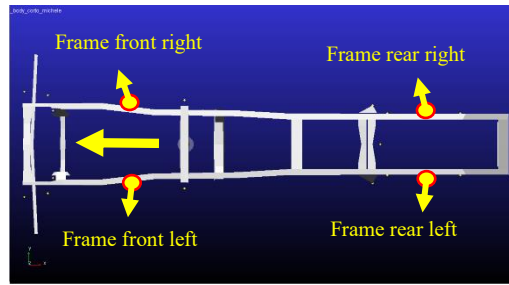


Figure 100- Accelerometers positioning

Frame front left:

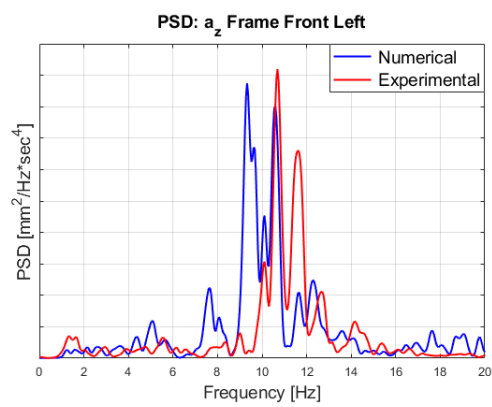


Figure 101- PSD of accelerations of frame front left

Frame front right:

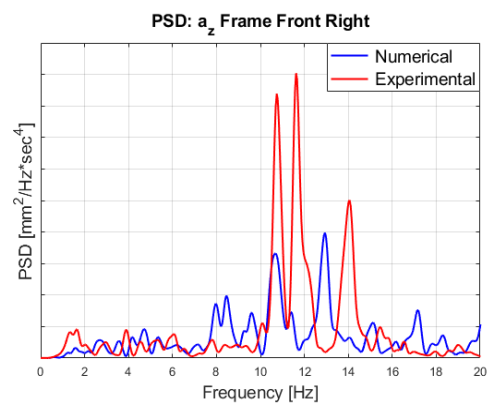


Figure 102- PSD of accelerations of frame front right

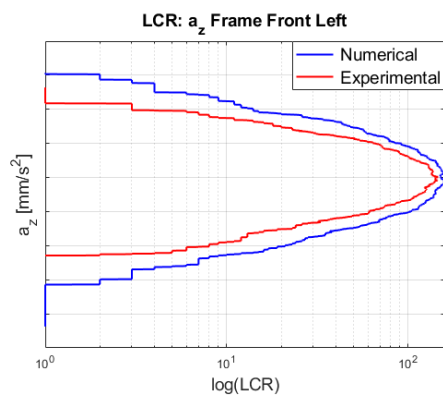


Figure 103- LCR of accelerations of frame front left

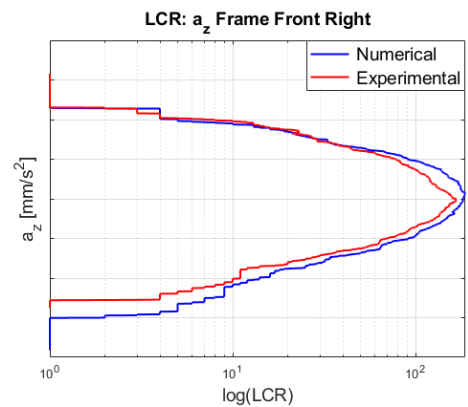


Figure 104- LCR of accelerations of frame front right

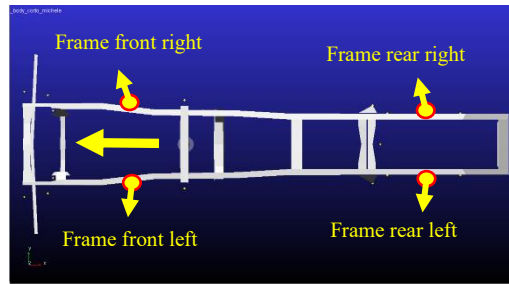


Figure 105- Accelerometers positioning

Frame rear left:

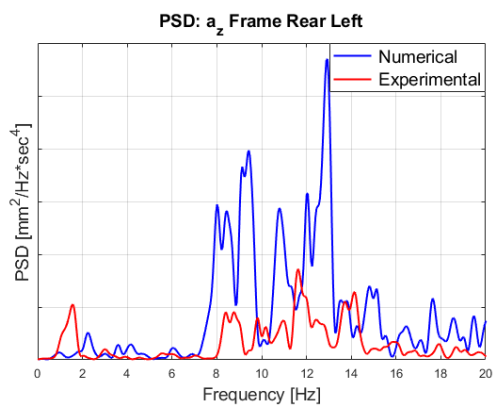


Figure 106- PSD of accelerations of frame rear left

Frame rear right:

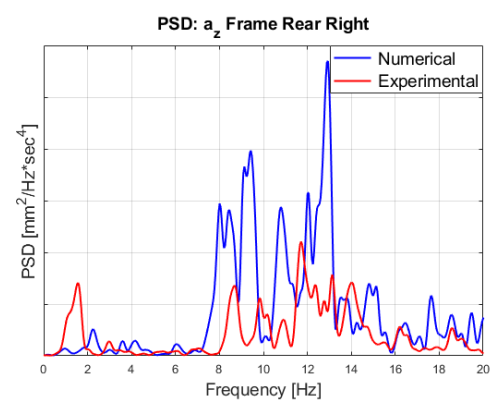


Figure 107- PSD of accelerations of frame rear right

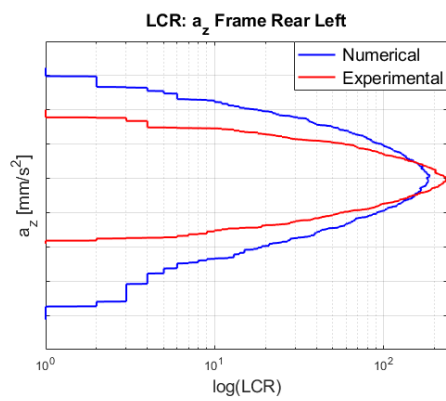


Figure 108- LCR of accelerations of frame rear left

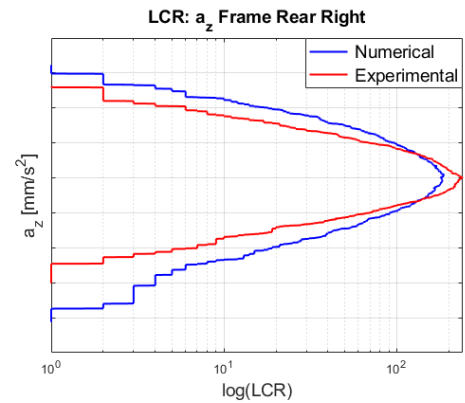


Figure 109- LCR of accelerations of frame rear right

These results obtained in the loaded condition at 40 km/h are good especially with regards to the accelerations recorded on the rear axle. In the front axle we have differences probably due to the

load distribution. In fact, the front axle is loaded about 400 kg less than the on road truck for the reasons explained in [Section 1.5](#).

Differences are noticed between the accelerometers positioned on the frame, especially the rear ones. The bands of frequencies showed by PSD are respected but the amplitudes are different in PSD and LCR diagrams both. The reason can be linked to the behavior of the rear air-springs and bushings not matching with the real ones.

4.4.2 45 km/h constant speed

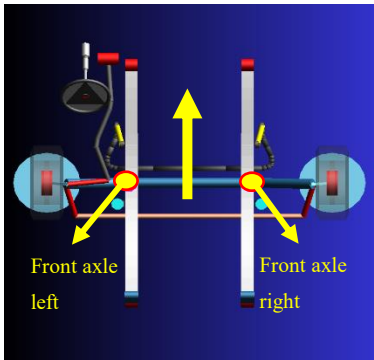


Figure 110- Accelerometers positioning

| Front axle left: | Front axle right: |
|---|---|
| <div> <div> <div>PSD: a_z Front Axle Left</div> </div> <div>Figure 111- PSD of accelerations of front axle left</div> </div> | <div> <div> <div>PSD: a_z Front Axle Right</div> </div> <div>Figure 112- PSD of accelerations of front axle right</div> </div> |
| <div> <div> <div>LCR: a_z Front Axle Left</div> </div> <div>Figure 113- LCR of accelerations of front axle left</div> </div> | <div> <div> <div>LCR: a_z Front Axle Right</div> </div> <div>Figure 114- LCR of accelerations of front axle right</div> </div> |

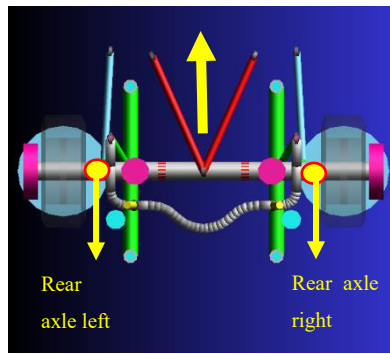
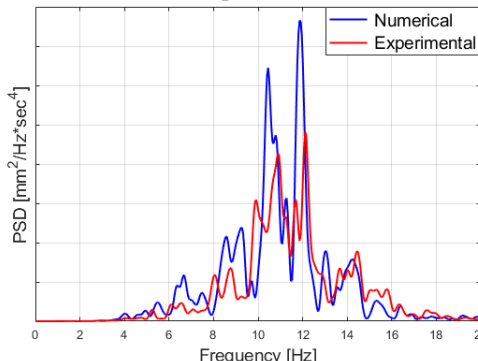
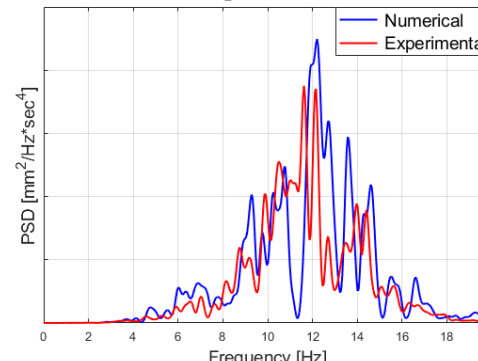
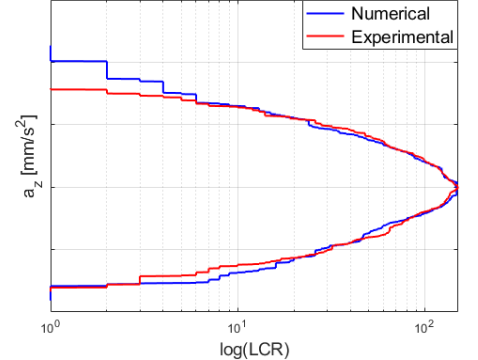
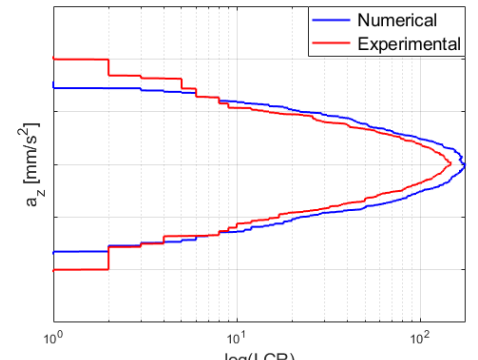


Figure 115- Accelerometers positioning

| Rear axle left: | Rear axle right: |
|--|--|
| <p data-bbox="446 801 638 828">PSD: a_z Rear Axle Left</p>  <p data-bbox="284 1227 769 1258">Figure 116- PSD of accelerations of rear axle left</p> | <p data-bbox="1021 801 1212 828">PSD: a_z Rear Axle Right</p>  <p data-bbox="858 1227 1343 1258">Figure 117- PSD of accelerations of rear axle right</p> |
| <p data-bbox="446 1384 638 1411">LCR: a_z Rear Axle Left</p>  <p data-bbox="284 1809 769 1841">Figure 118- LCR of accelerations of rear axle left</p> | <p data-bbox="1021 1384 1212 1411">LCR: a_z Rear Axle Right</p>  <p data-bbox="858 1809 1343 1841">Figure 119- LCR of accelerations of rear axle right</p> |

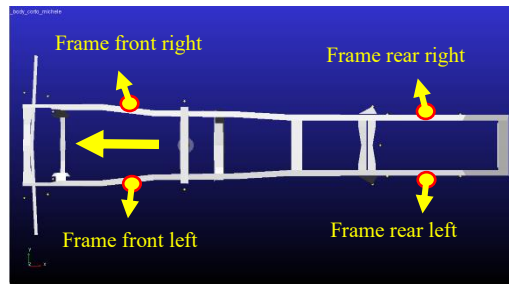


Figure 120- Accelerometers positioning

Frame front left:

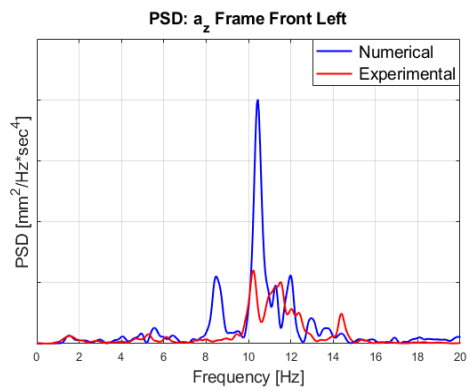


Figure 121- PSD of accelerations of frame front left

Frame front right:

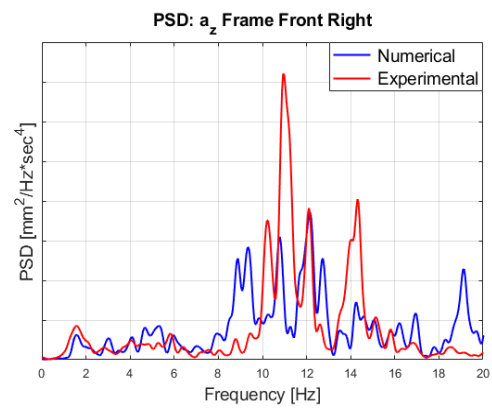


Figure 122- PSD of accelerations of frame front right

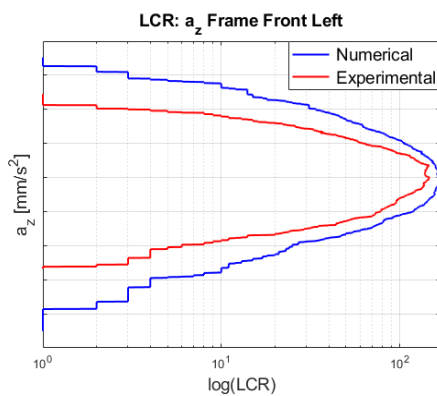


Figure 123- LCR of accelerations of frame front left

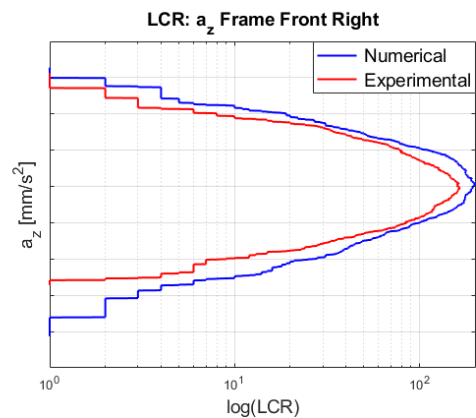


Figure 124- LCR of accelerations of frame front right

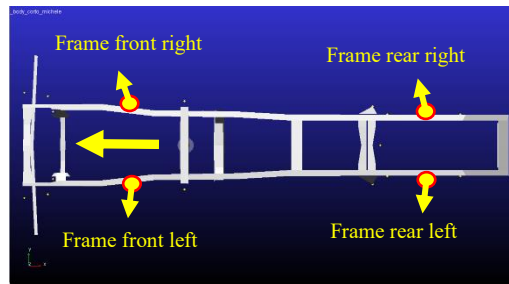
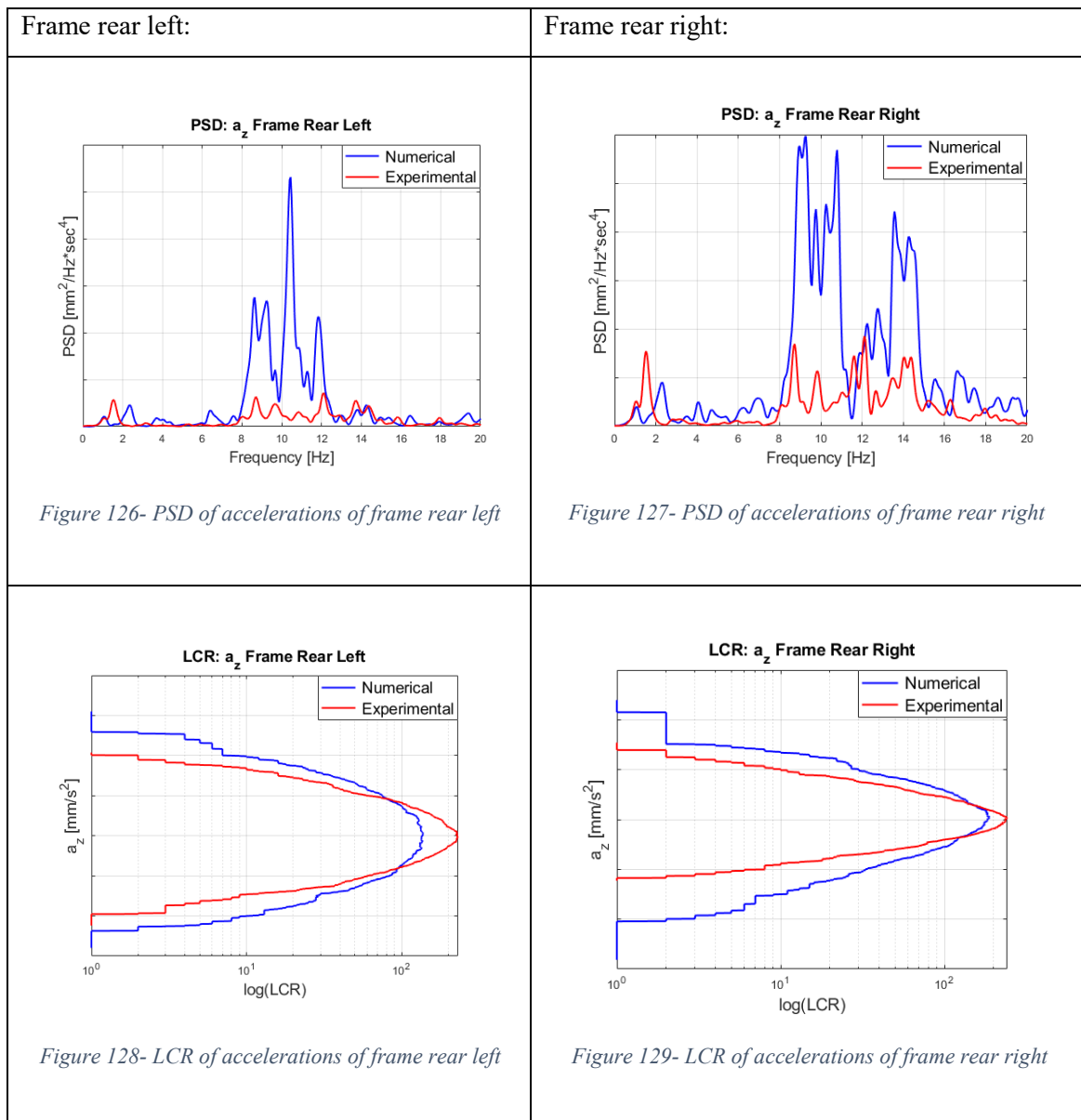


Figure 125- Accelerometers positioning



These results obtained in the loaded condition at 45 km/h are good and the same considerations done for the loaded condition at 40 km/h can be repeated.

4.3.3 15-30 km/h constant acceleration

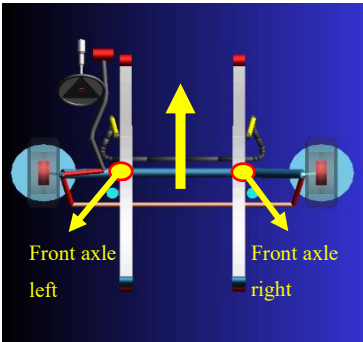
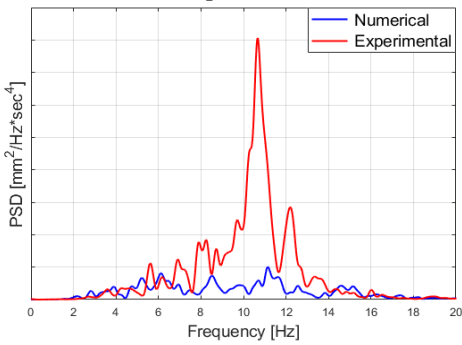
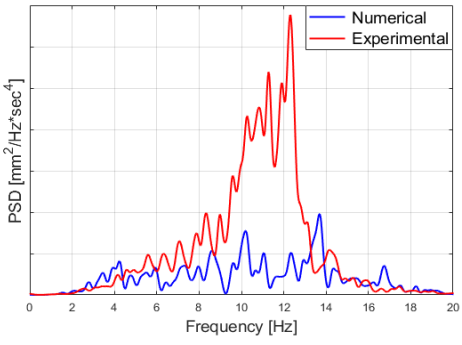
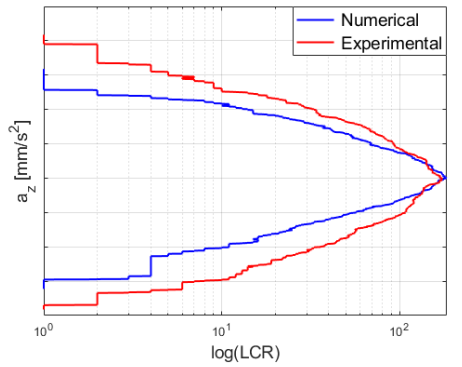
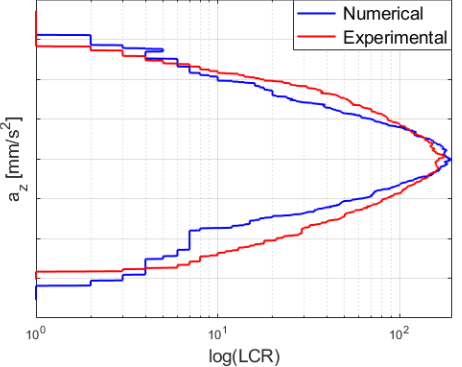


Figure 130- Accelerometers positioning

| Front axle left: | Front axle right: |
|--|---|
| <div><p>PSD: a_z Front Axle Left</p><p>Figure 131- PSD of accelerations of front axle left</p></div> | <div><p>PSD: a_z Front Axle Right</p><p>Figure 132- PSD of accelerations of front axle right</p></div> |
| <div><p>LCR: a_z Front Axle Left</p><p>Figure 133- LCR of accelerations of front axle left</p></div> | <div><p>LCR: a_z Front Axle Right</p><p>Figure 134- LCR of accelerations of front axle right</p></div> |

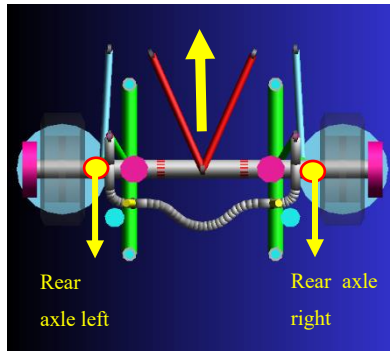


Figure 135- Accelerometers positioning

Rear axle left:

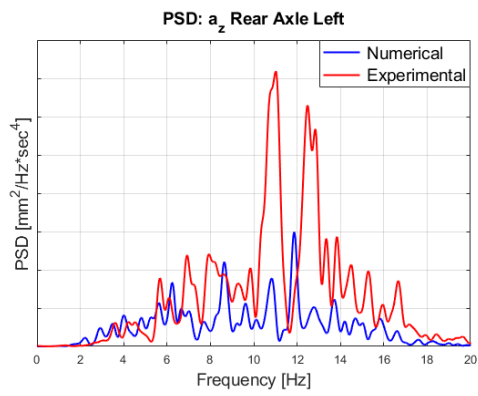


Figure 136- PSD of accelerations of rear axle left

Rear axle right:

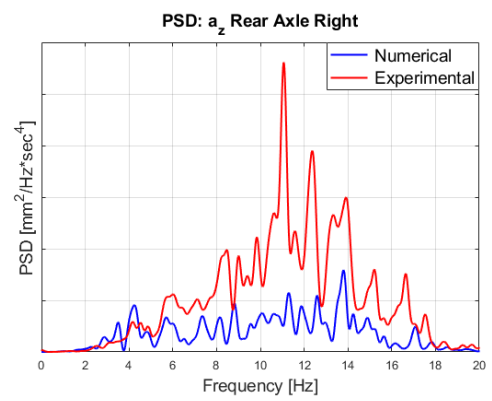


Figure 137- PSD of accelerations of rear axle right

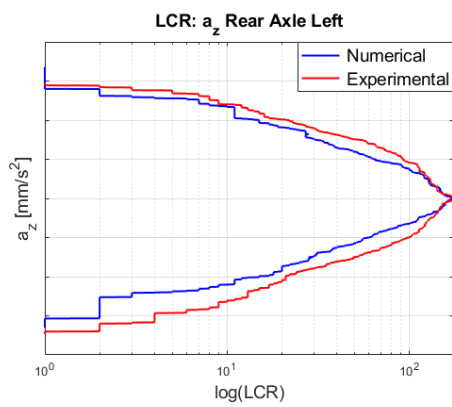


Figure 138- LCR of accelerations of rear axle left

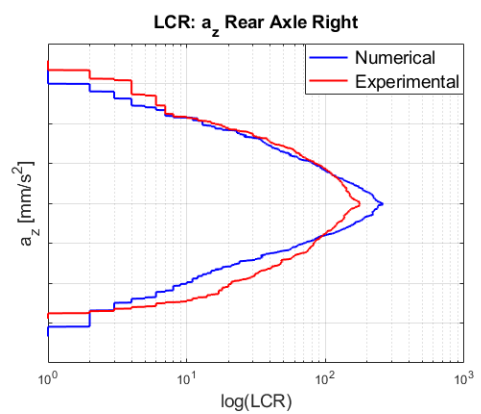


Figure 139- LCR of accelerations of rear axle right

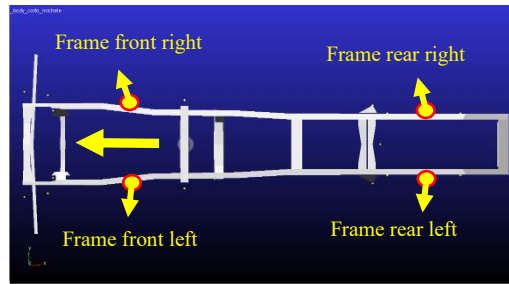


Figure 140- Accelerometers positioning

Frame front left:

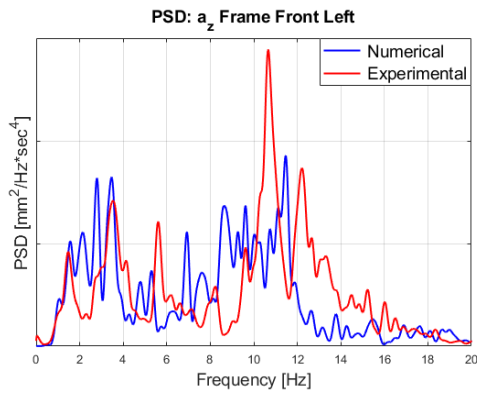


Figure 141- PSD of accelerations of frame front left

Frame front right:

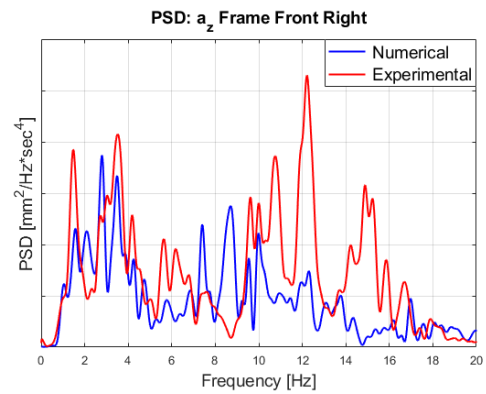


Figure 142- PSD of accelerations of frame front right

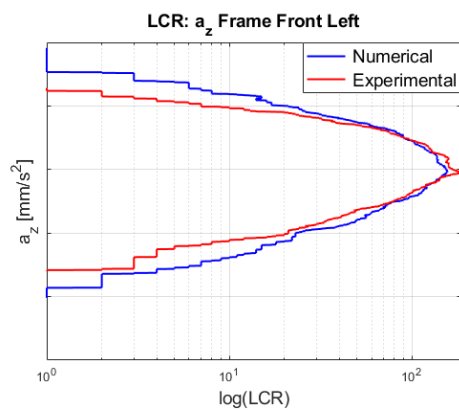


Figure 143- LCR of accelerations of frame front left

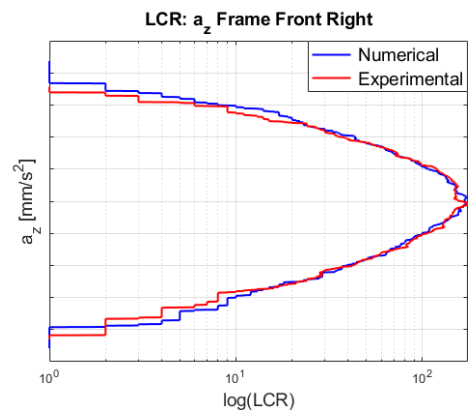


Figure 144- LCR of accelerations of frame front right

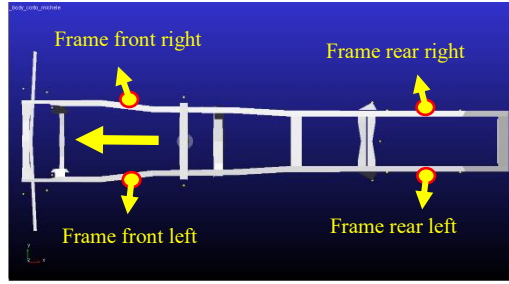


Figure 145- Accelerometers positioning

Frame rear left:

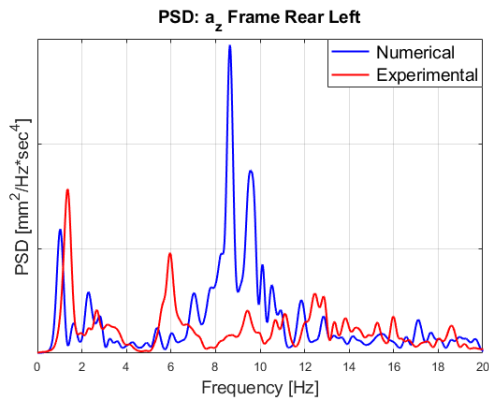


Figure 146- PSD of accelerations of frame rear left

Frame rear right:

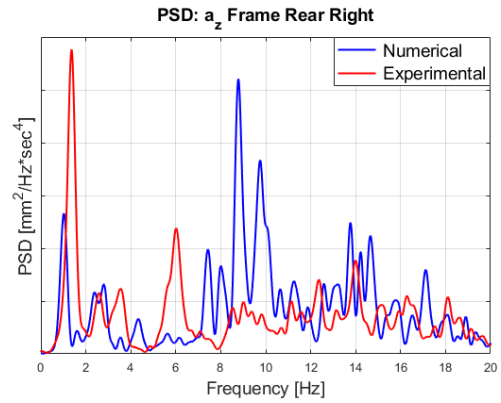


Figure 147- PSD of accelerations of frame rear right

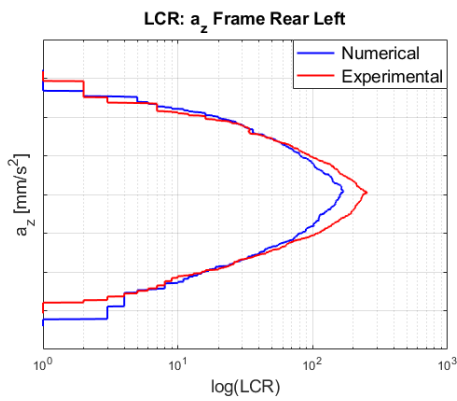


Figure 148- LCR of accelerations of frame rear left

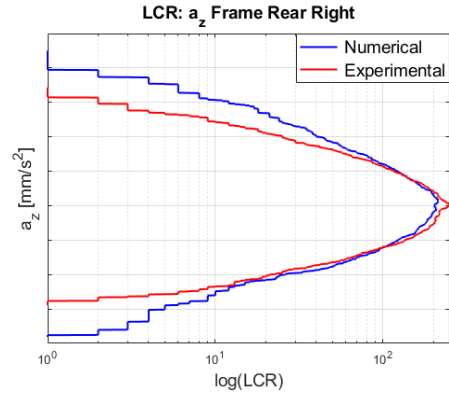


Figure 149- LCR of accelerations of frame rear right

These results obtained in the loaded condition at 15 km/h are not very good especially with regards to the PSD. The band of frequencies are always similar but the amplitudes very different. On the contrary, the correlation showed by LCR graphs are good.

Chapter 5. Conclusions and future perspectives

In this Master Thesis, the study of the first correlation between numerical and experimental comfort analysis of Iveco Stralis was presented. The study was carried out through experimental tests (Belgian block track, Markbronn proving ground, Germany) and numerical simulations (MSC Adams/Car) in order to evaluate the FTire model and suspension systems behavior of the multibody model respect the on-road truck.

The output data coming from the numerical and the experimental tests were vertical accelerations in time domain, registered by eight accelerometers positioned on the axles and the chassis of the truck.

The experimental results have been recorded, filtered and re-sampled by Iveco engineering office and are assumed as reference for the simulation ones.

The numerical simulations have been performed reproducing the real test conditions (speed, tire inflation pressure, load distribution, etc.) on the 3D reproduction of Markbronn track (OpenCRG format), using a complete multibody model of the truck.

The correlation has been conducted using two different techniques, typical of non-deterministic signals: the power spectral density (PSD) and the level crossing rate (LCR).

The obtained results can be considered satisfactory, considering that are the first outcomes obtained without changing the model property files and characteristics. The best outcomes are related to the unloaded condition, in which the load distribution is compliant with the on-road truck.

Concerning the PSD comparison, it can be said that the band of frequencies corresponds and the order of magnitude of values are the same. The amplitudes sometimes could appear very different, but it must be taken into account that we are dealing with square modulus, so differences are amplified. The LCR analysis can be considered fitting in the major part of the tests.

The study linked to this thesis concerns vibrations between 0 and 20 Hz and. Properly, it is not a comfort study aimed at improving the driver and passenger driving experience, but a preliminary evaluation of the FTire model and suspension systems response of the multibody model respect the on-road truck, performing the same track in the same test conditions. The multibody model developed is multipurpose because can be used not only for handling but also for studies concerning comfort, durability and fatigue.

Clearly, this is not an arrival point but a starting point for a sensitivity analysis and the parameter tuning of the multibody model. A sensitivity analysis is necessary to know which parameters and how they influence the results. The parameter tuning is required in order to have a multibody model more and more accurate and that behaves as close as possible to the real one. An accurate model can be obtained adjusting tire parameters, air springs and bushings properties files, masses and inertias of parts and so on. In this way the validation of the model can be pursued. Subsequently,

the validated model can be used to improve future heavy-duty vehicles and for other kinds of analysis mentioned before.

List of Symbols and Abbreviations

δ : steering wheel angle

δ_1 : steering angle of the wheel inside the curve

δ_2 : steering angle of the wheel outside the curve

Θ : roll angle

β : sideslip angle

$d\psi/dt$: yaw rate

a_y : lateral acceleration

F_z : vertical load

K_β : sideslip gradient

K_{us} : understeering gradient

l : vehicle wheelbase

t : vehicle track

ADAS: advanced driver-assistance systems

CRG: curved regular grid

FTire: flexible structure tire model

ISO: International Organization of Standardization

LCR: level crossing rate

NVH: noise, vibration and harshness

PSD: power spectral density

SAE: Society of Automotive Engineers

Bibliography

- [1]. Galvagno Enrico, Velardocchia Mauro (2017). “Meccanica del veicolo”, C.L.U.T. Editrice.
- [2]. Galvagno Enrico, Velardocchia Mauro. Notes of “Meccanica del veicolo” course, Polytechnic of Turin, Italy.
- [3]. Amati Nicola. “Notes of Chassis design course”, Polytechnic of Turin, Italy.
- [4]. Genta Giancarlo, Morello Lorenzo. (2009). “The automotive chassis. Vol. 1-2”, Springer.
- [5]. Vella Angelo. “Multibody modelling of a heavy-duty truck and analysis of the effect of frame flexibility on vehicle dynamics” (2018). Mechanical Engineering Master Theses, Polytechnic of Turin, Italy.
- [6]. Iveco internal reports.
- [7]. MSC Software (2015). “Adams/Help (Adams 2015.1)”.
- [8]. MSC Software Japan. (2015). “Leaf spring toolkit for Adams 2015.1. User’s guide”.
- [9]. Abhijit Londhe, Suhas Kangde, Nanrayana Moorthy. (2012). “Evaluation of vehicle systems structural durability using PSD based fatigue life approach”, 2012-01-0953 SAE International.
- [10]. Gabriele Fichera, Marco Scionti, Francesca Garesci. (2007). “Experimental correlation between the road roughness and the comfort perceived in bus cabins”, 2007-01-0352 SAE International.
- [11]. Asif Basha Shaik Mohammad, Ravindran Vijayakumar, Nageshwarrao.P. (2017). “Vibroacoustic optimization of tractor cabin and correlation with experimental data”, 2017-01-1847 SAE International.
- [12]. Arvind K. Jain, Sathish Madaswamy, Sudarsanam S., Venkat Srinivas. (2013). “Assessment of ride in a heavy commercial truck using numerical simulation methods and correlation with test”, 2013-26-0151 SAE International.
- [13]. Hans R. Dorfi. (2004). “Tire cleat impact and force transmission: modeling based on FTire and correlation to Experimental data”, 2004-01-1575, SAE International.
- [14]. Wheeler Andrew, "Computational Tire Models and their Effectiveness" (2013). Mechanical Engineering Undergraduate Honors Theses, University of Arkansas, Fayetteville.
- [15]. Cosin scientific software. “FTire – Flexible structure tire model. Modelization and parameter specification”.
- [16]. Friederichs Jan. “FTire modeling and validation report”. FKA mbH Aachen, Germany.
- [17]. Stefan Pyrek. “Tyre measurements and parameter identification for a tyre simulation model”. FKA mbH Aachen, Germany.
- [18]. Rakesh Hari Borse. (2015). “Analysis, creation and extraction of three-dimensional road profiles using open CRG tool”, ISSN 2395-1621, International Engineering Research Journal.

- [19]. Potò Vivien, Csepinszky Andras, Barsi Arpad. (2018). "Representing road related laserscanned data in curved regular grid: a support to autonomous vehicles", Volume XLII-2, 2018, The International Archives of the Photogrammetry, Remote Sensing and Spatial Information Sciences.
- [20]. Dr. Rauh Jochen. (2005). "Road simulation CRG (curved regular grid) Road data format overview", Daimler-Chrysler.
- [21]. Dr. Rauh Jochen. (2008). "OpenCRG. A unified approach to represent 3D road data in tyre simulation", AK 6.1.3, Daimler.
- [22]. OpenCRG. (2017). "User manual", VI2009.050, VIRE Simulationstechnologie GmbH.
- [23]. Molinari Filippo, Mesin Luca. Notes of "Elaborazione di segnali biomedici" course, Polytechnic of Turin, Italy.
- [24]. Fasana Alessandro, Marchesiello S. (2006). "Meccanica delle vibrazioni", C.L.U.T Editrice.
- [25]. Association Française de Normalisation. (2004). "Norme Internationale ISO 4138", Third Edition, ISO Editeur.
- [26]. Association Française de Normalisation (2003). "Norme Internationale ISO 7401", Second Edition, ISO Editeur.

Sitography

- [1]. IVECO Italy: <https://www.iveco.com>
- [2]. Cosin scientific software: <https://www.cosin.eu>
- [3]. OpenCRG: www.opencrg.org
- [4]. VIRES Simulationstechnologie GmbH: <https://vires.com>

Acknowledgements

In questa pagina si conclude un altro capitolo della mia vita. Sicuramente il capitolo più bello e interessante, ma allo stesso tempo duro e pieno di momenti difficili.

Il ringraziamento più grande va a mia *Mamma*, a mio *Papà* e a mia *Sorella*, i quali hanno sempre creduto in me, mi hanno sempre supportato e non mi hanno mai fatto mancare nulla. È grazie a loro che sono la persona che conoscete oggi ed è grazie ai loro sacrifici quotidiani che tutto questo cammino è stato possibile. Mantenere un figlio all'Università e lontano da casa non è sicuramente facile, dal punto di vista economico ma soprattutto dal punto di vista sentimentale, ne sono consapevole. Ma voglio dirgli che io ci sono e ci sarò sempre per loro, e che gli voglio un mondo di bene.

Ringrazio i miei *Nonni*, che hanno contribuito non poco alla mia educazione e che hanno avuto sempre una parola di conforto e dell'ottimo cibo a darmi la carica per andare avanti.

Ringrazio la mia fidanzata *Amanda* che ha reso speciali questi ultimi anni, con il suo sorriso, il suo amore, la sua positività e la sua dolce "pazzia". La ringrazio per aver reso più semplici i momenti difficili e per sopportarmi dal punto di vista caratteriale. Tutto ciò nonostante i sacrifici per la lontananza dalla sua bellissima Isola Verde e dalla sua famiglia, che ringrazio altrettanto per avermi accolto splendidamente. Spero la Vita mi permetta di condividere con lei tantissimi altri capitoli.

Ringrazio i miei *coinquilini e amici*, in particolare *Mattia Ghio* e *Fabio Salmone*, con cui sono legato dal primo anno di liceo. Con loro ho condiviso tutti gli alti e bassi del periodo universitario. Anche il loro aiuto ha contribuito non poco al raggiungimento della Laurea.

Ringrazio il *Dott. Nosenzo*, la *Dott.ssa Capitelli*, l'*Ing. Morello* per avermi accettato in un'azienda importante come Iveco, per avermi trattato come un collega fin da subito e per aver contribuito alla mia formazione professionale.

Ringrazio il *Prof. Velardocchia* e il *Prof. Galvagno* per avermi seguito eccellentemente e costantemente in questi otto mesi di attività.

Ringrazio tutti i ragazzi e le ragazze del *Team H2politO* con cui ho condiviso tre anni formidabili. Ci sono stati momenti belli e momenti meno belli, ma insieme abbiamo superato tutto. In particolare, ringrazio *Giuseppe Basso*, *Pietro Polignano*, *Mariano Della Ripa*, *Matilde Tinti* e *Marco Pedana*, con i quali ho condiviso non solo l'esperienza lavorativa ma anche i weekend di studio intenso e le cene improvvisate. Saranno sempre nel mio cuore.

Infine, ringrazio la *Vita*, che finora mi ha regalato tutto ciò che si può desiderare. Mi ha donato la salute, mi ha fatto nascere nella famiglia migliore al mondo, mi ha fatto conoscere la persona che amo e che mi ama, mi ha fatto incontrare tante persone lungo il cammino che sono diventate più di semplici amici e mi ha fatto crescere nel paese più bello di tutti, l'Italia. Sono fortunato.

